Finite Element Analysis of Elastic-Plastic Anisotropic Soils

by

Atul Nanda

dissertation submitted to the Faculty of the

Virginia Polytechnic Institute and State University

in partial fulfillment of the requirements for the degree of

Doctor of Philosophy

in

Civil Engineering

APPROVED:

T.Kuppusamy

G.W.Clough

J.N.Reddy

J.H.Hunter

R.D.Krebs

December 1986

Blacksburg, Virginia

Finite Element Analysis of Elastic-Plastic Anisotropic Soils

by

Atul Nanda

T.Kuppusamy

Civil Engineering

(ABSTRACT)

Elastic-plastic stress-strain models are developed for initially anisotropic soils. The models are developed for both total stress (undrained) analyses and for effective stress (drained) analyses. For anisotropic undrained cohesive soils under monotonic loading an elastic-plastic isotropic-hardening model is developed. For complex loading conditions the model is extended using multisurface plasticity. For effective stress analyses of soils, the Cam-Clay model concepts are generalized for initially anisotropic soils. Both isotropic and anisotropic hardening are used in the model. The behavior of the models is investigated under several loading conditions and some comparisions are made with experimental triaxial data. A nonlinear three-dimensional finite element program is developed in which the models are implemented. An updated Lagrangian large displacement analysis is also included. The constitutive models developed are used to investigate the influence of initial anisotropy on the bearing capacity, deformation and pore pressure development under footings in both plane-strain and three dimensional conditions. It is found that for the range of anisotropy encountered in the field, the deformation and bearing capacity are significantly different.

Acknowledgements

The author wishes to express his gratitude to Professor T. Kuppusamy, his thesis chairman for his stimulating discussions and continious encouragement. Appreciation is also expressed to Professors G.W. Clough, J.N. Reddy, R.D. Krebs and J.H. Hunter who critically reviewed this manuscript.

Table of Contents

List of Figures

List of Tables

List of Symbols

A Hardening Modulus

a Size of Consolidation Surface

a_0 Size of Yield Surface

B Strain-Displacement Matrix

b Anisotropy Ratio

C Cohesion

D Elastic Matrix

$\mathbf{D}^{ep}$ Elastic-Plastic Matrix

$d\mu$ Translation Constant

$d\bar{\varepsilon}^p$ Incremental Equivalent Strain

E Anisotropic Matrix

E_i Elastic Moduli

e void ratio

e_0 Initial Void Ratio

e^p Plastic Void Ratio

F Yield Function

$\mathbf{F}_i$ Anisotropic Vector

G_{ij} Shear moduli

H Hardening Modulus

K Plastic Modulus

$\mathbf{K_G}$ Stiffness Matrix

$\mathbf{K_e}$ Element Stiffness Matrix

K_0 Coefficient Lateral Stress

K_b Soild-Fluid Bulk Modulus

M Distortion Matrix

n Slope of Failure Surface

$\mathbf{N}_i$ Shape Function

$\mathbf{n}_f$ Gradient of Yield Function

$\mathbf{n}_q$ Graident of Potential Function

n_1 Exponent for Elastic Constants

P Size of Yield Surface

p Mean Pressure

P_L Limit Load

Q Potential Function

R Load Vector

R_{ij} Anisotropic Bearing Capacity Ratio

S Deviatoric Stress Vector

S_i Undrained Yield Strength

$\mathbf{T}_\epsilon$ Transformation Matrix

$\mathbf{T}_\sigma$ Transformation Matrix

$\mathbf{U}^G$ Global Displacement Vector

U Pore-Pressure

u Displacement

X_i Yield Strengths

α Translation Vector

δ Vertical displacement

δ_r Distance

ε Strain

ε^e Elastic Strain

ε^p Plastic Strain

γ Material Constant

λ Slope of Loading Curve in Consolidation Test

κ Slope of Unloading Curve in Consolidation Test

η Curve Fit Constant

ν_{ij} Possions Ratio

σ Stress Vector

$\bar{\sigma}$ Equivalent Stress

φ Friction Angle

τ^{∇} Jaumann Stress

ω_{ij} Rotation Tensor

Ω Residual Load Vector

CHAPTER 1

INTRODUCTION

Almost all soils exhibit some degree of anisotropic behavior. Yet in most analysis the influence of anisotropy is neglected. However, the presence of anisotropy in soils can significantly influence the analysis, in particular the analysis of stresses and displacements under foundations, bearing capacity , stability of embankments and slopes, and earth pressures on retaining structures.

The classical methods of analysis in soil mechanics treat the problem of deformation and stability separately, i.e., settlement analysis and bearing capacity calculations. Soils continuously yield, thereby showing that deformation and failure analyzes cannot be seperated. Also, in most of the classical methods, the soil is treated as an isotropic media. For deformation analysis the soil is treated as an elastic solid and for stability analysis it is treated as a rigid-plastic body. Only in a few cases is the anisotropy of the soil included in the analysis. In these cases, the theory of anisotropic elasticity is used for deformation analysis and an anisotropic failure criteria is used for stability analysis. However, the real behavior of soils is too complex to be modeled by such simple theories. With the development of numerical

methods, particularly the finite element method, it is now possible to do a complete analysis of soil mechanics problems, i,e., an incremental elastic-plastic analysis can be done so that the continious yielding nature of soils can be included in the analysis. In recent, years a large number of constitutive models have been developed to analyze the behavior of soils. These models, along with the finite element method, have been used to analyze problems in soil mechanics. Most of these models treat the soil as an isotropic media.

The behavior of soils is generally nonlinear, anisotropic, hysteretic and rate and path dependent. In the past the theory of plasticity has been successfully used to predict stresses, strains and limit loads under different loading conditions. Elasto-plastic models have been developed for both static and cyclic loading conditions and have been used under a wide variety of loading conditions. Because the behavior of soils is very complex, no single model can be used for all possible loading conditions. For small strains a simple elasticity model can be used. For large strains and under monotonic loading conditions a nonlinear elasticity model or a simple isotropic hardening plasticity model can be used with accuracy. However, under a general varying state of stress, an advanced plasticity model is necessary to obtain good results.

While a large amount of work has been done in the elasto-plastic analysis of isotropic materials, little work has been done in the elasto-plastic analysis of initially anisotropic materials. This is unfortunate, as most soils exhibit some degree of anisotropy. It is essential that initial anisotropy be included in the analyzes of geotechnical problems, as anisotropy can influence bearing capacity, deformations, earth-pressures and stability of geotechnical structures.

The aim of this thesis is to extend the classical isotropic elastic-plastic models to account for the initial anisotropy of the soil. These models will be developed for undrained and effective stress analyzes of soils, and will account for both initial and induced anisotropy of the soil. The models will be implemented for the finite element analysis of a number of problems in soil mechanics.

This thesis has been divided into seven Chapters. In Chapter 2 the causes and types of anisotropy in soils are briefly discussed. The basic concepts of the theory of plasticity and various isotropic and anisotropic yield criteria are reviewed. Also, some of the results obtained from the limit analysis of anisotropic materials are discussed.

In Chapter 3 elastic-plastic constitutive models are developed for the undrained behavior of anisotropic clays. Both isotropic hardening and multisurface theories are used in development of the model. The general response of the model is investigated under simple loading conditions and some comparisions are made with experimental data.

In chapter 4 elastic-plastic constitutive models are developed for the anisotropic behavior of both clays and sands. These models can be used for both drained and undrained conditions. Both isotropic hardening and kinematic hardening theories are used in developing the models. The response of the models is investigated and some comparisions are made with experimental data

Chapter 5 describes the implementation of the models into finite element analysis. A three-dimensional finite element program was developed for nonlinear analysis of soils. The models developed in Chapters 3 and 4 have been implemented into the program. As plastic deformation can lead to large displacements, geometric nonlinearity was also considered. A large deformation capability based on the updated Lagrangian formulation has been implemented in the program.

In chapter 6 strip and rectangular footings on anisotropic soils are analyzed by the finite element method under both drained and undrained conditions. The influence of anisotropy is investigated on both the deformation and failure of the footings. The finite element analysis takes into account the initial anisotropy of the soil, three-dimensional stress conditions and the influence of overconsolidation on the deformation and failure of the footings. The influence of initial anisotropy on the pore pressure development, yielding below the footing and surface displacement profiles is also analyzed. The influence of anisotropy on the stability and deformation of an embankment is also investigated.

Finally, in Chapter 7 the summary and conclusions derived from this study are presented.

CHAPTER 2

PLASTICITY OF ANISOTROPIC SOILS

Introduction

In this chapter the causes of anisotropy in soils and their stress-strain- strength behavior is briefly examined. The anisotropic behavior of soils under both drained and undrained conditions are discussed.

As the theory of plasticity will be used to develop the models, the basic concepts of the theory of plasticity as applied to anisotropic materials are briefly discussed and the various anisotropic yield criteria examined. Also, some of the classical methods of limit analysis and the relevant results obtained by these methods for anisotropic media are investigated.

Causes of Anisotropy

Almost all soils exhibit anisotropic behavior in both strength and stress-strain response. Anisotropy in soils is caused by the manner of deposition and the non-uniform initial state of stress in the soil. The anisotropy arises due to the difference in vertical and horizontal stresses which develop during deposition and this leads to prefered orientation of the soil structure (26). Futher anisotropy could develop due to the complex stress history experienced in the past by the soil. This includes deposition,erosion, geologic movements and earthquake motions.

The anisotropic response of soils can be seperated into two parts; inherent anisotropy and induced anisotropy. Inherent anisotropy is the anisotropy exhibited in strength and stress strain response upon initial loading. If samples of an unstressed anisotropic media are tested , in directions which are mutually perpendicular, different stress-strain behavior will be observed (see Figure 2.1). This includes the initial elastic moduli, as well as the ultimate strength. This type of behavior is called initial anisotropy.

Induced anisotropy is the anisotropy developed in soils due to the loading process. Load an initially isotropic material in one direction and unload. Reload the same sample in a direction normal to the first loading direction. The stress-strain response of the two cases may be different. Thus an initially isotropic material has become anisotropic. This type of behavior is called induced anisotropy. Usually the two types of anisotropy exist simultaneously. Under undrained conditions many clays exhibit induced anisotropy. If the loading process causes rotation of the principal stresses, the undrained stress strain behavior may be anisotropic (22). As this anisotropy is caused due to loading and depends on the stress path, it is also called induced anisotropy.

The anisotropic behavior of sands has been examined by many researchers (2,3,68). Experiments carried out under both triaxial and plane strain conditions on sand samples inclined to the direction of deposition indicate anisotropy in both strength and stress-strain re-

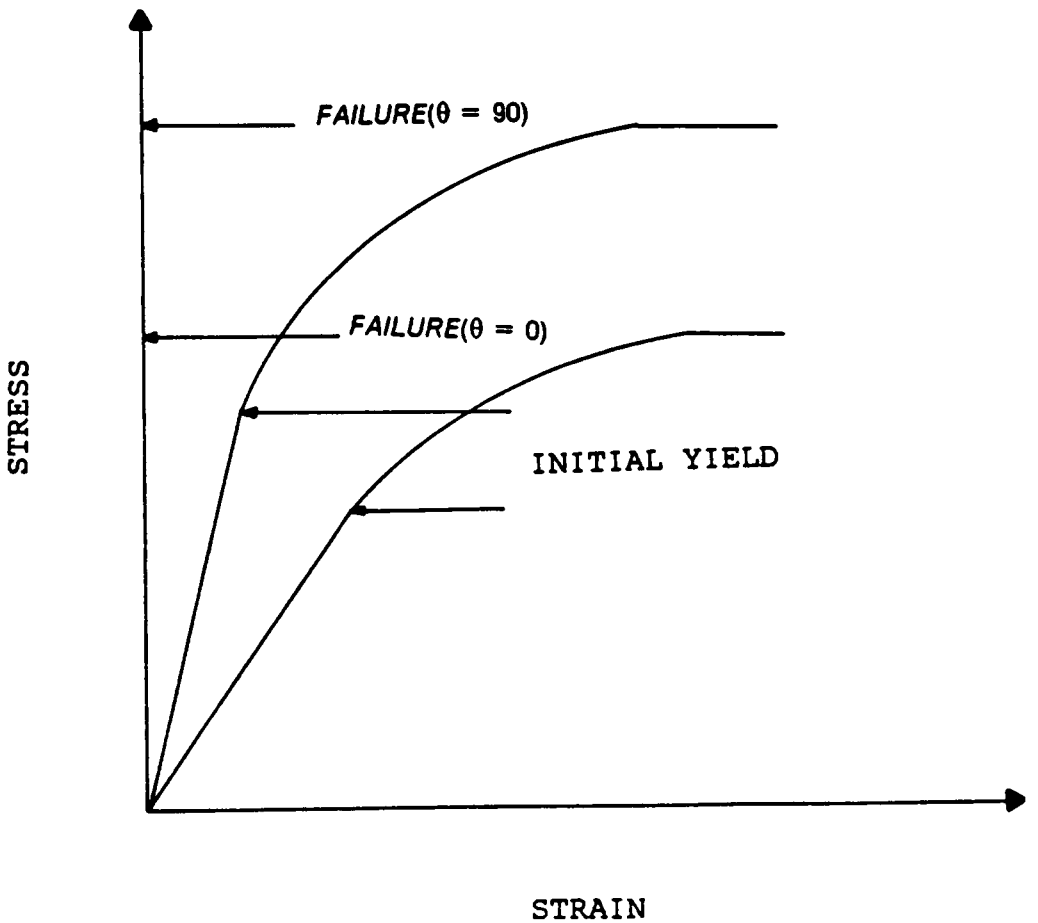

Figure 2.1 General Response of Anisotropic materials

sponse. The angle of internal friction can vary between 2 to 8 degrees over the angle of internal friction measured in the direction of depositation. The strains can vary by over 200 percent. Anisotropy in sands arises chiefly due to the mode of deposition of the sand layer. This leads to preffered orientation of the sand grains. Figure 2.2 shows the strength and stress-strain variation with the angle of loading for triaxial tests on sand (2).

Initial anisotropy is exhibited by clays under undrained conditions (1,8,13,22,41,59,60). The anisotropic behavior of undrained clay is due both to the mode of sedimentation and the previous stress history experienced by the soil. Many overconsolidated clays and clays consolidated under an anisotropic stress state also exhibit anisotropic behavior. The drained response of these same clays may be isotropic. The undrained anisotropic behavior is due to the previous stress history of the clay and due to different stress paths during loading. This can result in anisotropic undrained behavior, while the drained response is essentially isotropic. The undrained shear strength can vary by over 50% in two mutually perpendicular directions and the elastic moduli can differ by a factor greater than 2.0. This is important in the short term analysis of structures on clay. Initial anisotropy can influence both bearing capacity and deformation. Figure 2.3 shows the stress-strain response of London clay under undrained conditions (1). The stress strain response is plotted for a horizontal sample (θ = 0.) and for a vertical sample (θ = 90.). The clay displays anisotropy both in the elastic response as well as in the strength.

Under drained conditions, some sensistive and overconsolidated clays exhibit anisotropic response (36,41,69). Limited data is available for the drained anisotropic behavior of clays. Anisotropy is exhibited both in strength and stress-strain behavior. The variation in strength can be up to 50% and the elastic moduli can vary by over 200% (69). Figure 2.4 shows the stress-strain response of a senstitive clay under drained triaxial conditions (69). The stress strain response is plotted for samples inclined at various angles to the horizontal. Both the stress strain response as well as the volume change exhibit anisotropy.

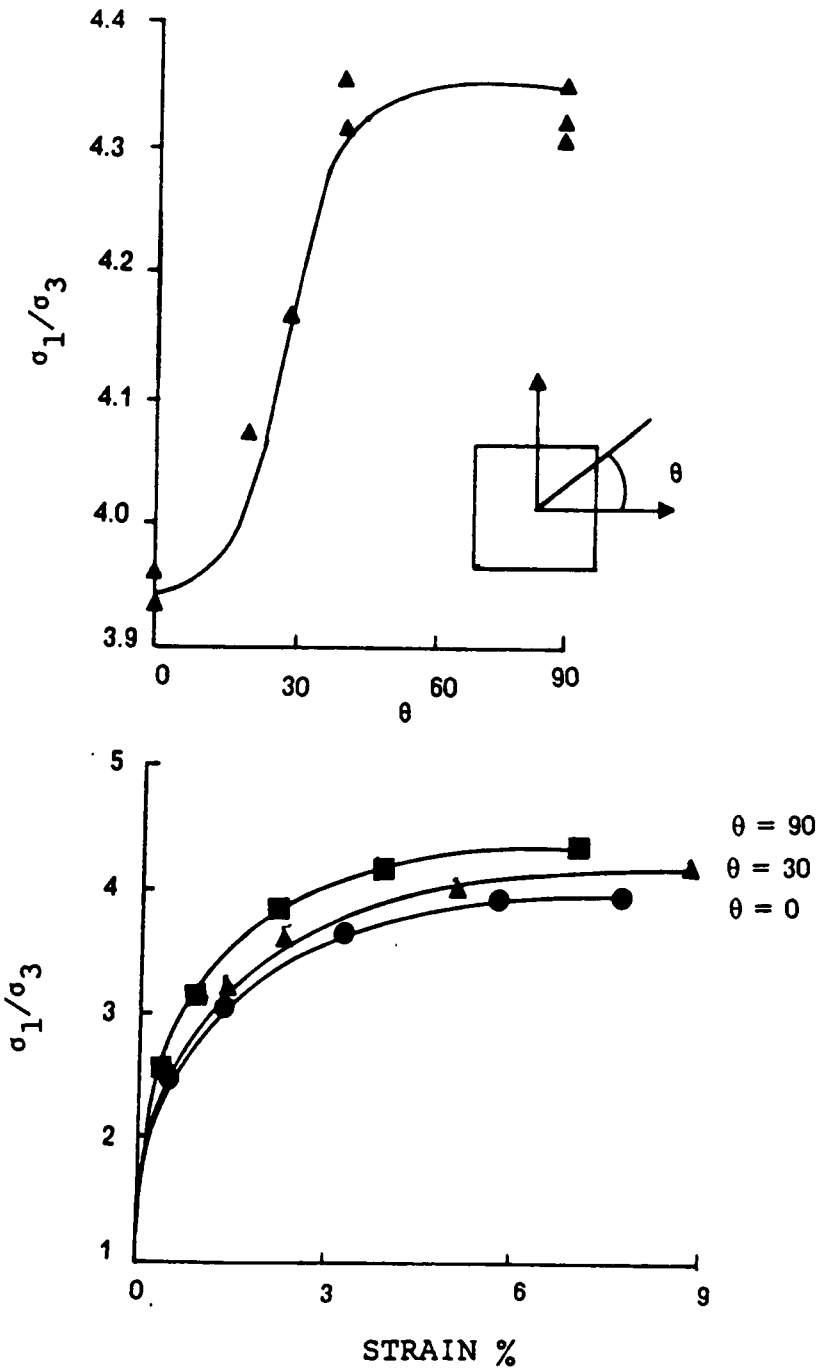

Figure 2.2 Anisotropic Behavior of Sands(Ref-2)

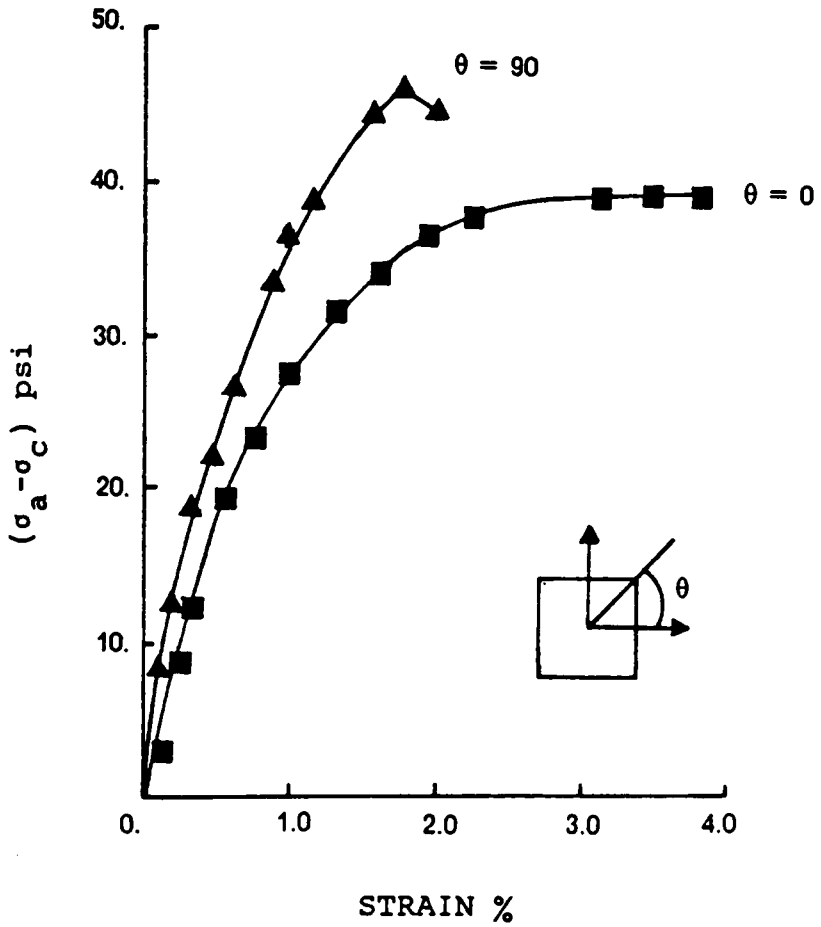

Figure 2.3 Anisotropic Behavior of Undrained Clays (Ref-1)

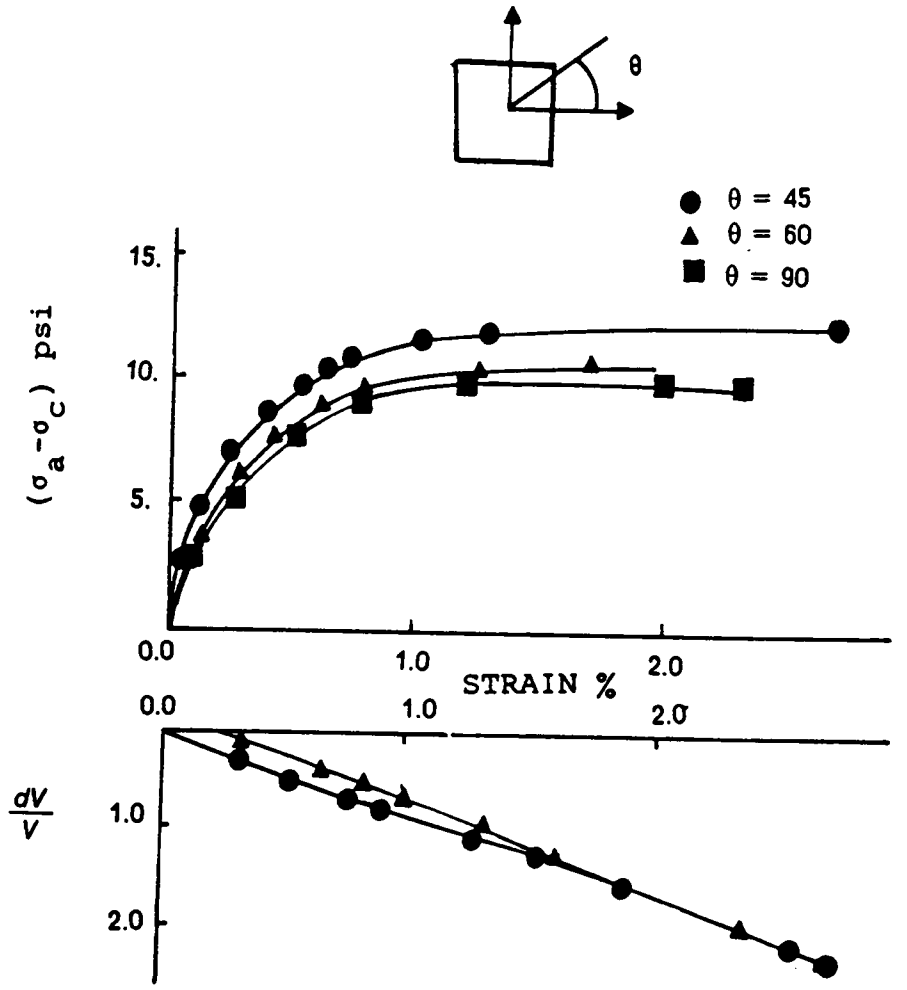

Figure 2.4 Anisotropic Behavior od Drained Clays (Ref-69)

Plasticity Theory

The basic assumption in the theory of plasticity is that, there exists a yield surface in the stress space, such that, for all states of stress within the surface, the response of the material is elastic. States of stress on the surface exhibit elastic-plastic response. No state of stress is allowed outside this surface. In general the yield surface is of the form,

$$F(\sigma, \alpha, k) = 0 \tag{2.1}$$

where σ is the stress vector, α is the translation vector and k is a scalar parameter. Where for $F < 0$, the response is elastic and for $F = 0$, the response is elastic-plastic. The various forms of $F(\sigma, \alpha, k)$ will be discussed in the next section.

It is assumed in the incremental theory of plasticity that the incremental strain can be separated into an elastic component and a plastic component (29,72).

$$d\varepsilon = d\varepsilon^e + d\varepsilon^p \tag{2.2}$$

where $d\varepsilon$ is the total incremental strain vector, $d\varepsilon^e$ is the elastic incremental strain vector and $d\varepsilon^p$ is the incremental plastic strain vector. It is further assumed that there exists a plastic potential and that the plastic incremental strain vector is proportional to the gradient of this potential. This is the normality condition (72,29).

$$d\varepsilon^p = \lambda \frac{\partial Q}{\partial \sigma} \tag{2.3}$$

where Q is the plastic potential and λ is a proportionality constant to be determined by the consistency condition. This condition states that during deformation the stress point should not penetrate the yield surface. This is given as,

$$dF = 0 \tag{2.4}$$

Equation 2.3 can also be written as (42),

$$d\varepsilon^p = \mathbf{n}_q(\mathbf{n}_f^T d\sigma)/K \tag{2.5}$$

Where K is the plastic modulus and $\mathbf{n}_q$ *and* $\mathbf{n}_f$ are the normalized potential and yield function gradients (42) given by,

$$\mathbf{n}_q = \frac{\partial Q}{\partial \sigma}((\frac{\partial Q}{\partial \sigma})^T(\frac{\partial Q}{\partial \sigma}))^{-1/2} \tag{2.6}$$

$$\mathbf{n}_f = \frac{\partial F}{\partial \sigma}((\frac{\partial F}{\partial \sigma})^T(\frac{\partial F}{\partial \sigma}))^{-1/2}$$

If Q = F, then the material is said to have an associated flow rule; if Q is not the same as F, then the material has a non-associated flow rule. In this thesis, only associated flow rules will be used, as this results in a symmetric stiffness matrix. In general, most frictional materials require non-associated flow rules. However, the increase in accuracy obtained by using a non-associated flow rule is offset by a reduction in computing costs due to lesser computer storage and computation time.

Further the elastic strain increment is given as,

$$d\varepsilon^e = \mathbf{D}^{-1} d\sigma \tag{2.7}$$

where **D** is the elastic constitutive matrix. Substituting the flow rule and the above equation into equation (2.2).

$$d\varepsilon = \mathbf{D}^{-1} d\sigma + \mathbf{n}_q(\mathbf{n}_f^T d\sigma)/K \tag{2.8}$$

Solving for $d\sigma$

$$d\sigma = (\mathbf{D} - \mathbf{D}\mathbf{n}_f^T \mathbf{n}_q \mathbf{D}/(K + \mathbf{n}_f \mathbf{D}\mathbf{n}_q))d\varepsilon \tag{2.9}$$

Equation 2.9 can be written as,

$$d\sigma = (\mathbf{D} - \mathbf{D}^p)d\varepsilon = \mathbf{D}^{ep} d\varepsilon \tag{2.10}$$

Where $\mathbf{D}^{ep}$ is the elastic-plastic matrix and $\mathbf{D}^{p}$ is the plastic matrix.

Anisotropic Yield Criteria

In the previous section, a brief description of the theory of plasticity and yield criteria was given. In this section, some of the yield criteria used for anisotropic materials will be discussed. The yield criteria will be classified as pressure-independent criteria and pressure dependent criteria. Pressure-independent yield criteria are used for materials whose yielding is independent of the the hydrostatic pressure. These yield criteria are used for undrained analysis. Pressure-independent yield criteria are used for materials whose yielding depends on the hydrostatic pressure, such as sands and effective stress analysis of clays.

Some commonly used pressure-independent yield criteria are the Von-Mises and the Tresca criteria (29,39). The commonly used pressure-dependent yield criteria are the Mohr-Columb and the Drucker-Prager criteria (15).

The most important pressure-independent yield criteria for anisotropic materials is the Hill's criteria. This is a generalization of the Von-Mises criteria for anisotropic media(29). It is given by;

$$\bar{F}(\sigma_2 - \sigma_3)^2 + \bar{G}(\sigma_3 - \sigma_1)^2 + \bar{H}(\sigma_1 - \sigma_2)^2 + 2L\sigma_4^2 + 2M\sigma_5^2 + 2N\sigma_6^2 = 1 \qquad (2.11)$$

Where

$$\bar{F} = \frac{1}{2}\left(\frac{1}{X_2^2} + \frac{1}{X_3^2} - \frac{1}{X_1^2}\right)$$

$$\bar{G} = \frac{1}{2}\left(\frac{1}{X_3^2} + \frac{1}{X_1^2} - \frac{1}{X_2^2}\right)$$

$$\bar{H} = \frac{1}{2}\left(\frac{1}{X_1^2} + \frac{1}{X_2^2} - \frac{1}{X_3^2}\right)$$

$$L = \frac{1}{2S_1^2} \qquad M = \frac{1}{2S_2^2} \qquad N = \frac{1}{2S_3^2}$$

Where X_1, X_2 and X_3 are the yield strengths in the 1,2 and 3 directions. S_1 is the the shear strength in the 2-3 plane, S_2 is the shear strength in the 1-3 plane and S_3 is the shear strength in the 1-2 plane.

Some generalizations of the Mohr-Columb criteria for anisotropic media have also been developed by Baker and Krizek (4) and Livhen and Schlarsky (34). Here, a variation of C and φ is assumed. Where C is the cohesion and φ is the angle of internal friction.

$$C = C_{max} - (C_{max} - C_{min}) \sin^2\psi$$

$$\tan\varphi = \tan\varphi_{max} - (\tan\varphi_{max} - \tan\varphi_{min}) \sin^2\psi \qquad (2.12)$$

$$\psi = \beta - (45 - \frac{\varphi}{2})$$

where β is the orientation of the failure plane. These criteria are not convenient for numerical analysis as the orientation of the failure plane has to be determined.

Another important yield criteria for anisotropic materials is the Wu-Tsai yield criteria (64).

$$\mathbf{F_1}\sigma + \sigma^T\mathbf{F_2}\sigma = 1 \qquad (2.13)$$

where $\mathbf{F_1}$ is a 6-1 vector and $\mathbf{F_2}$ is a 6-6 matrix of material properties. The coefficients of these are to be determined experimentally. This is a very complete yield criteria. In its general form, it is pressure-dependent but can be easily reduced to a pressure-independent form, and this can be used for materials which exhibit different strengths in tension and compression.

Similar criteria for more general cases is given by Goldenblat-Kopnov (72);

$$(\mathbf{F_1}\sigma)^a + (\sigma^T\mathbf{F_2}\sigma)^b + \ldots\ldots = 1 \qquad (2.14)$$

where $\mathbf{F}_1$ and $\mathbf{F}_2$ are matrices of material parameters as in equation 2.13, and a and b are constants. This criteria is too complex for practical purposes. A more convenient criteria for pressure-independent materials was given by Drucker and Edelmam (23). This can easily be generalized for pressure-dependent materials;

$$(\mathbf{S} - \boldsymbol{\alpha})^T \mathbf{E} (\mathbf{S} - \boldsymbol{\alpha}) = 1 \tag{2.15}$$

where $\boldsymbol{\alpha}$ are tensors that locate the surface in stress space, $\mathbf{S}$ are deviatoric stress vectors and E is the anisotropic/distortion matrix. This criteria has been used for anisotropically hardening materials.

Another approach is to use tensor functions to express yielding (10). The yield function is expanded as a tensor polynomial in terms of plastic strains, the coefficients of which are to be determined experimentally. This form is not very easy to use in practice, as a large number of coefficients are to be determined.

Hardening Rules

To describe the complete elastic-plastic response, the hardening behavior has to be described. Figure 2.5 illustrates the uniaxial stress-strain response of an ideal elastic-plastic material. Along OA the response is elastic. Along AB plastic response is observed. At B the material unloads in an elastic mode upto D. From D to B the material loads in an elastic mode up to B. Any loading above B is plastic. This increase of yield strength upon reloading is called 'hardening'. Hardening can be linear or nonlinear. Most soils exhibit nonlinear hardening. The plastic modulus can vary from infinity (initial yield) to zero at failure. However in many cases linear hardening is a suitable approximation. The two basic types of hardening rules used in the theory of plasticity are isotropic hardening and kinematic or anisotropic hardening.

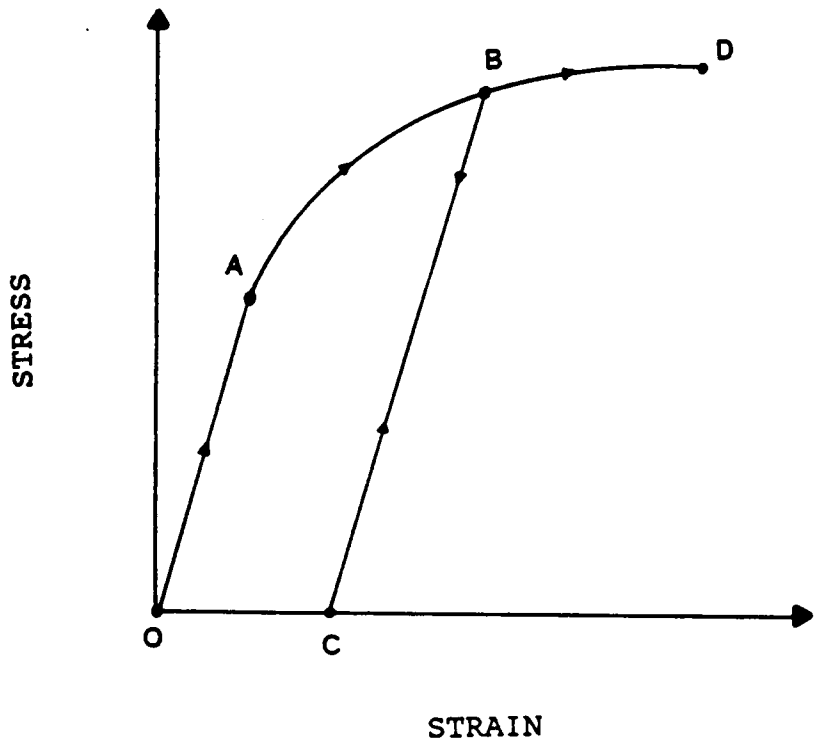

Figure 2.5 Hardeing Behavior

Figure (2.6) illustrates isotropic hardening. As the stress point moves outward in stress space from the initial surface, the yield surface expands uniformally with the stress point without distortion. For isotropic hardening the yield function can be written as;

$$F = F(\sigma,k) \tag{2.16}$$

Where k is a scalar called the hardening parameter and usually represents the size of the yield surface.

Figure (2.6) also illustrates kinematic hardening. As the stress point moves in stress space, the yield surface translates in stress space without changing shape or size. For kinematic hardening, the yield function can be written as;

$$F = F(\sigma, \alpha) \tag{2.17}$$

where α is the translation vector. The translation vector represents the position of the yield surface in stress space. The translation of the yield surface in stress space is specified by a translation rule. Several translation rules exist. Two of the more common rules are described below;

$$\alpha = c\varepsilon^{p} \tag{2.18}$$

$$d\alpha = d\mu(\sigma - \alpha) \tag{2.19}$$

where c and $d\mu$ are constants to be determined from the consistency condition and, $d\alpha$ is the incremental translation vector.

In general, the stress strain behavior of many materials is very complex; hence, both isotropic hardening and kinematic hardening have to be used. More complex types of hardening will be described in the next two chapters.

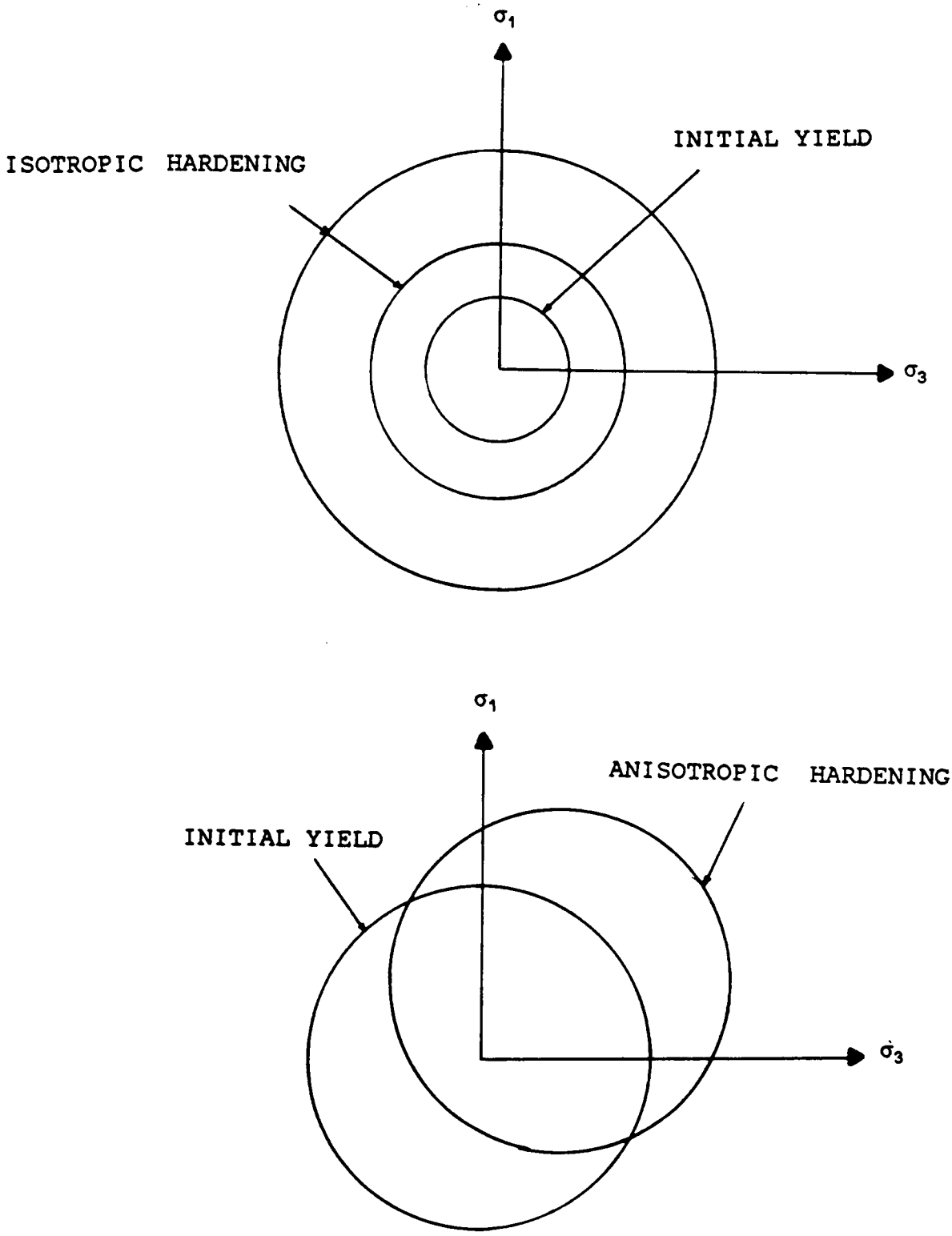

Figure 2.6 Isotropic and Kinematic Hardening

Limit Analysis of Anisotropic Media

There are three methods used for limit analysis, the slip-line method, the theorems of limit analysis(upper and lower bound theorems) and the limit equilibrium method. In the slip-line method, the equations of equilibrium and the yield criteria are combined to give a set of differential equations in the yielded area. These equations are transformed to curvilinear coordinates, such that the transformed coordinates coincide at every point in the yielded region with the direction of slip. These are known as the slip-line field. These, along with the boundary conditions are used to study the state of stress in the yielded zone and compute the limiting condition. This method is described in detail by Sokolovskii (63), where several approximate methods are developed to compute limit loads of structures, stability of slopes and earth pressures for isotropic soils.

Slip-line solution for the ultimate load of a rigid punch on a semi-infinite anisotropic media under plane strain conditions was obtained by Hill (29). The above solution was extended by Davis and Christian (19) to obtain bearing capacity factors for strip footings on undrained anisotropic clays.

The theorems of limit analysis give an estimate of limit loads. In the lower bound-theorem, a stress field is assumed which does not violate either the yield condition or the equilibrium equations. This theorem gives a lower bound-estimate of the limit load. In the upper-bound theorem a kinematically admissible velocity field is assumed and the limit load is calculated by equating the rate of internal and external work. This gives an upper bound estimate of the limit loads.

The limit theorems have been applied to some cases involving anisotropic media. The bearing capacity and slope stability problems under undrained conditions have been analyzed by Chen (15). He also analyzed slope stability under drained conditions. He assumed that the cohesion varies with direction, while the friction angle is constant in all directions. The bearing capacity of a strip on an anisotropic soil which exhibits both anisotropic cohesion and

friction angle has been analyzed by Livheh.M and Shklarsky.E (34) for the special case where the anisotropy of cohesion is identical to the anisotropy of the friction angle. This solution has limited application, as such a case is unlikely to be encountered in reality.

The limit equilibrium method has been traditionally used in soil mechanics for approximate stability analysis. In this method, a critical failure surface is obtained. This failure surface is used to calculate the limit load. The advantage of this method is that it is easy to use. However, it does not yield either an upper-bound or a lower-bound solution.

The methods of limit analysis determine the limit loads, but give no information about the deformation. In practice, both the collaspe load and the deformation are required. The finite element method along with elastic-plastic models can be used to calculate both limit loads and deformations.

CHAPTER 3

MODELS FOR PRESSURE-INDEPENDENT MEDIA

Introduction

In this Chapter, new models are developed for initially anisotropic pressure-independent media. These models can be applied to the short-term, undrained analysis of clays, metals, composites and other initially anisotropic materials. The models are applicable for both initial and induced anisotropy.

In section 3.2, the elasticity of an anisotropic body is reviewed. The experimental determination of the elastic constants are briefly described. In section 3.3, an elastic-plastic model for an initially orthotropic pressure-independent media with isotropic work hardening is developed. Determination of the parameters required for the model are also described. In section 3.4, an anisotropic-hardening multisurface model for an initially orthotropic pressure-independent media is developed and the determination of the parameters required

is also discussed. Finally, in section 3.5, the general response of the above models and comparison with experimental data for both isotropic and anisotropic materials are presented.

Anisotropic Elasticity

The theory of anisotropic elasticity has been developed in detail by Lekhitsky (33), where several analytical solutions of practical value have been given. Elastic analysis of anisotropic soil under both drained and undrained conditions has been investigated by Feda (24), Pickering(49) and Gibson (26). Several solutions of practical value can also be found in (26). Here a brief introduction to the theory of anisotropic elasticity is given.

The relation between stress and strain for an elastic body is given as;

$$\sigma = D\varepsilon \tag{3.1}$$

where σ is the stress vector (6-1), ε is the strain vector (6-1) and **D** is a (6-6) symmetric elastic constitutive matrix.

For a general anisotropic elastic body, 21 elastic constants are required. However, here only an orthotropic elastic body will be considered.

An elastic body that has 3 planes of elastic symmetry is called an orthotropic body(figure 3.1). It requires 9 independent elastic constants. The stress strain relations for an orthotropic elastic body in the material principal planes are given in appendix A. The nine constants are the moduli E_1 , E_2 and E_3 , the shear moduli G_{12} , G_{23} *and* G_{13} , and the Poissons ratios ν_{ij} . For an incompressible media, that is one with no volume change, only 6 elastic constants are required. Imposing the condition of incompressibility $\varepsilon_v = 0$,the magnitude of the Poissons ratios can be determined in terms of the elastic moduli (appendix A).

An elastic body that has a plane of isotropy is called a cross anisotropic body (figure 3.2). Five independent elastic constants are required in this case. For an cross anisotropic body in the material principal planes, the strain and stress relations are given in appendix A. Here

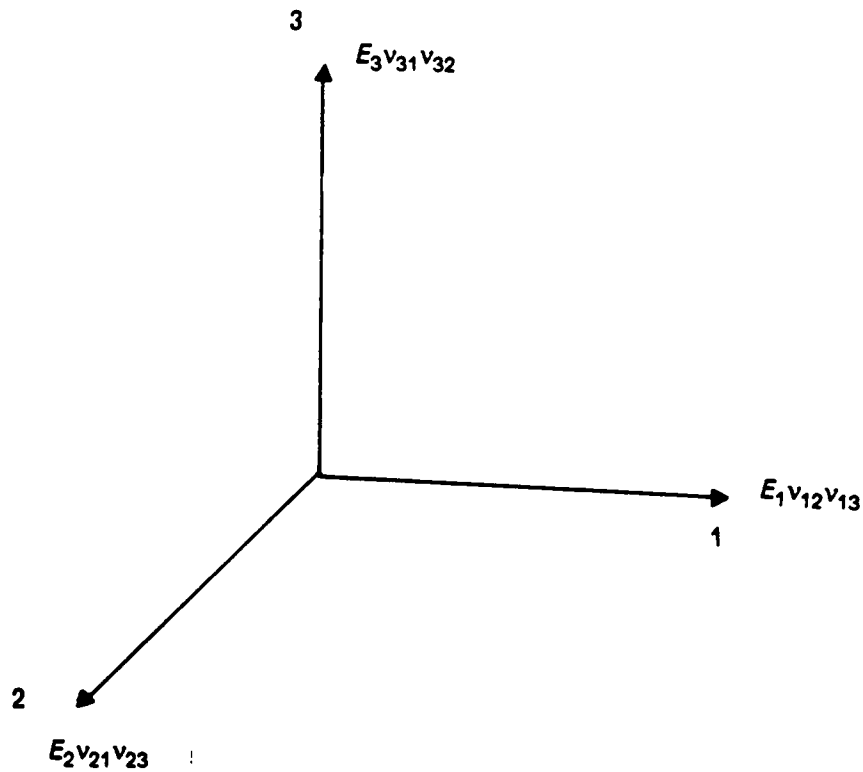

Figure 3.1 Orthotropic Elastic Body

the constants are E and v the Youngs modulus and Poissons ratio in the plane of isotropy and $E^{\times}$ and $v^{\times}$ the Youngs modulus and Poissons ratio out of plane. $G^{\times}$ is the out of plane shear modulus. For an incompressible cross-anisotropic media, only 3 constants are required (appendix-A). It should be noted that the above equations are valid only in the principal planes. In other cases, appropiate transformations should be used. These are described in appendix-A.

Finally, for an isotropic elastic solid only two elastic constants are required. Where E and v are the Youngs modulus and Poissons ratio. For an incompressible media only one constant E is required ($v = .50$)

The elastic constants can be determined from triaxial tests (37,26). The procedure for determining the elastic constants for a cross- anisotropic material from triaxial tests is described below. For a cross-anisotropic material, three elastic constants, the elastic moduli in the horizontal direction (1-direction), the elastic moduli in the vertical direction (3-direction), and the out of plane shear modulus are required.

The elastic moduli can be determined by conducting tests in the horizontal and vertical directions;

$$E_1 = \frac{d\sigma_1}{d\varepsilon_1} \tag{3.2}$$

$$E_3 = \frac{d\sigma_3}{d\varepsilon_3} \tag{3.3}$$

The shear moduli can be determined from a test on an inclined sample. Transforming the stress strain equations;

$$\frac{1}{G_{12}} = \left(\frac{1}{E_i} - \frac{\cos^4\theta}{E_2} - \frac{\sin^4\theta}{E_1}\right)\frac{1}{(\sin^2\theta\cos^2\theta)} + \frac{2\nu_{21}}{E_1} \tag{3.4}$$

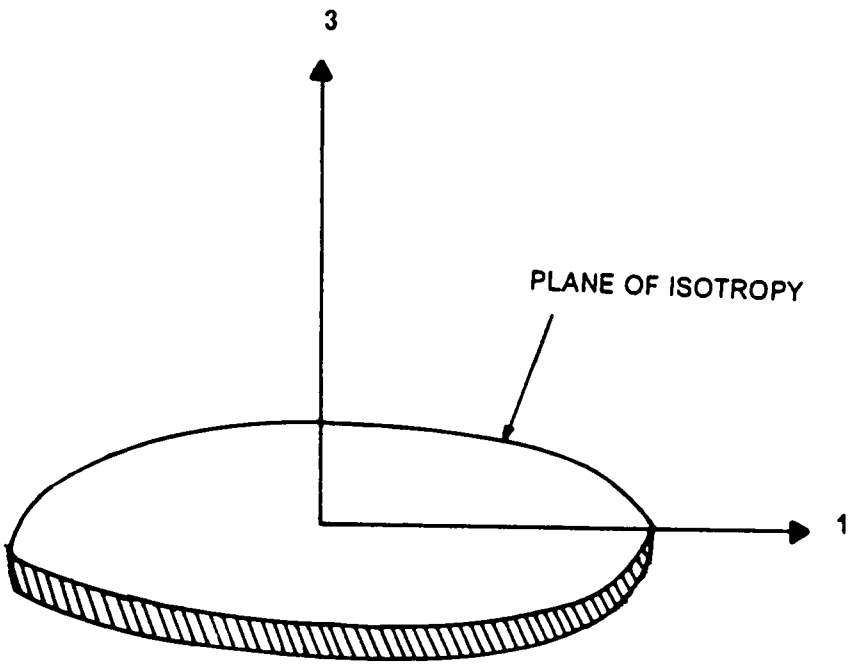

Figure 3.2 Cross-Anisotropic Elastic Body

Where E_i is the modulus measured in the inclined test and θ is the angle of inclination from the 1 axis. For undrained analysis the value of ν can be determined from the incompressibility condition.

Isotropic-Hardening Model (IHM-PI)

In this section, a pressure-independent, elastic-plastic model is developed for an initially orthotropic media. The model can distinguish between elastic and plastic strains. Also the loading/unloading conditions can be easily determined. The models based on nonlinear elasticity (such as the hyperbolic model), are not capable of this. It is assumed that the hardening is isotropic, i.e. the initial anisotropy of the material does not change during deformation. Hence, the model cannot account for induced anisotropy. Also unloading is assumed elastic. Therefore, the model is limited to monotonic loading conditions.

The above assumptions limit the applicability of this model. However, the model is simple and easy to implement. A more general model which overcomes the above limitations will be presented in the next section.

The first elastic-plastic model for initially orthotropic materials was developed by Hill (29). This model is a generalization of the Von-Mises work-hardening model. The Hill's yield criteria is described in Chapter-2. Most other models for initially orthotropic materials with isotropic hardening are based upon modifications of Hill's theory (27,59,60,66,62). Here a work hardening model with isotropic-hardening is developed and the elasto-plastic constitutive matrix is derived. For an isotropic-hardening model the yield function is of the form (figure 3.3);.

$$F(\sigma,k) = 0 \tag{3.5}$$

Where k, the hardening parameter is a scalar which is a monotonically increasing function of plastic deformation (plastic work). The form of $F(\sigma,k)$ is chosen as;

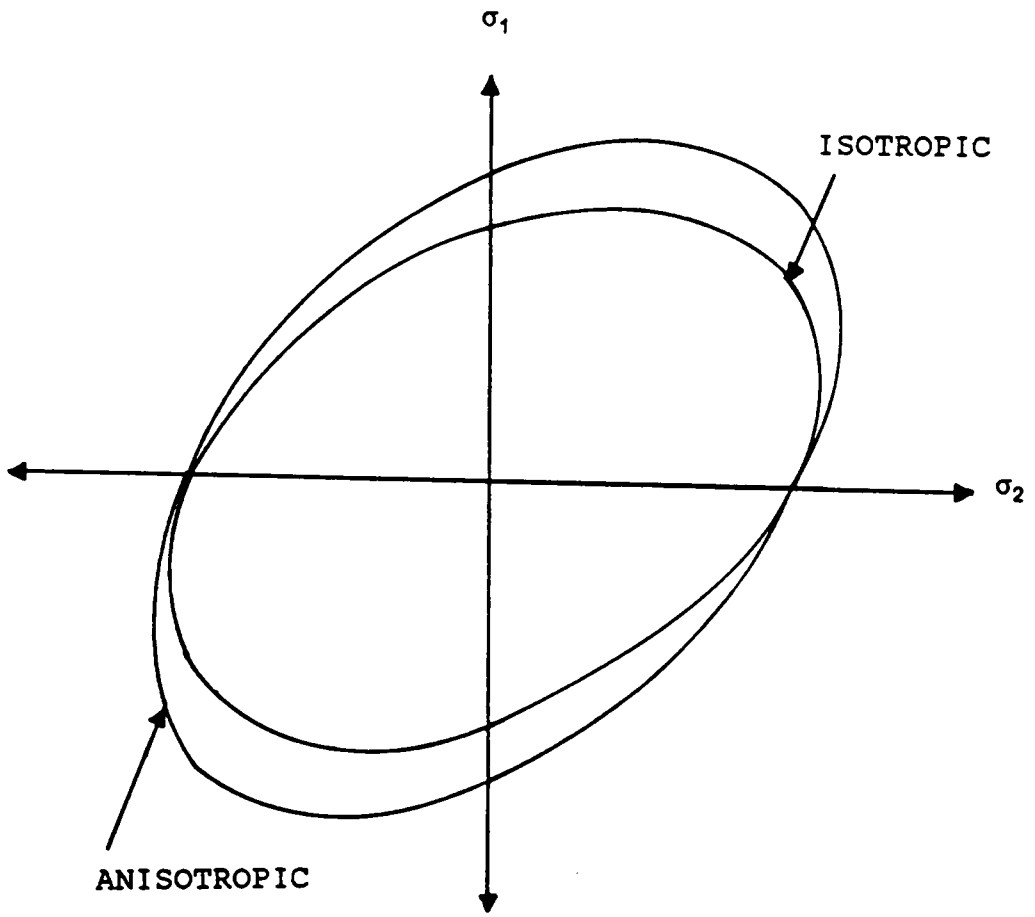

Figure 3.3 Isotropic-Hardening Model

$$F(\sigma,k) = \sigma^T \mathbf{M} \sigma - P^2(k) = \bar{\sigma}^2 - P^2(k) = 0 \tag{3.6}$$

where $\bar{\sigma}$ is called an equilvalent stress. This is a general quadratic form. **M** is the distortion matrix, P(k) is the size of the surface. For an orthotropic media **M** in the material principal planes is given as;

$$\mathbf{M} = \begin{vmatrix} M_{11} & M_{12} & M_{13} & 0 & 0 & 0 \\ M_{21} & M_{22} & M_{23} & 0 & 0 & 0 \\ M_{31} & M_{32} & M_{33} & 0 & 0 & 0 \\ 0 & 0 & 0 & M_{44} & 0 & 0 \\ 0 & 0 & 0 & 0 & M_{55} & 0 \\ 0 & 0 & 0 & 0 & 0 & M_{66} \end{vmatrix} \tag{3.7}$$

M has 9 independent constants. Where M_{11} ,M_{22} and M_{33} are related to the yield normal strengths in the 1, 2 and 3 directions and M_{44} ,M_{55} and M_{66} are related to the shear strengths. M_{12} ,M_{23} and M_{13} are the coupling terms. The pressure-independent condition is obtained by imposing the incompresibility condition;

$$\varepsilon_v^p = \lambda\left(\frac{\partial F}{\partial \sigma_1} + \frac{\partial F}{\partial \sigma_2} + \frac{\partial F}{\partial \sigma_3}\right) = 0 \tag{3.8}$$

Substitute equation (3.6) into equation (3.8). Solving for M_{12} ,M_{23} and M_{13} ;

$$\begin{aligned} M_{12} &= -.5(M_{11} + M_{22} - M_{33}) \\ M_{13} &= -.5(M_{11} + M_{22} - M_{22}) \\ M_{23} &= -.5(M_{22} + M_{33} - M_{11}) \end{aligned} \tag{3.9}$$

Hence, for a incompressible orthotropic media , only 6 independent constants are required.

In this formulation, it will be assumed that the coefficients of **M** is constant during deformation. Futher **M** is normalized by setting $M_{11} = 1.0$.

For a cross anisotropic media with the plane of isotropy in the 1-2 plane, only 3 independent constants M_{11}, M_{33} and M_{66} are required because;

$$M_{11} = M_{22}$$

$$M_{55} = M_{66} \tag{3.10}$$

For an isotropic media, only one constant is required. In this case **M** is given by;

$$\mathbf{M} = \begin{vmatrix} 1.0 & -.5 & -.5 & 0 & 0 & 0 \\ -.5 & 1.0 & -.5 & 0 & 0 & 0 \\ -.5 & -.5 & 1.0 & 0 & 0 & 0 \\ 0 & 0 & 0 & 3. & 0 & 0 \\ 0 & 0 & 0 & 0 & 3. & 0 \\ 0 & 0 & 0 & 0 & 0 & 3. \end{vmatrix} \tag{3.11}$$

Substituting equation 3.11 into equation 3.6, the resulting yield condition will reduce to the Von-Mises yield condition. It has been assumed in the model, that the coefficients of M are constant with deformation,i.e., the anisotropy does not change during deformation. A more general formulation could include the variation of M with plastic strains(distortional hardening). However this would result in a large number of additional parameters.

Derivation of Elastic-Plastic Matrix

As explained in Chapter 2, the total incremental strain is expressed as the sum of the elastic and plastic incremental strains;

$$d\varepsilon = d\varepsilon^e + d\varepsilon^p$$

$$d\varepsilon^e = \mathbf{D}^{-1} d\sigma \tag{3.12}$$

$$d\varepsilon^p = \lambda\left(\frac{\partial Q}{\partial \sigma}\right)$$

where λ is a constant to be determined. The other terms have been defined previously. Substituting the expressions for the elastic and plastic incremental strains into the equation for total incremental strain;

$$d\varepsilon = \mathbf{D}^{-1} d\sigma + \lambda\left(\frac{\partial Q}{\partial \sigma}\right) \tag{3.13}$$

As the stress point cannot penetrate the yield surface, the consistency condition requires;

$$dF = \left(\frac{\partial F}{\partial \sigma}\right)^T d\sigma - A\lambda = 0 \tag{3.14}$$

where $A = -\frac{\partial F}{\partial k}\frac{dk}{\lambda}$

Substitute equation 3.13 in equation 3.14;

$$d\sigma = \mathbf{D}^{ep} d\varepsilon \tag{3.15}$$

Where the elastic-plastic matrix is,

$$\mathbf{D}^{ep} = \mathbf{D} - \left(\mathbf{D}\left(\frac{\partial Q}{\partial \sigma}\right)^T \left(\frac{\partial F}{\partial \sigma}\right)\mathbf{D}\right)/\left(A + \left(\frac{\partial F}{\partial \sigma}\right)^T \mathbf{D}\left(\frac{\partial Q}{\partial \sigma}\right)\right) \tag{3.16}$$

Where A is proportional to the hardening modulus. In this model an associated flow rule will be used, i.e. F = Q.

To obtain a complete discription of the elastic-plastic process, A has to be evaluated. In the work-hardening model the scalar hardening parameter is chosen as the plastic work done during deformation. The work-hardening model has been commonly used for isotropic media. Zienkiewicz (70) developed a method to evaluate A for an isotropic media. Here a method is

presented to evaluate A for an initially anisotropic material. The incremental plastic work is given as;

$$dk = \sigma^T d\varepsilon^p = \bar{\sigma} d\bar{\varepsilon}^p \tag{3.17}$$

Where dk is incremental plastic work, $\bar{\sigma}$ is an equivalent stress defined in equation 3.6 and $d\bar{\varepsilon}^p$ an equivalent incremental strain given below;

$$d\bar{\varepsilon}^p = \frac{\sigma^T d\varepsilon^p}{\bar{\sigma}} \tag{3.18}$$

Substitute equations 3.17 and 3.12 in the expression for A.

$$A = -\frac{\partial F}{\partial k}\sigma^T \frac{\partial Q}{\partial \sigma} \tag{3.19}$$

Solving for $\frac{\partial F}{\partial k}$, by substituting equation 3.6 and 3.17;

$$\frac{\partial F}{\partial k} = -2P\frac{\partial P}{\partial k} = -2\frac{\partial \bar{\sigma}}{\partial \bar{\varepsilon}^p} \tag{3.20}$$

Substitute equation 3.20 into equation 3.19;

$$A = 2\frac{\partial \bar{\sigma}}{\partial \bar{\varepsilon}^p}\sigma^T \frac{\partial Q}{\partial \sigma} \tag{3.21}$$

Define $H = \frac{\partial \bar{\sigma}}{\partial \bar{\varepsilon}^p}$ as the plastic modulus, therefore;

$$A = 2H\sigma^T\left(\frac{\partial Q}{\partial \sigma}\right) \tag{3.22}$$

Derermination of Parameters

In this section, a method will be given to determine the components of the **M** matrix and H the hardening modulus from undrained triaxial tests. For a cross-anisotropic media, three elastic constants, three plastic constants, the hardening modulus and the strength at initial yield are required. The procedure to determine the elastic constants is given in section 3.2. The plastic constants are determined from the failure stresses in undrained triaxial tests. It has been assumed in this model that the anisotropy does not change during deformation, i.e. the anisotropy at initial yield is identical to the anisotropy at failure. Here the components of the M-matrix will be calculated from the failure stresses. The size of the yield surface at initial yield is calculated from the stresses at initial yield.

Consider a triaxial test in 1-direction (figure 3.4);

$$F(\sigma,k) = \sigma^T \mathbf{M} \sigma - P(k)^2 = M_{11} S_1^2 - P(k)^2 = 0 \tag{3.23}$$

Solving for P(k) as $M_{11} = 1.0$;

$$P = S_1 = \sigma_1 - \sigma_c \tag{3.24}$$

where S_1 is the failure strength in the 1-direction and σ_c is the confining pressure. The size of the yield surface at initial yield is determined by substituting the value of σ_1 at initial yield into equation 3.24. Consider a similar test in the 3-direction(figure 3.5);

$$F(\sigma,k) = \sigma^T \mathbf{M} \sigma - P(k)^2 = M_{33} S_3^2 - P(k)^2 = 0 \tag{3.25}$$

Solving for M_{33} ;

$$M_{33} = \frac{S_1^2}{S_3^2} \tag{3.26}$$

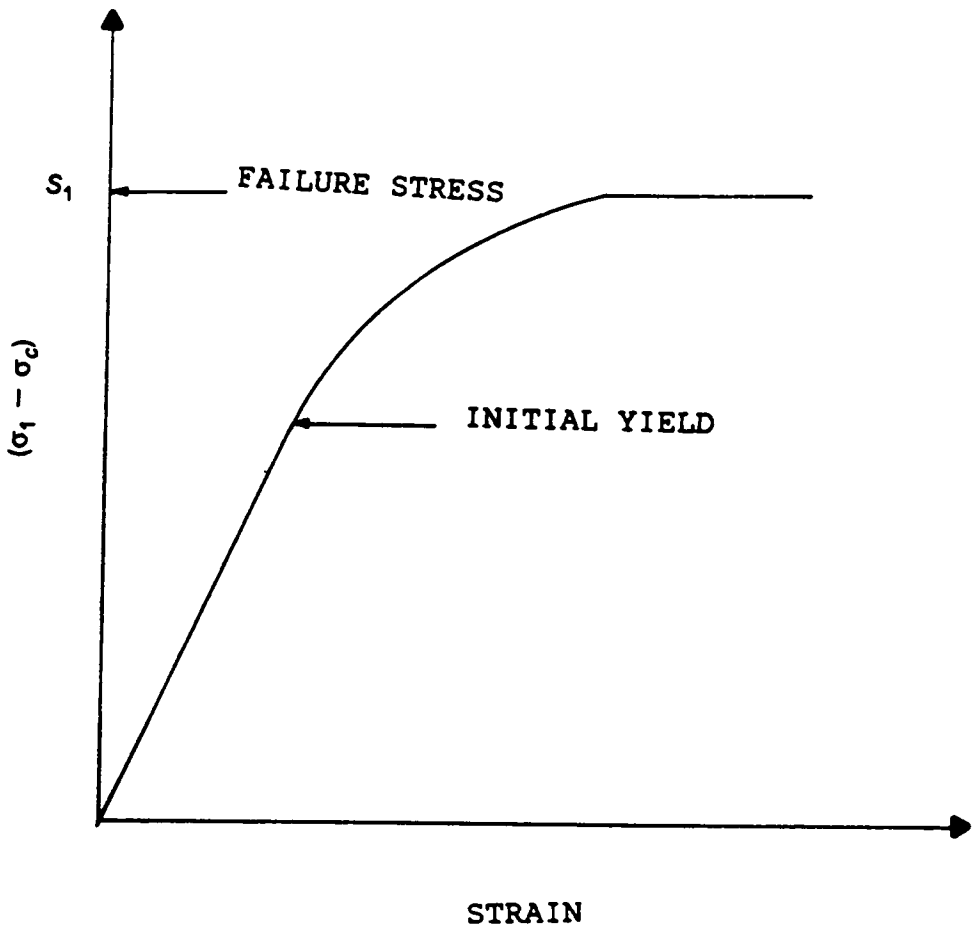

Figure 3.4 Triaxial Test-Horizontal Direction

where S_3 is the yield strength in the 3-direction. To determine M_{66}, a test on a sample inclined at an angle theta to the material principal planes is required. Let σ_a be the axial stress at failure and σ_c be the confining pressure in the triaxial test. Using the tranformation matrix in appendix-A, the stresses in the material principal planes can be determined. let these be σ_{ax}, σ_{cx} and τ. Substitute into equation 3.6;

$$F(\sigma,k) = \sigma^T \mathbf{M} \sigma - p^2(k) = M_{33}\sigma_{ax}^2 - M_{33}\sigma_{ax}\sigma_{cx} + \sigma_{cx}^2 + M_{66}\tau^2 - P^2(k) = 0 \tag{3.27}$$

Solving for M_{66};

$$M_{66} = \frac{(P^2 - M_{33}(\sigma_{ax}^2 - \sigma_{cx}\sigma_{ax}) + \sigma_{cx}^2)}{\tau^2} \tag{3.28}$$

The determination of H is described below. For a test in the 1-direction, $\bar{\sigma}$ reduces to S_1. Substituting in equation 3.18;

$$d\bar{\varepsilon}^p = \frac{\sigma^T d\varepsilon^p}{\bar{\sigma}} = d\varepsilon_1^p \tag{3.29}$$

Therefore;

$$H = \frac{dS_1}{d\varepsilon_1^p} \tag{3.30}$$

where H is the slope of the stress versus the plastic strain curve.

To get an expression for the hardening modulus, the stress strain curve can be approximated by the Ramberg-Osgood model (30,56)shown in figure 3.6;

$$\varepsilon = \frac{\sigma}{E} + K(\frac{\sigma}{E})^{\eta} \tag{3.31}$$

Where E is the initial modulus and K and η are curve fit constants determined from;

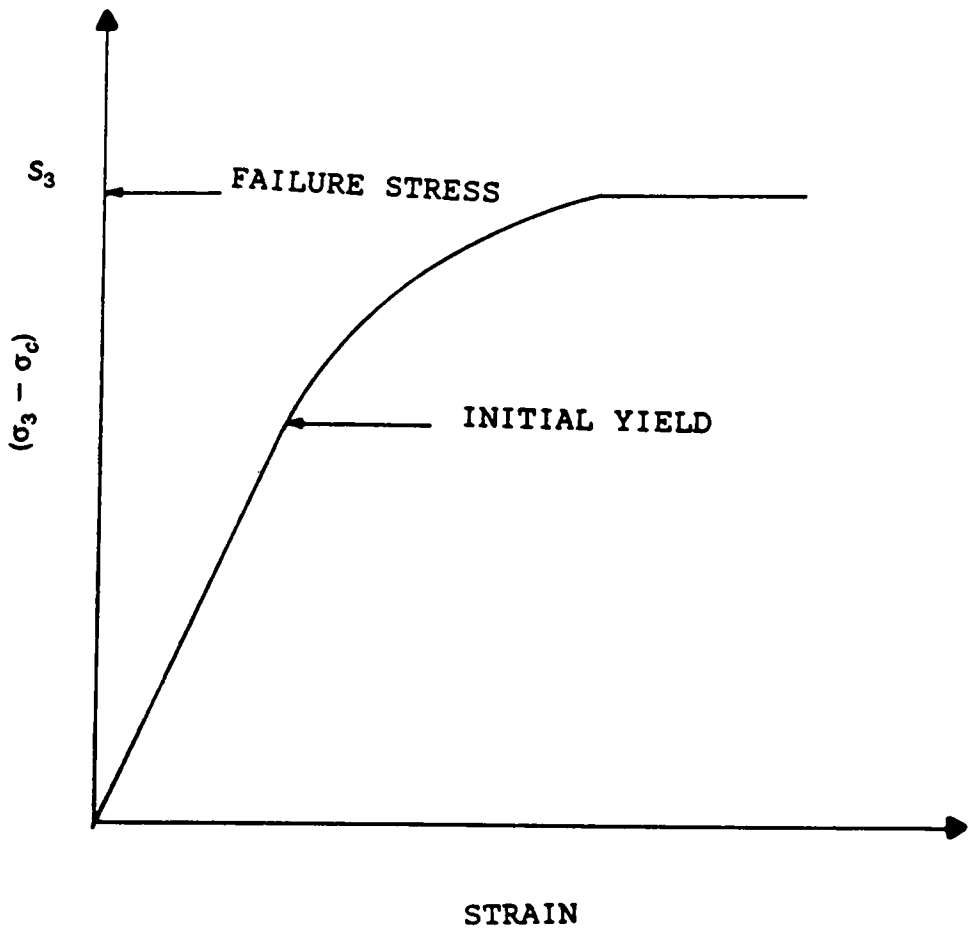

Figure 3.5 Triaxial Test-Vertical Direction

$$K = \frac{(1 - m_1)(\frac{E}{\sigma_1})^{\eta} - 1}{m_1} \tag{3.32}$$

$$\eta = 1 + \frac{\log(\frac{1 - m_1}{1 - m_2})}{\frac{m_2}{m_1}\log(\frac{\sigma_1}{\sigma_2})}$$

$$H = \frac{E}{\eta K(\frac{\sigma}{E})^{\eta} - 1}$$

where $m_i = \frac{E_i}{E}$ at $\sigma = \sigma_i$

For practical purposes the size of the yield surface and the moduli could be normalized by yhe mean effective pressure in the ground. Then the parameters could be determined at any mean effective pressure.

An elastic-plastic work hardening model for initally orthotropic pressure-independent materials was developed. An expression for the hardening modulus was derived and a procedure for determining experimentally the plastic parameters and the plastic modulus derived. The model described here can be used for the undrained analysis of anisotropic clays under monotonic loading conditions. This model has been implemented in a finite element program which will be described in Chapter 5.

Multisurface Model (MSM-PI)

The model described in the previous section cannot account for induced anisotropy. The anisotropy for the material remains unchanged during deformation. Further unloading is purely elastic. Real materials show both induced anisotropy and reverse plasticity. In this section a multisurface model is developed which can account for both types of behavior.

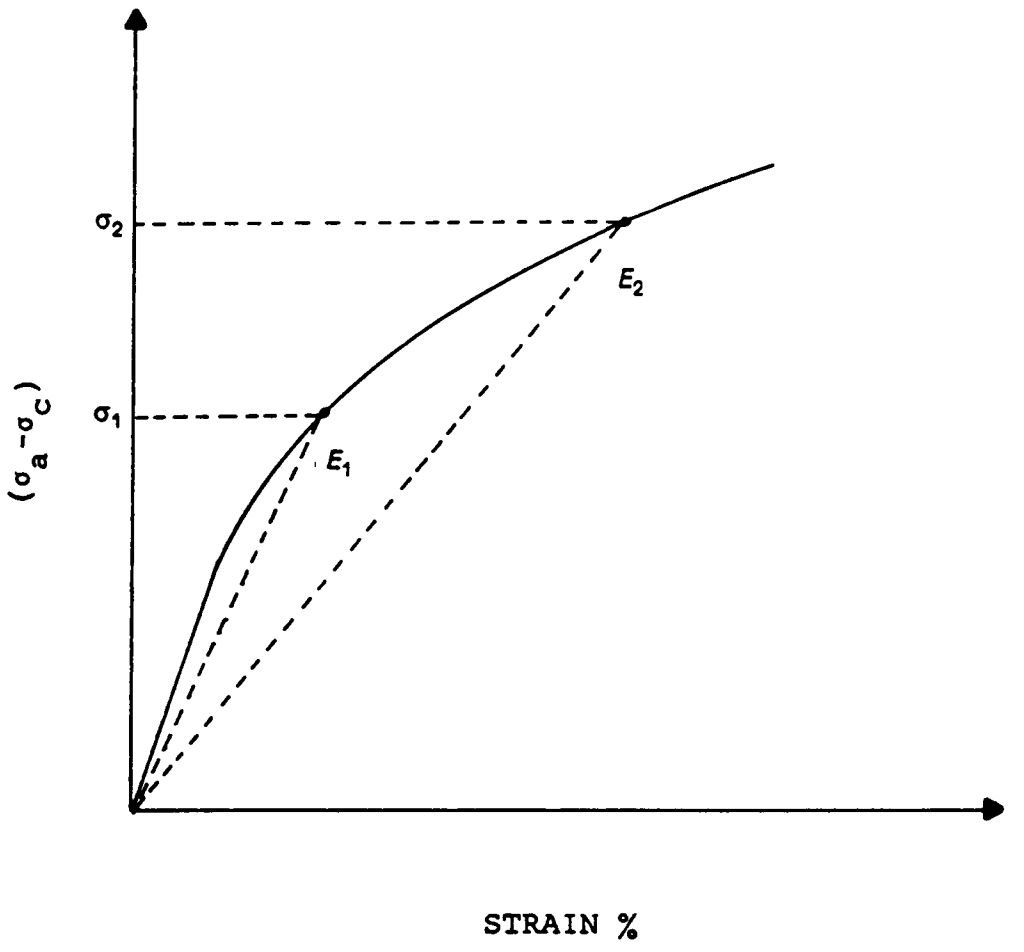

Figure 3.6 Derermination of Hardening Modulus

The first elastic-plastic model for an isotropic pressure-independent material with anisotropic-hardening was developed by Prager (72); subsequently several other models with anisotropic-hardening were proposed. The expression for some of the hardening rules is given in Chapter-2. Another approach to anisotropic-hardening was taken by Baltov and Sawczuk (6). The yield function was expanded as a tensor polynomial in terms of the plastic strains, the coefficients of which were determined experimentally. These models gave good results for simple loading conditions. To model material behavior under complex loading conditions, the multisurface models (43) and the bounding surface models (16,32) were developed.

However, most of the models were proposed for initially isotropic materials. Only a few models attempted to account for the initial anisotropy of the material. Edelman and Drucker (23) and Dafalias (17) proposed models for initially orthotropic materials, but did not implement these models. Here a multisurface model is developed for pressure-independent initially orthotropic materials.

The multisurface model was first proposed by Mroz (43). The stress space is assumed to contain a finite number of yield surfaces, each with a constant plastic moduli. As the stress point moves from its initial state it engages the first yield surface. The surface translates in stress space with the stress point. A translation rule is prescribed such that no surface intersects another. The surfaces engaged by the stress point translate together without intersection, the plastic modulus used is that of the current surface. A surface not engaged does not influence deformation (figure 3.7).

During unloading, the stress point detaches itself from the current surface. Till the stress point again engages the first surface the response is elastic. Once the first surface is engaged, plastic deformation occurs. Hence the model exhibits reverse plasticity and induced anisotropy (figure 3.7). This model has been applied to metals (43) and to the undrained behavior of clays (52,53). The model described in this section is an extension of the isotropic-hardening model developed in the previous section, to account for anisotropic-hardening.

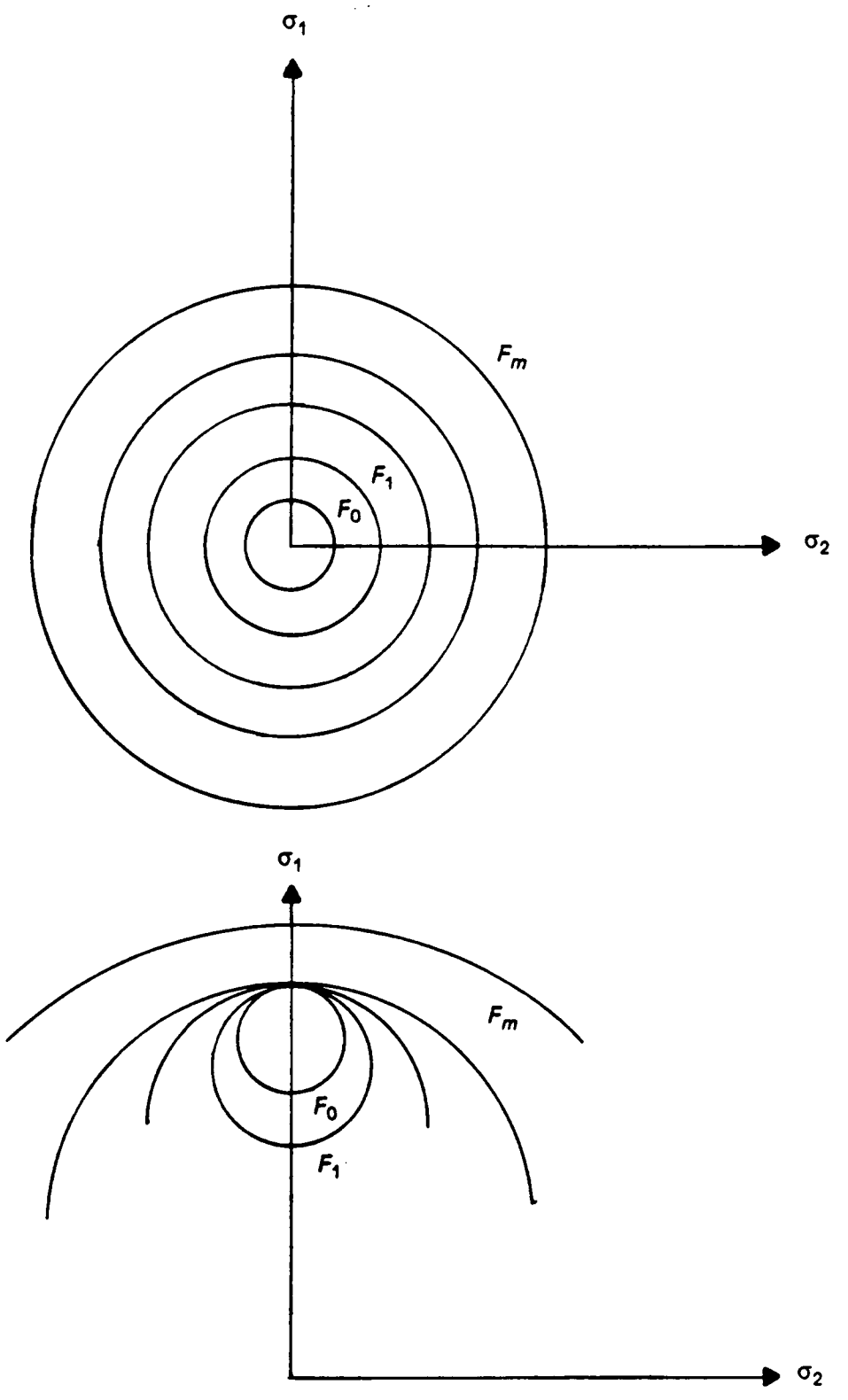

Figure 3.7 Multisurface Model

This model can account for initial orthotropy, induced anisotropy, and reverse plasticity. The two-surface model will be discussed in detail in the next Chapter.

Derivation of Elastic-Plastic Matrix

The yield function chosen for the yield surfaces is of the form;

$$F^m = (\sigma^m - \alpha^m)^T \mathbf{M} (\sigma^m - \alpha^m) - (P^m)^2 = 0 \tag{3.33}$$

where m is the surface number. **M** is the distortion matrix(pressure independence condition imposed), which is the same for all surfaces and is to be constant during deformation. The distortion matrix is described in the previous section. α is the translation vector which locates the surface in stress space. P is the size of the yield surfaces and is assumed constant during deformation.

The Mroz translation rule is assumed (43),

$$d\alpha = d\mu(\sigma^{m+1} - \sigma^m) \tag{3.34}$$

where $d\alpha$ is the incremental translation vector and $d\mu$ is a constant to be determined from the consistency condition. σ^m and σ^{m+1} are the stresses on the m surface and the projected stresses on the m+1 surface at the congugate point (figure 3.8). Where σ^{m+1} is determined from,

$$\frac{(\sigma^m - \alpha^m)}{P^m} = \frac{(\sigma^{m+1} - \alpha^{m+1})}{P^{m+1}} \tag{3.35}$$

Solving for σ^{m+1} an expression for the incremental translation vector can be obtained (43).

$$d\alpha = d\mu((P^{m+1} - P^m)\sigma^m - (\alpha^m P^{m+1} - \alpha^{m+1} P^m)) \tag{3.36}$$

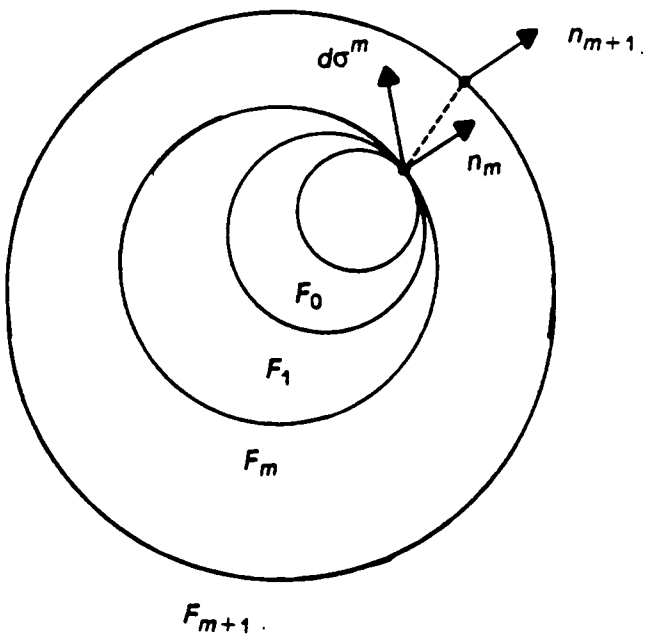

Figure 3.8 Translation Rule

The constant $d\mu$ is obtained from the consistency condition, i.e., the stress point remain on the yield surface.

$$\frac{\partial F}{\partial \sigma}(d\sigma - d\alpha) = 0 \tag{3.37}$$

The elastic-plastic constitutive can be written as;

$$d\sigma = \mathbf{D}^{ep} d\varepsilon \tag{3.38}$$

Where $\mathbf{D}^{ep}$ is given as;

$$\mathbf{D}^{ep} = \mathbf{D} - \frac{(\mathbf{D}\mathbf{n}^T\mathbf{n}\mathbf{D})}{(K + \mathbf{n}^T\mathbf{D}\mathbf{n})} \tag{3.39}$$

where $\mathbf{D}^{ep}$ is the elastic-plastic matrix and K is the plastic modulus and **n** are the normalized gradients given in equation 2.5.

Determination of Parameters

A method is given to determine the parameters required for the multi-surface model for a cross-anisotropic material, from undrained triaxial tests. For a cross-anisotropic material, three elastic constants, three yield strengths and the plastic modulus and size of each surface are required. The elastic constants are determined as before (section 3.2). The plastic constants are calculated from the failure stresses.

For a cross-anisotropic material with the 1-2 plane as the plane of isotropy, when the initial values of α are zero, a test in the 1-direction;

$$F(\sigma, \alpha) = M_{11}S_1^2 - P(k)^2 = 0 \tag{3.40}$$

Solving for P(k) as $M_{11} = 1.$,

$$P = S_1 = (\sigma_1 - \sigma_c) \tag{3.41}$$

S_1 is the yield stress and where σ_c is the confining pressure. From a similar test in the 3-direction,

$$M_{33} = \frac{S_1^2}{S_3^2} \tag{3.42}$$

where S_1 and S_3 are the yield stresses in the 1 and 3 directions respectively. M_{66} can be calculated from a test on an inclined specimen (section 3.3).

To calculate the plastic modulus and the sizes of each surface, linearize the stress strain curve into several linear segments, each linear segment representing a surface in stress space and having a constant plastic modulus. The plastic modulus is determined from the flow rule (equation 2.5). Linearizing the stress-strain curve in the 1-direction, the plastic modulus of each surface (linear segment) can be calculated;

$$K = \frac{2}{3}\left(\frac{dS_1}{d\varepsilon_1^p}\right) \tag{3.43}$$

The size of each surface can be calculated from the stress-strain curve in the 1-direction, as $P^m = S_1$ (Figure 3.9).

Again the sizes of the yield surfaces and the moduli can be normalized by the mean effective pressure in the ground. To summarise, in the above section an elastic-plastic multi-surface model has been described. The elastic-plastic matrix and the translation rule have been derived. The model developed here can model both initial and induced anisotropy of clays under undrained conditions.

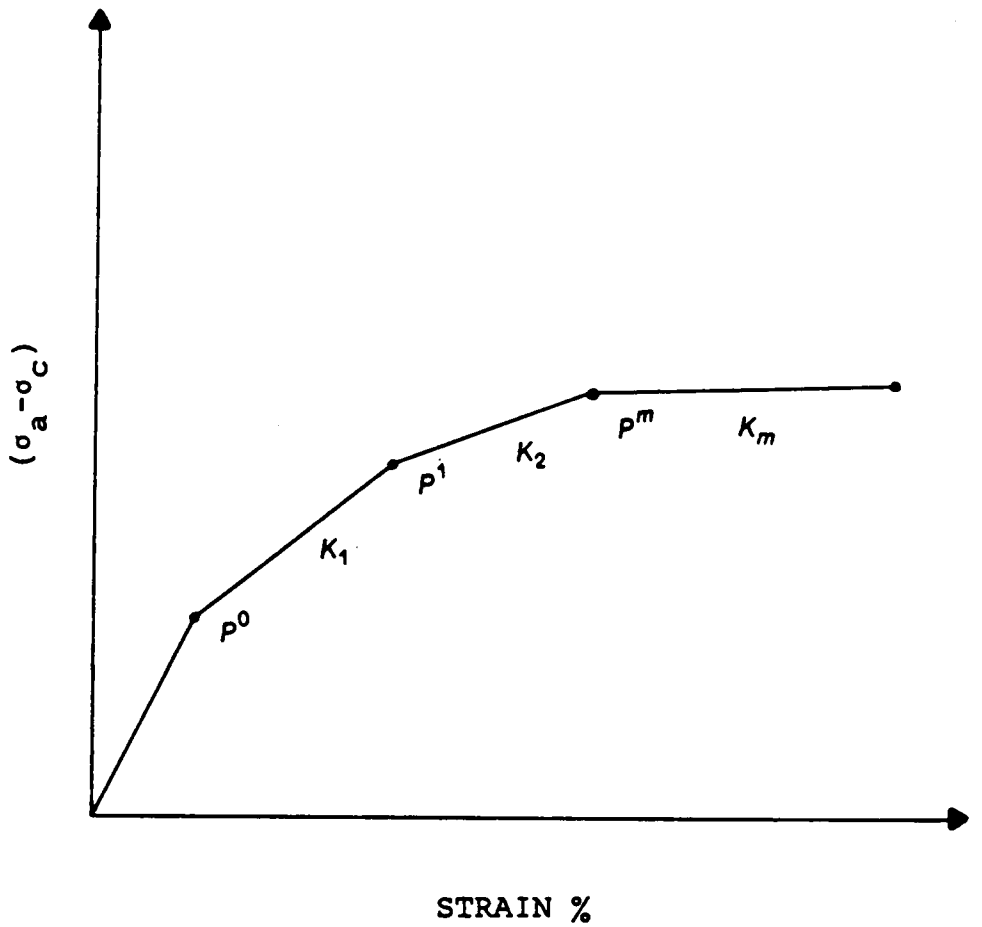

Figure 3.9 Determination of Plastic Modulus

General Response and Comparison

In this section the general response of the models described in the previous sections will be investigated. Also some comparisons will be made with experimental data. The models have been implementated in a finite element program. In this section one element is used to simulate test conditions. The purpose is to study the model response and to validate the finite element program.

To study the response of inclined specimens, the stiffness matrix is transformed from the material principal plane to the global refrence system using the transformation matrix described in the appendix A. The angle of inclination of the specimen is used to determine the components of the transformation matrix.

(1) Strength Variation

Figure 3.10 shows the variation in strength for a cross-anisotropic sample, calculated using the failure criteria given in equation 3.4. For a cross-anisotropic material, three strengths are required. These are the strength in the vertical direction (S_{u0}), the strength in the horizontal direction (S_{u90}) and a strength in an intermediate direction (S_{u45}). The following values have been assumed,

S_{u0} = 10.0 psi

S_{u90} = 2.5 psi

S_{u45} = 5.5 psi

Using the above values the components of the **M** matrix can be calculated, using the procedure described in section 3.3.

M_{11} = 1.0

M_{33} = .0625

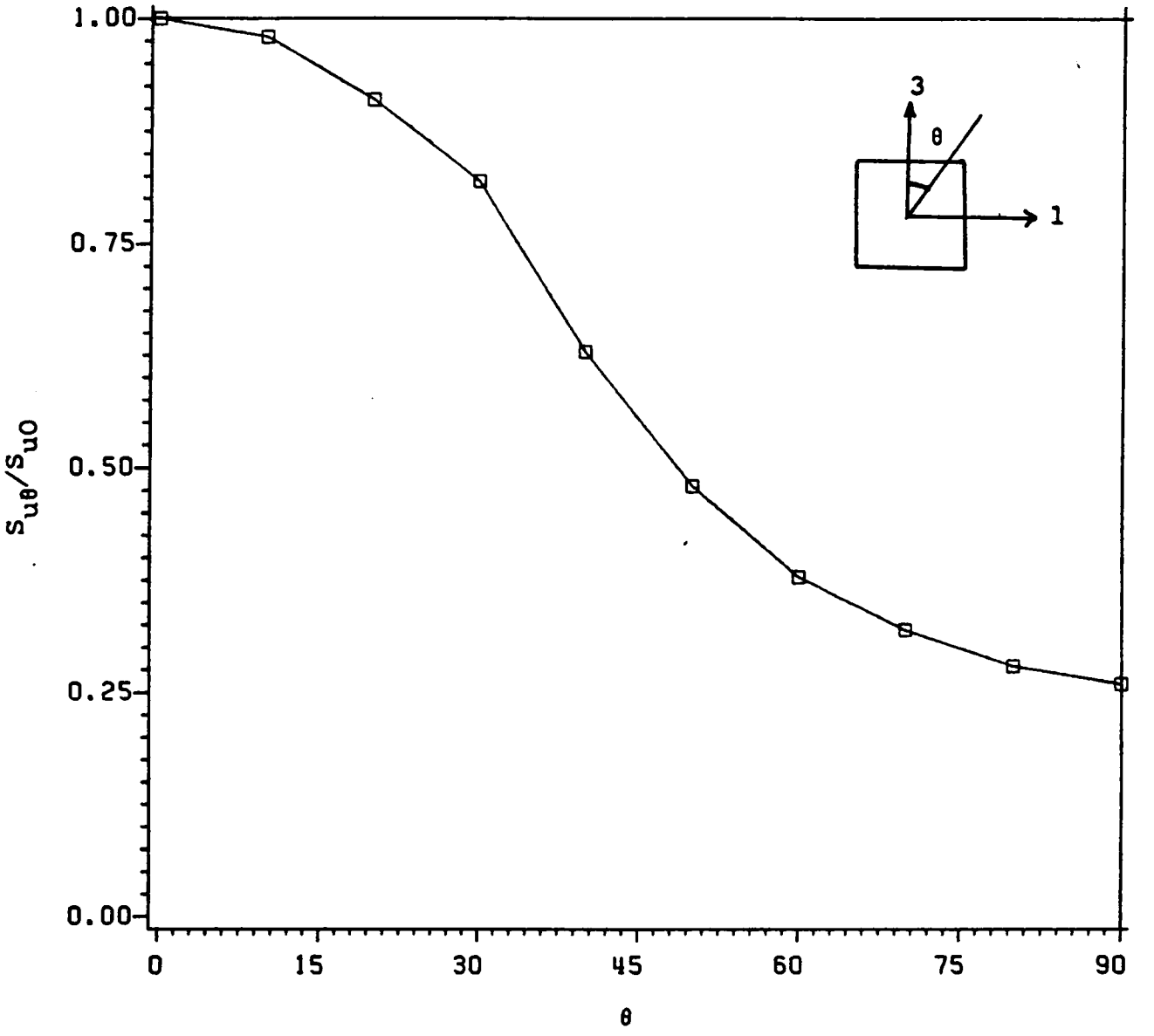

Figure 3.10: Undrained Anisotropic Strength Variation

$M_{66} = 1.85$

The variation in strength can then be calculated by using the transformation given in appendix A.

The variation in strength predicted above, is commonly observed in undrained clays (12). The failure criteria used can model any quadratic variation in strength.

(2) Stress strain response of isotropic-hardening model

In this section the response of the isotropic-hardening model is studied. For the isotropic hardening model the following parameters are required.

(a) Elastic moduli and Poissons ratios (calculated from the incompressibility condition): For a cross-anisotropic material, with the 1-2 plane as the plane of isotropy, three elastic parameters E_1, E_3 and G_{13} are required.

(b) Yield strengths (components of the M-matrix): For the cross-anisotropic material, three yield strengths P, M_{33} and M_{66} and the initial size of the yield surface are required.

(c) Ramberg-Osgood parameters K and η (determined from a stress strain curve, equation 3.32)

To study the response of the model, the stress strain data of anisotropic Kalonite clay from Mitchel (41) is used (see Figure 3.11). In Figure 3.11 σ_a is the axial stress, σ_c is the confining pressure and θ is the angle of inclination from the horizontal direction. Mitchel (41) conducted undrained triaxial tests on anisotropic Kalonite clay, in both the horizontal ($\theta = 0.$) and vertical ($\theta = 90.$) directions. The horizontal direction will also be reffered as the 1-direction, and the vertical direction will be reffered as the 3-direction. A triaxial test in the horizontal (1-direction, $\theta = 0.$) direction is a test in which the axial stress is applied in the 1-direction

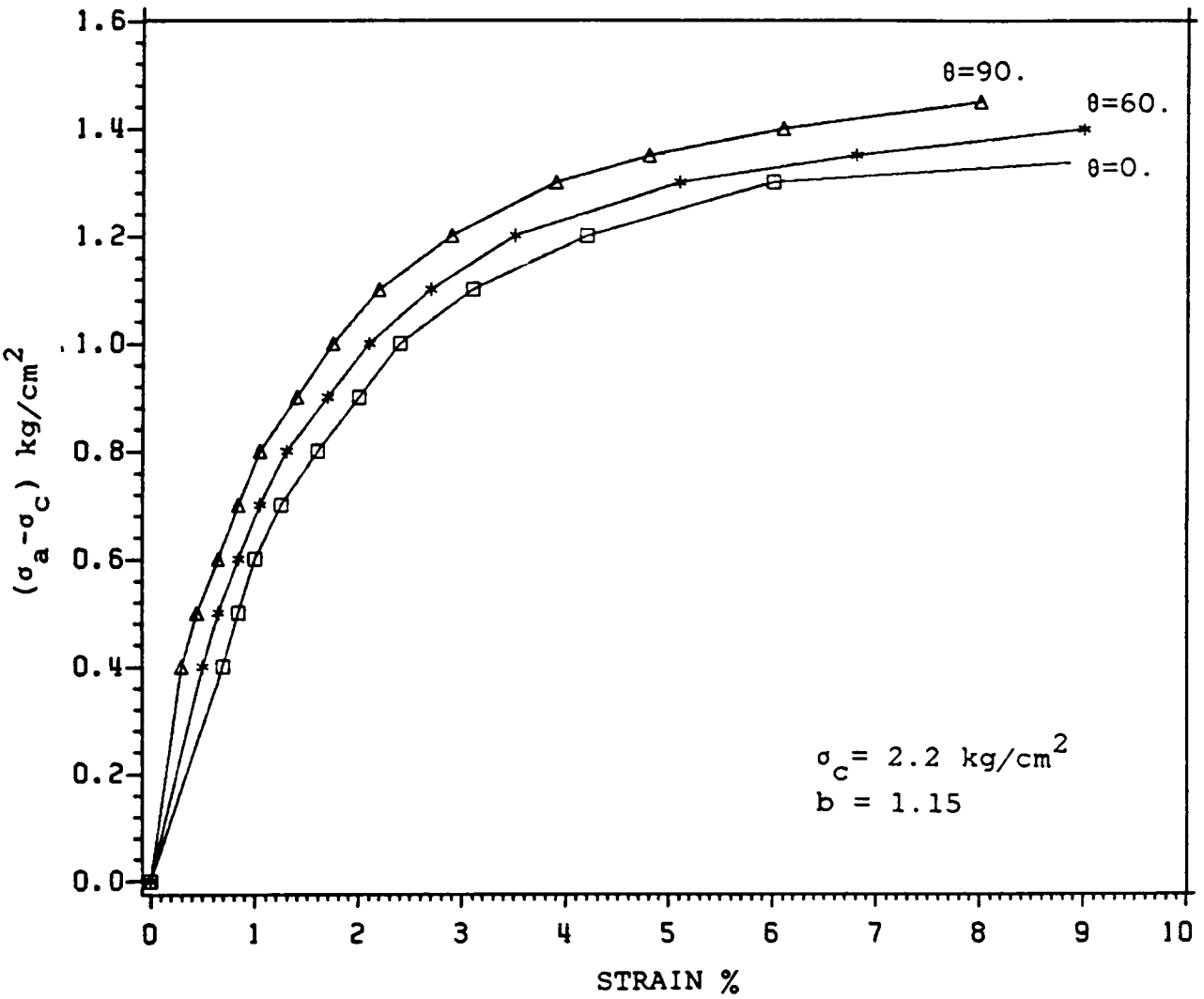

Figure 3.11: Undrained Response of Kaolinite Clay

and the confining pressure is applied in the other two directions. This data is sufficient to model the response in the material principal planes. To study the response of inclined specimens, the shear modulus G_{13} and M_{66} are to be determined. In this analysis, a stress-strain curve for a specimen inclined at an angle of 60. degrees to the horizontal plane is assumed, and the parameters required for the model are calculated from these three curves (figure 3.11).

The elastic moduli are calculated from the stress-strain curves in the horizontal and vertical directions. The out of plane shear moduli is calculated from the stress-strain curve of the inclined specimen (section 3.2). The plastic constants are calculated from the failure stresses in the horizontal, vertical and inclined specimens (section 3.3). The Ramberg-Osgood parameters are determined from the stress strain curve in the horizontal direction. These are then used to study the response of specimens inclined at various angles to the horizontal plane. The parameters used in the analysis are given below.

E_1 = 67.0 kg/cm^2

E_3 = 78.0 kg/cm^2

G_{13} = 26.5 kg/ cm^2

P = .40 kg/ cm^2 (initial size)

M_{33} = .75

M_{66} = 2.25

K = 940.

η = 2.46

Figure 3.12 shows the experimental (and assumed) and the predicted stress-strain response in the triaxial test as the cross-anisotropic sample is rotated with respect to the principal material directions. It is observed that as the angle of inclination of the specimen increases, the stress-strain curves exhibit both a stiffer elastic response and a higher failure strength. The response is typical of undrained samples of clays (1,41). Note the strains are in percent.

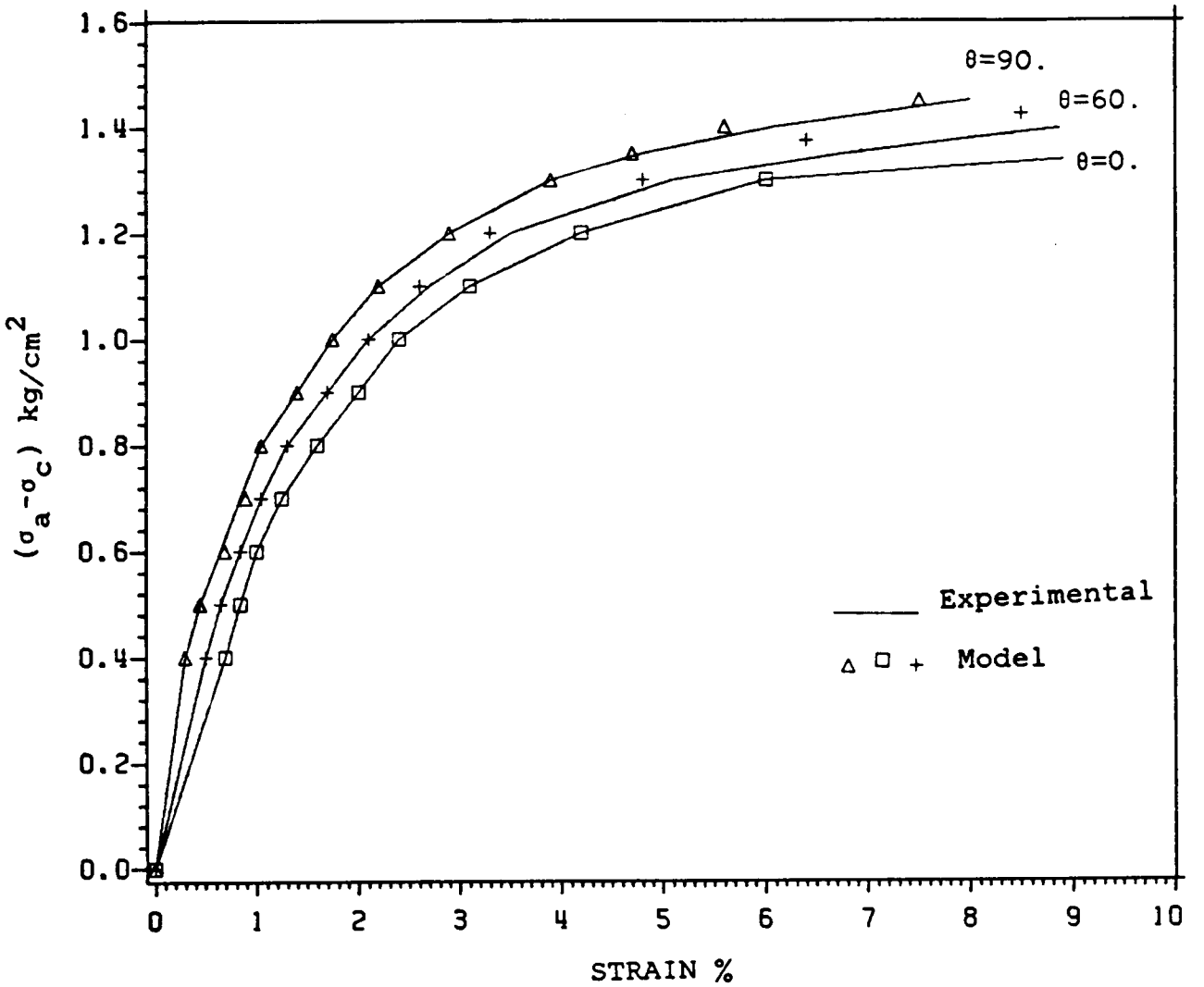

Figure 3.12: Predicted Response of Kaolinite Clay

In the next example the response of the model is investigated for increasing values of anisotropy. To study the influence of anisotropy, a parameter b is defined as the ratio of the strength in the vertical direction to the strength in the horizontal direction. A value of b=1. implies an isotropic clay and increasing values of b imply increasing anisotropy of the clay. To study the influence of strength anisotropy only, the elastic response of the soil is assumed to be elastic. The parameters used in the analysis are;

$E = 67.0$ kg/ cm^2

$K = 940.$

$\eta = 2.46$

$P = .40$ kg/ cm^2 (initial)

$M_{33} = \frac{1}{b^2}$

As the response of the clay is investigated only in the material principal planes, the shear terms are not needed. Figure 3.13 shows the influence of anisotropy on the stress-strain response of undrained clays. Four cases are analyzed, b=1.0, b=1.15, b=1.42 and b=2.0. The value b=1.0 implies an isotropic clay. By increasing the values of b, the influence of strength anisotropy on the stress-strain response can be analyzed. A stiffer response and higher strength is observed as the ratio increases.

(3) Multisurface Model Response

To study the response of the multisurface model the stress strain data of anisotropic London clay by Atkinson (1) is used. The following parameters are used in the analysis.

$E_1 = 3500.$ psi

$E_3 = 4200.$ psi

$M_{33} = .64$

Where 1 is the horizontal direction and 3 is the vertical direction. As the stress strain response is required only in the material principal planes, the shear terms are not required. The multisurface model also requires a stress strain curve which is linearized into several

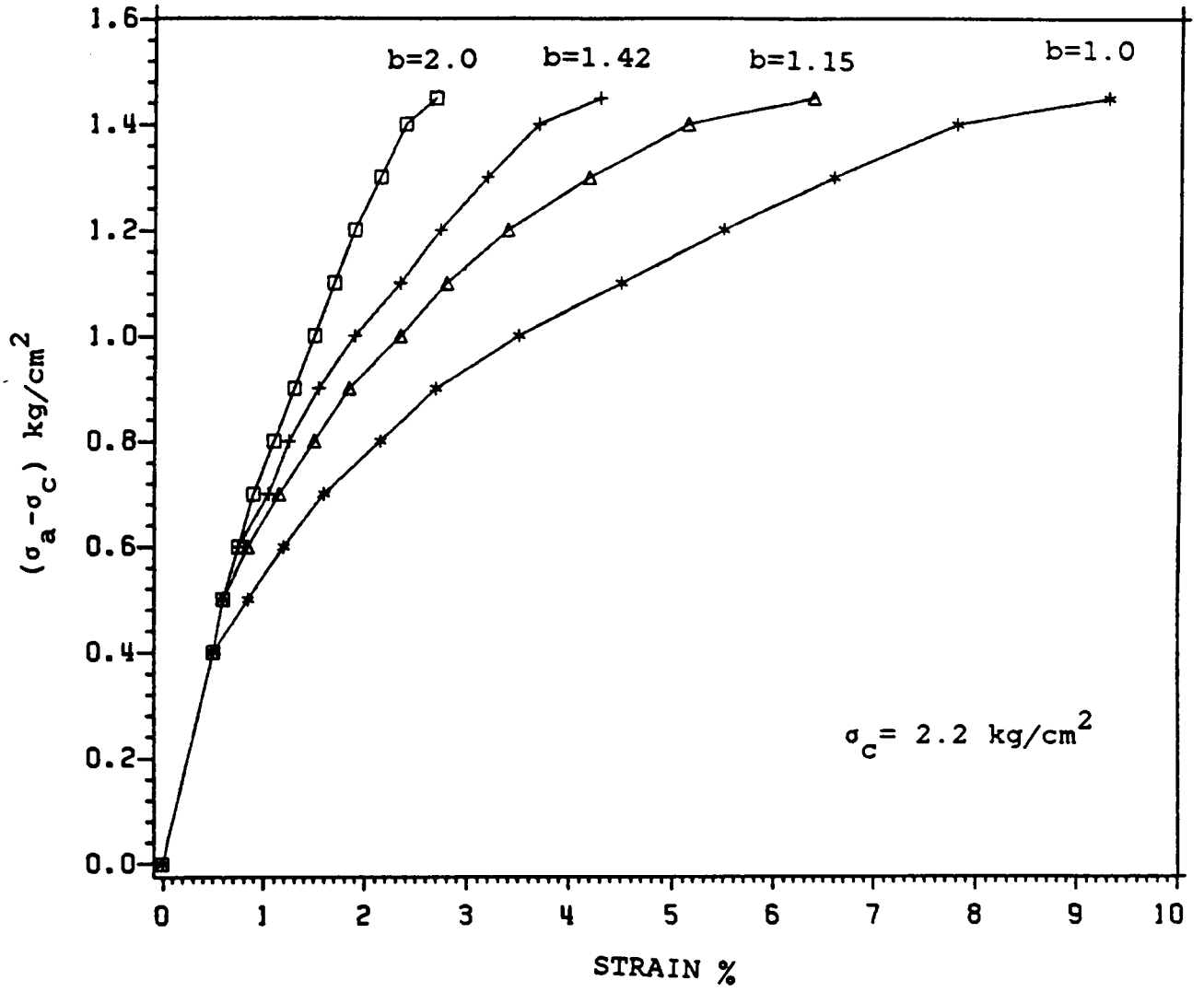

Figure 3.13: Influence of anisotropy on undrained response

linear segments (each linear segment representing a surface). The plastic modulus and size of each surface is calculated from equation 3.43 (see section 3.4). In this case the stress strain curve in the horizontal direction is linearized. It is linearized into five segments (5-surfaces). The surface parameters are given in table 3.1.

In figure 3.14, the response of the multisurface model is investigated under a single cycle of loading. The figure shows the stress strain response in both the horizontal and vertical directions. The model can predict reverse plasticity and the hysteris loop.

(4) Comparison with Experimental Data

In this section, some comparison with experimental data is made for both isotropic and anisotropic media. Both the isotropic-hardening model and the multisurface model will be used in the following analysis. As the response is required only in the material principal planes, M_{66} and G_{13} are not required. As before σ_a is the axial stress and σ_c is the confining pressure. Direction-1 refers to the horizontal direction as well as to $\theta = 0.$ and direction-3 refers to the vertical direction and to $\theta = 90.$ degrees.

Figure 3.15a shows the stress strain response of Kalonite clay (5) under undrained triaxial conditions consolidated under a confining pressure of 58.0 psi. The model parameters were calculated from figure 3.15a for both the isotropic-hardening model (Ramberg-Osgood parameters) and the multisurface model (5 surfaces). The parameters used are given below and in table 3.2.

Isotropic Hardening Model-Parameters

$E = 6500.$ psi

$K = 362000000.$ psi

$\eta = 4.45$

$P = 15.$ psi (initial)

These parameters are used to recalculate the stress strain response of the clay at a confining pressure of 58. psi and also the response at a confining pressure of 40. psi (figure 3.15b) Excellent agreement was observed in both cases.

Table 3.1 Properties for multisurface model-London clay

N	size(p) psi	modulus(k) psi
1	10.00	10000.
2	20.00	2215.
3	30.00	760.0
4	37.00	90.00
5	39.00	10.00

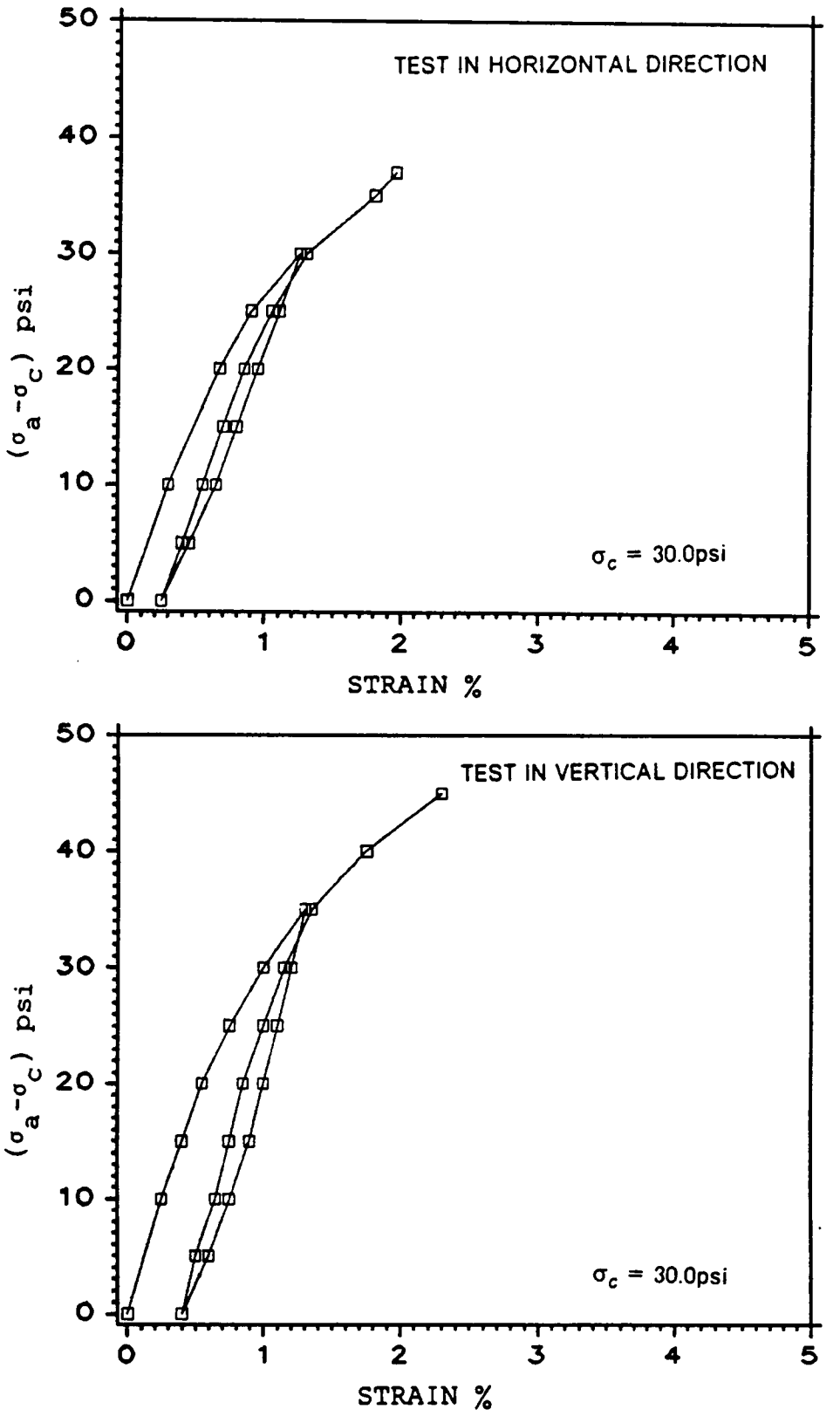

Figure 3.14: Response of Multisurface Model

Table 3.2 Properties for multisurface model-Isotropic Kaolinite

N	size(p) psi	modulus(k) psi
1	15.00	20000.
2	25.00	8930.00
3	35.00	2033.00
4	45.00	854.0
5	55.00	00.00

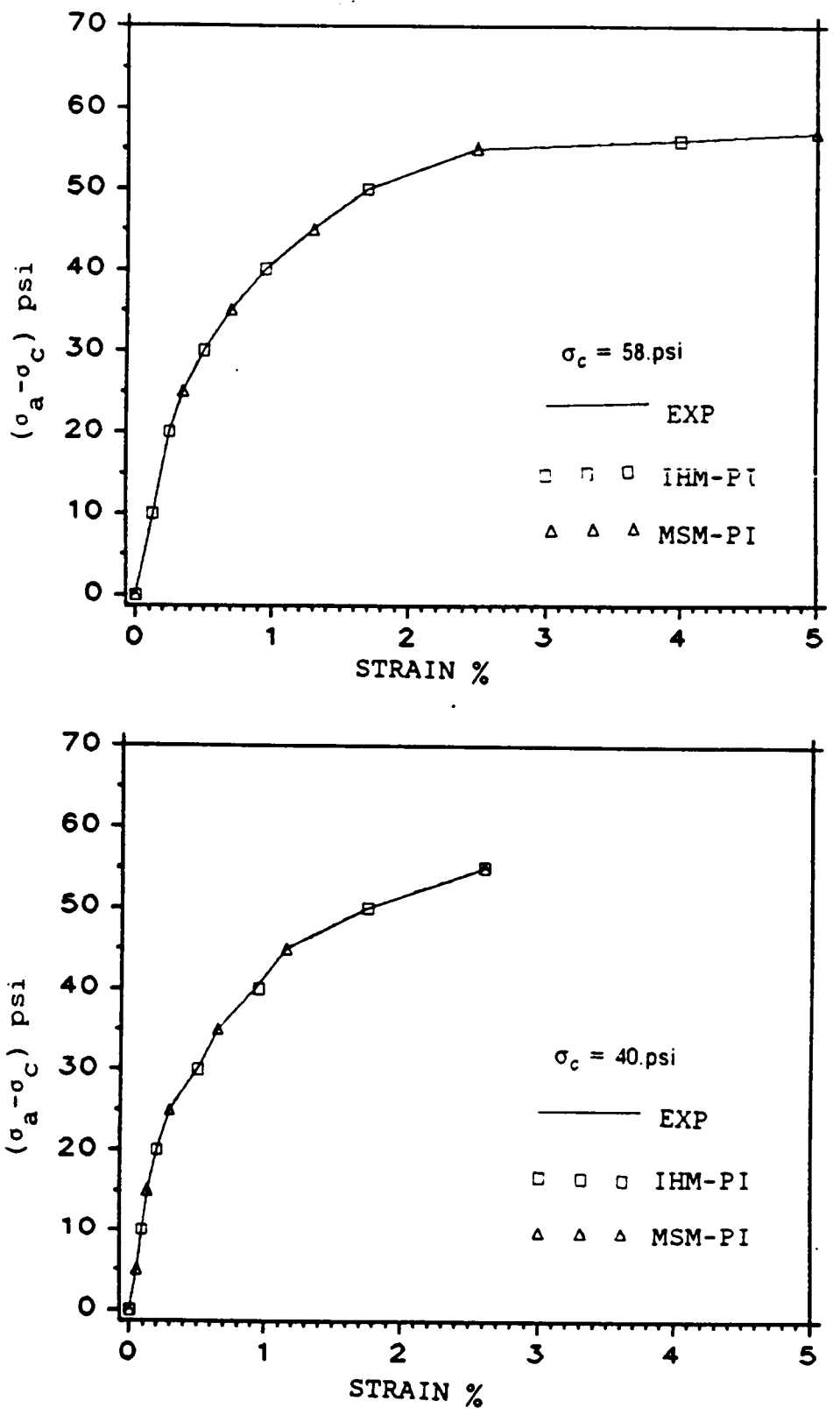

Figure 3.15: Comparison of model prediction with experimental data-Isotropic Kaolinite clay

Figure 3.16a shows the stress strain response of San Francisco bay mud(11) sheared under undrained triaxial conditions. The model parameters for both the isotropic-hardening model and the multisurface model were calculated from the stress-strain curve of figure 3.16a. Then these were used to predict the stress strain response of the same clay which was anisotropically consolidated with a horizontal confining pressure of 2.08 kg/ cm^2 and a vertical confining pressure of 3.18 kg/ cm^2 (figure 3.16b). The parameters used in the analysis are given below and in table 3.3;

Isotropic-Hardening Model-Parameters

E = 145. Kg/ cm^2

K = 1920000.

η =3.58

P = .7 kg/cm^2 (initial)

Both the isotropic-hardening model and the multisurface model predictions compare well with the experimental data.

Figure 3.17 illustrates the stress strain response of anisotropic kaolinite clay (41), specimens of which were sheared both in the horizontal and vertical directions under undrained triaxial conditions. Figure 3.17a compares the stress strain response with the results of the isotropic-hardening model. The model parameters were calculated from the horizontal curve and were used to predict the stress strain response in both the horizontal and vertical directions. Figure 3.17b also compares the experimental data with the results of the multisurface model. Again the model parameters were calculated from the horizontal curve (5 surfaces were used in the analysis). The parameters used in the analysis are given below and in table 3.4;

Isotropic Hardening Model-Parameters

E_1 = 67.0 kg/cm^2

E_3 = 78.0 kg/cm^2

K = 940.

η = 2.46

Table 3.3 Properties for multisurface model-Bay mud

N	size(p) kg/cm^2	modulus(k) kg/cm^2
1	.7000	214.00
2	1.000	48.00
3	1.250	17.10
4	1.500	9.600
5	1.650	00.00

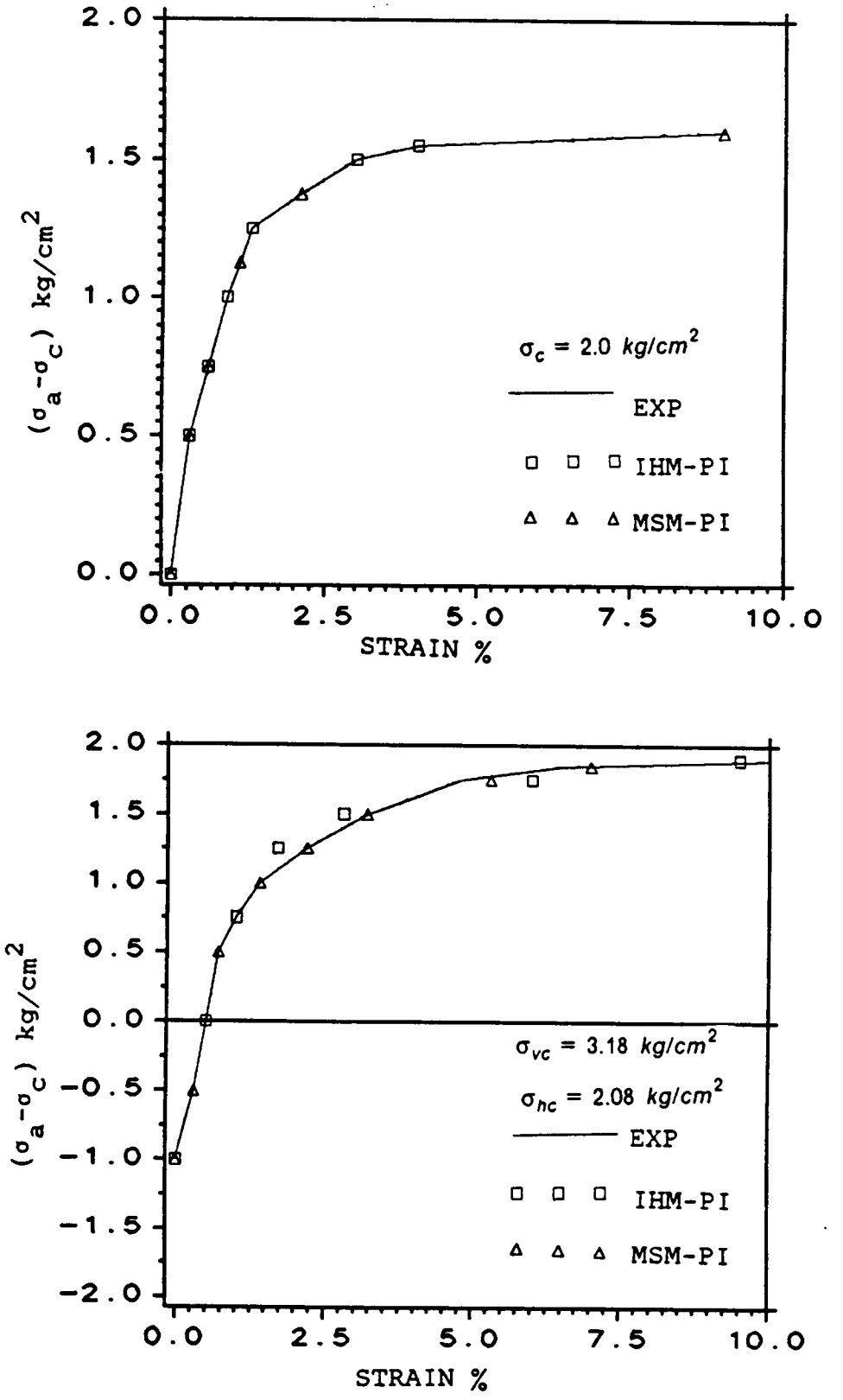

Figure 3.16: Comparison of model prediction with experimental data-Bay mud

M_{33} = .75

P = .40 kg/cm^2 (initial)

Good agreement is observed in both cases.

Figure 3.18 compares the stress strain response of anisotropic clay (1) with the results of both the isotropic-hardening model and the multisurface model. Figure 3.18a compares the experimental stress strain response of anisotropic London clay in both the horizontal and vertical directions with the results of the isotropic-hardening model. Again the parameters for the models were calculated from the stress-strain curve in the horizontal direction. These parameters were used in the models to predict the stress-strain response in both the vertical and horizontal directions. Figure 3.18b compares the experimental results with the predictions of the multisurface model. The plastic modulus was calculated from the horizontal curve, using five linear segments. The parameters used in the analysis are given below and in table 3.5;

Isotropic Hardening Model-Parameters

E_1 = 3500. psi

E_3 = 4200. psi

K = 3000000. psi

η = 4.69

P = 10.0 psi (initial)

Good agreement is observed in both cases.

The models could be used to predict the response of the specimens in any inclined directions, however limited data was available. The comparisons made in this section prove the capability of the models to predict the stress strain behavior of anisotropic undrained clays.

Table 3.4 Properties for multisurface model-Anisotropic Kaolinite

N	size(p) kg/cm^2	modulus(k) kg/cm^2
1	.4000	200.00
2	.6000	65.5
3	1.000	14.00
4	1.200	6.200
5	1.350	0.000

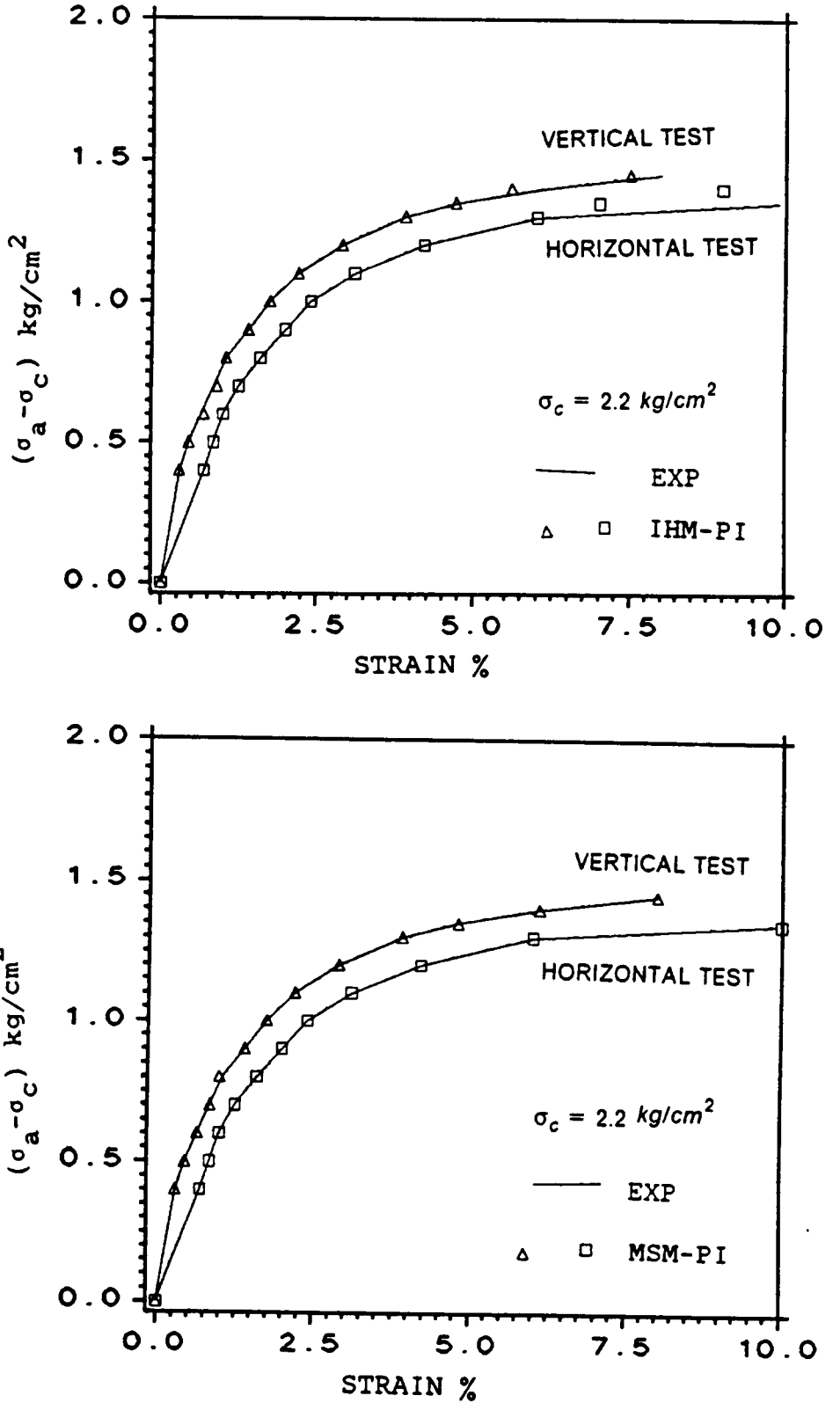

Figure 3.17: Comparison of model prediction with experimental data-Anisotropic Kaolinite clay

Table 3.5 Properties for multisurface model-Anisotropic London clay

N	size(p) psi	modulus(k) psi
1	10.00	10000.
2	20.00	2215.
3	30.00	760.0
4	37.00	90.00
5	39.00	10.00

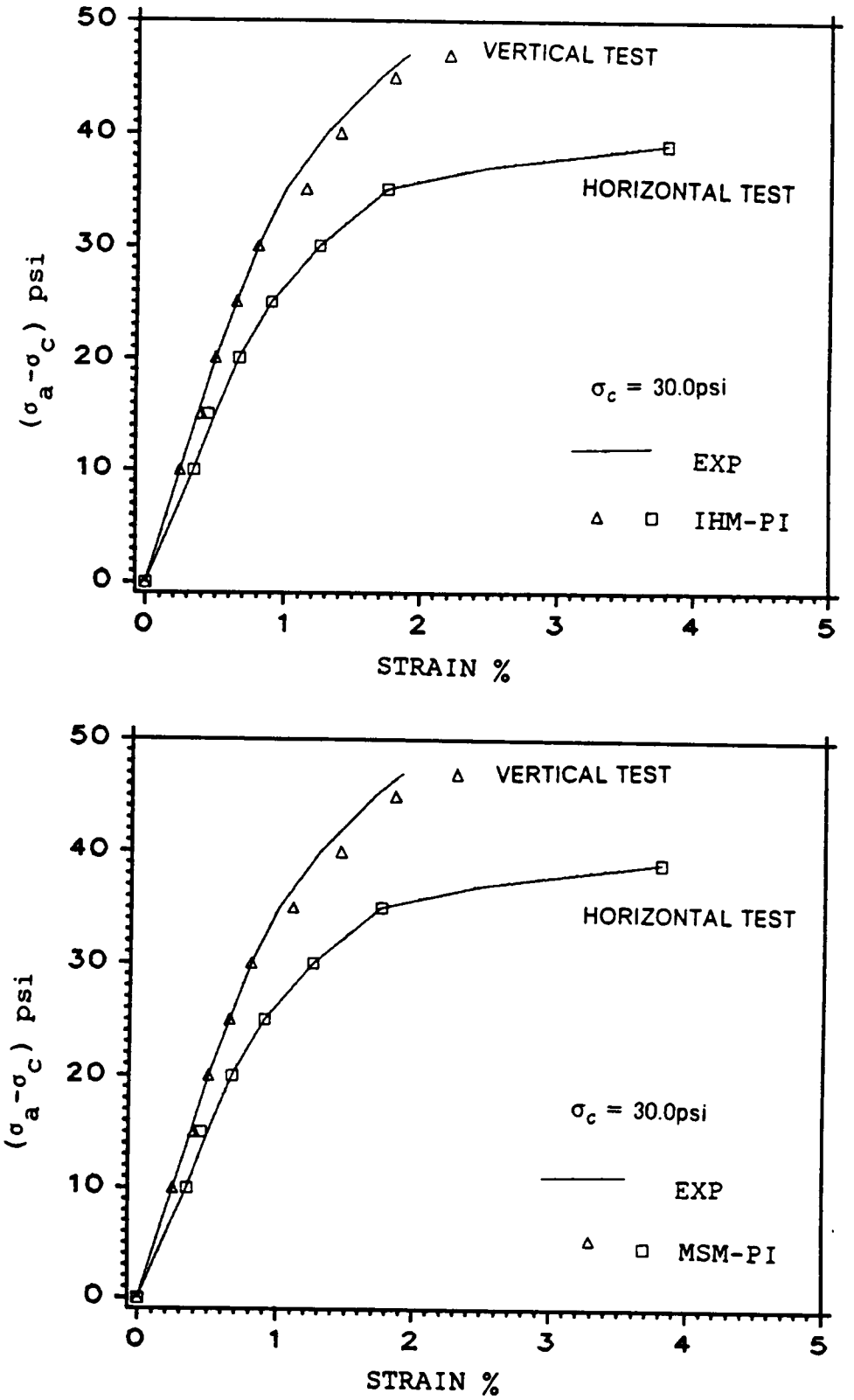

Figure 3.18: Comparison of model prediction with experimental data-Anisotropic London clay

CHAPTER 4

MODELS FOR PRESSURE-DEPENDENT MEDIA

Introduction

In the previous Chapter models were developed for elastic-plastic pressure-independent media. These models can be applied to non-granular or non-frictional media, and the short-term undrained analysis of clays. In this Chapter, pressure-dependent elastic-plastic models are developed for granular or frictional media and as such they can be applied to effective stress analysis of soils.

The basic features of a pressure-dependent model are described in Chapter 2. Mohr-Coulomb and Drucker-Prager models are the earliest models of this type. Drucker, Gibson and Henkel (21) suggested the modification of the models to include work hardening for soils. Roscoe, Schofield and Wroth (57) developed the Cam-Clay model based on the isotropic work hardening theory. This model was later modified by Roscoe and Burland (58) to include shear distortion and is called the modified Cam-clay model. These models were subsequently

generalized by Zienkiewicz and Naylor (70) and Bannerjee and Stipho (7) for finite element analysis.

Mroz, Norris and Zienkiewicz (44) and Prevost (54) developed kinematic hardening models for soils. These are called the multisurface models. In these models, several yield surfaces are used to describe the anisotropic yielding of soil. Later, the same concepts were used to develop the two-surface or the bounding surface model by Dafalias and Hermann (18) and Mroz, Norris and Zienkiewicz (44). These models are a special case of the multisurface models. The use of the two-surface models can reduce computational and storage costs with little loss of accuracy (55).

However, most of the models developed were for initially isotropic materials. The initial anisotropy of the of the soil was considered only in a few models. A cap model for transversely isotropic materials was developed by Baladi and Sandler (5). Ghaboussi and Momen (25) developed an isotropic-hardening model for initially transversely anisotropic sands. Both the above models were developed for transversely anisotropic soils and were based on the isotropic work hardening theory. Hence they are limited to monotonic loading conditions. Here, a pressure-dependent model for initially orthotropic soils is developed. Both isotropic-hardening and kinematic-hardening are employed. Hence, the model can be used for general loading conditions. The model can be applied to both sands and clays (both normally consolidated and over-consolidated).

This Chapter is divided into four sections. In section 4.2, an elastic plastic isotropic-hardening model for an initially orthotropic media will be described. In section 4.3, this model is extended to account for kinematic hardening. In section 4.4, the determination of the parameters required for the models are discussed. Finally in section 4.5, the general behavior of the models are investigated and some comparisons with experimental data are made.

Isotropic-Hardening Model (IHM-PD)

In this section, an elastic-plastic isotropic-hardening model for an initially orthotropic pressure-dependent media (granular or frictional) is developed. This model is based on the concepts developed by Roscoe, Schofield and Wroth (57) and Roscoe and Burland (58) and is generalized for initial orthotropy. The model in its general form can be applied to both sands and clays. As isotropic-hardening is used, the model is limited to monotonic loading conditions. Also the model gives reasonable results only for normally and lightly over-consolidated soils. The two-surface model described in the next section overcomes both the above limitations. The advantage of the isotropic-hardening model is that it is easy to implement and computational costs are low compared to the anisotropic-hardening models.

The failure surface is assumed to be of the form;

$$\bar{\sigma} = np$$

$$\bar{\sigma}^2 = \sigma^T \mathbf{M} \sigma \tag{4.1}$$

$$p = \frac{(\sigma_1 + \sigma_2 + \sigma_3)}{3}$$

Where p is the hydrostatic pressure and **M** is the distortion matrix (assumed to remain constant during deformation) previously described in Chapter 3 with the pressure independence condition imposed and n is a material constant (figure 4.1). Equation 4.1 represents a ellipital cone in the principal stress space.

The form of the yield surface is chosen as (figure 4.1);

$$F(p, \bar{\sigma}, k) = (p - a)^2 + \frac{\bar{\sigma}^2}{n^2} - a^2(k) = 0 \tag{4.2}$$

where k is the hardening parameter and 'a' is the size of the yield surface. Also, 'a' is equal to half the value of p_c , where p_c is the consolidation pressure. The yield surface is also called the consolidation surface or the bounding surface. Equation 4.2 represents an ellipsoid in principal stress space. For isotropic materials and under triaxial conditions the yield function reduces to the form developed by Roscoe and Burland (58) for the modified Cam-Clay model.

$$q = \sigma_1 - \sigma_c$$

$$p = \frac{(\sigma_1 + 2\sigma_c)}{3} \tag{4.3}$$

$$F(p,q,k) = (p - a)^2 + \frac{q^2}{n^2} - a^2(k) = 0$$

For states of stress within this surface, the response is elastic. For states of stress on the yield/consolidation surface the response is elastic plastic.

During loading, a stress point which is on the yield/consolidation surface moves outward. As the stress points moves outward the yield/consolidation surface expands with the stress point. During unloading, the stress point detaches itself from the yield/consolidation surface and the unloading is purely elastic. During reloading, the behavior is elastic till the stress point touches the yield/consolidation surface, after this elastic-plastic deformation takes place.

However, when the stress point reaches the failure surface, unlimited deformation occurs at constant stress and volume (figure 4.1). The behavior is perfectly elastic-plastic.

If initially the stress point is on the yield/consolidation surface, the soil is called normally-consolidated. If the stress point is within the yield/consolidation surface the soil is called over-consolidated. Here, only normally consolidated and lightly over-consolidated soils will be considered.

In general k the hardening parameter is a function of deviatoric and volumetric strains (46).

$$k = f_1(\varepsilon_d^p) + f_2(\varepsilon_v^p) \tag{4.4}$$

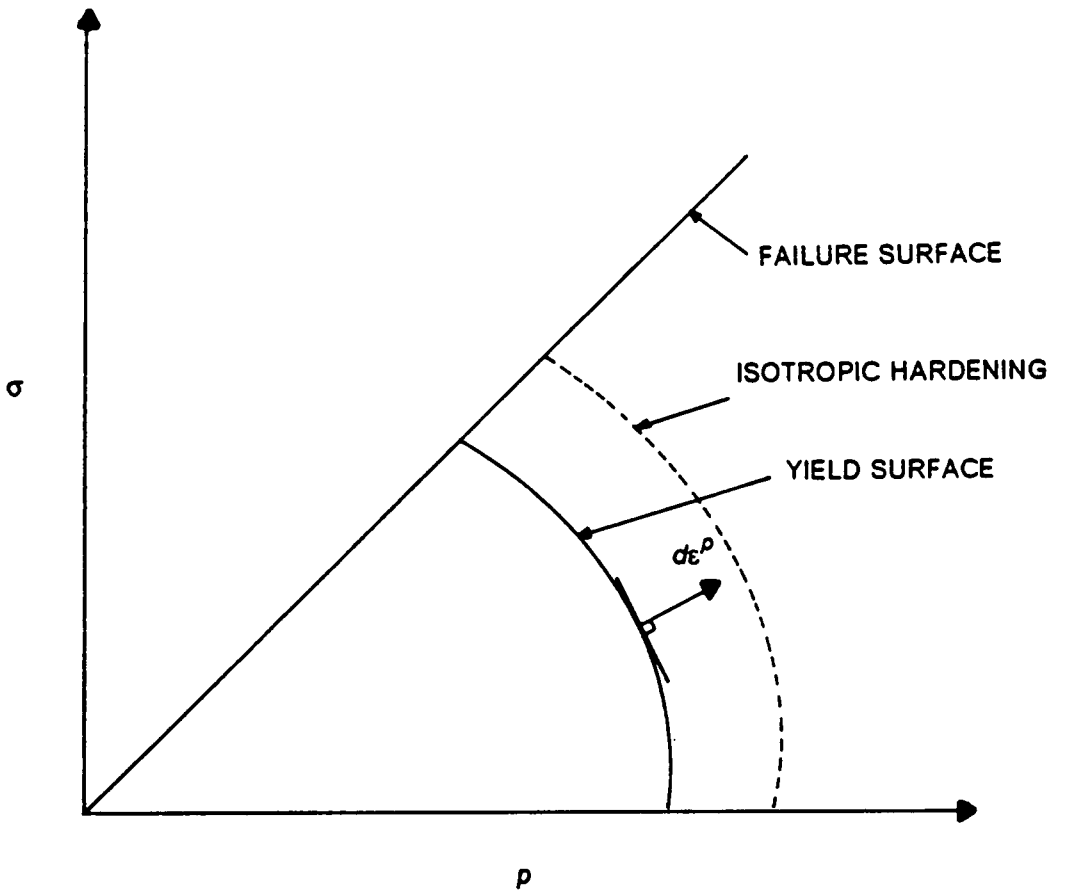

Figure 4.1 Pressure Dependent Isotropic Hardening Model

where ε_v^p is the plastic volume strain and ε_d^p is a measure of the deviatoric plastic strains.

However here only volumetric hardening will be considered;

$$k = -e^p \tag{4.5}$$

Where e^p is the plastic void ratio. In this formulation it has been assumed that the M-matrix remains constant during deformation. To have a more general formulation, the components of the M-matrix should be functions of the plastic strains. However this would increase the number of parameters needed for the model.

Derivation of Elasto-Plastic Matrix

In this section, the elasto-plastic matrix will be derived, using the above concepts. Differintating equation (4.2);

$$\frac{\partial F}{\partial \sigma} = \frac{2(p-a)}{3} + \frac{2\sigma^T \mathbf{M}}{n^2} \tag{4.6}$$

The plastic incremental strain is given as (42);

$$d\varepsilon^p = \frac{\mathbf{n}(\mathbf{n}^T d\sigma)}{K} \tag{4.7}$$

Where K is the plastic modulus and **n** are the normalized gradient. The consistency condition requires that the stress point does not penetrate the yield surface.

$$dF = (\frac{\partial F}{\partial \sigma})d\sigma + (\frac{\partial F}{\partial e^p})de^p = 0 \tag{4.8}$$

Where de^p is given as;

$$de^p = -(1 + e_0)d\varepsilon_v^p \tag{4.9}$$

Substitute equations (4.6), (4.7) and (4.9) into equation (4.8) and solve for K;

$$K = \frac{4(1 + e)p(p - a)da}{(\frac{\partial F}{\partial \sigma})^T(\frac{\partial F}{\partial \sigma})} \tag{4.10}$$

where $da = \frac{\partial a}{\partial e^p}$.

The total incremental strain can be separated into elastic and plastic components (42);

$$d\varepsilon = d\varepsilon^e + d\varepsilon^p$$

$$d\varepsilon^e = \mathbf{D}^{-1}d\sigma \tag{4.11}$$

$$d\varepsilon^p = \frac{\mathbf{n}(\mathbf{n}^T d\sigma)}{K}$$

Using the above relations, the elastic-plastic matrix can be obtained(42).

$$d\sigma = (\mathbf{D} - (\mathbf{D}\mathbf{n}^T\mathbf{n}\mathbf{D})/(K + \mathbf{n}^T\mathbf{D}\mathbf{n}))d\varepsilon \tag{4.12}$$

where **D** is the elastic matrix.

The evolution of the parameter 'a' has to be determined through the use of the isotropic consolidation test (figure 4.2). Assuming that the variation of 'a' with 'e' is given as (44);

$$a = a_i \exp(\frac{e_0^p - e^p}{\lambda - \kappa}) \tag{4.13}$$

$$da = \frac{\partial a}{\partial e^p} = \frac{-a_i}{\lambda - \kappa} \exp(\frac{e_0^p - e^p}{\lambda - \kappa}) \tag{4.14}$$

where a_0 is the size of the yield surface at initial consolidation pressure p_0 at void ratio e_0. λ is the slope of the loading path of the test and κ is the slope of the unloading path.

In the pressure-dependent model the elastic moduli are also pressure-dependent;

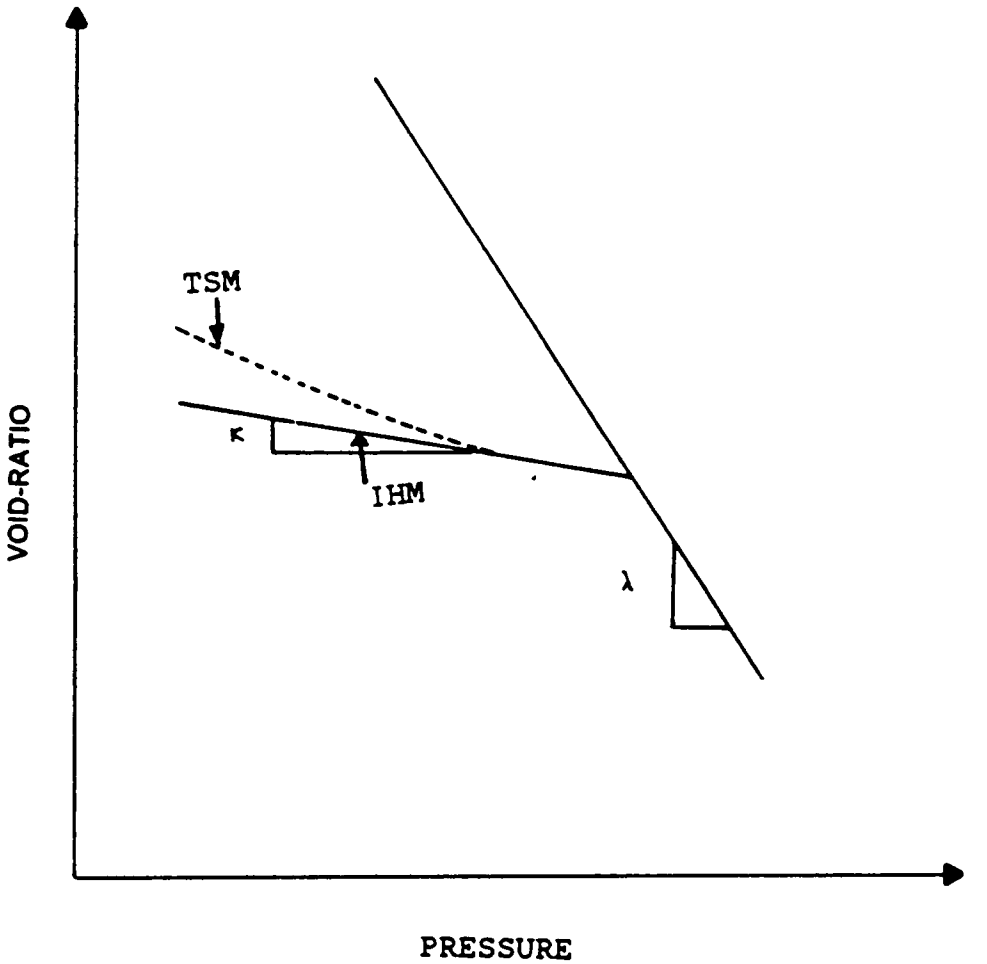

Figure 4.2 Isotropic Consolidation Test

$$E = E_i(\frac{p}{p_i})^{n1} \tag{4.15}$$

where n1 is a constant (n1 =1. for clays and n1 =.5 for sands) and E_i is the value of E at p = P_i

This model can also be applied to undrained analysis. For finite element calculations, the formulation of Bannerjee and Stipho (7) is used to impose the undrained conditions as follows.

$$\mathbf{u} = \mathbf{K}_b\boldsymbol{\varepsilon} \tag{4.16}$$

Where $\mathbf{K}_b$ is given as;

$$\mathbf{K}_b = K_b \begin{vmatrix} 1 & 1 & 1 & 0 & 0 & 0 \\ 1 & 1 & 1 & 0 & 0 & 0 \\ 1 & 1 & 1 & 0 & 0 & 0 \\ 0 & 0 & 0 & 0 & 0 & 0 \\ 0 & 0 & 0 & 0 & 0 & 0 \\ 0 & 0 & 0 & 0 & 0 & 0 \end{vmatrix}$$

where **u** is the pore pressure and K_b is the solid-fluid bulk modulus. This matrix is added to the constitutive matrix during assembly calculations. The pore pressure can be calculated from the strains using equation (4.16). This method gives good results for states of stress small compared to the failure stresses. Near collaspe conditions the numerical errors will create problems (7). For better results a pore pressure degree of freedom should be added to the element.

The model developed in this section can be used for normally-consolidated and lightly over-consolidated soils. It can model the initial anisotropy of the soil under both drained and undrained conditions.

Two-Surface Model (TSM)

In the previous section, an isotropic-hardening model was developed. This model is useful for modelling monotonic loading processes for normally-consolidated soils. For over-consolidated soils and under general loading conditions a anisotropic-hardening model is required. In this section, a Two-surface model is developed, which is a special case of the multisurface model. The model described in this section is a generalization of the model developed by Mroz, Norris and Zienkiewicz (44) for initially orthotropic media. The description of the model can be divided into two parts,

(1) when the stress point is on the bounding or consolidation surface (figure 4.3).

(2) when the stress point is within the bounding surface.

Case 1 is identical to the description given in the previous section and will not be discussed here. To model anisotropic-hardening, a new yield surface is introduced within the consolidation surface, the consolidation surface is also called the bounding surface. The yield surface translates and expands within the bounding surface. Therefore, it can model anisotropic-hardening. When the stress point is on the bounding surface, the yield surface also passes through the stress point. As the stress point moves outwards, both the bounding surface and the yield surface expand such that the ratio of their sizes remains constant (figure 4.3).

If the stress point is within the bounding surface, it can be either on the yield surface or inside the yield surface. If the stress point is within the yield surface, the response is elastic. If the stress point is on the yield surface, elastic-plastic deformation occurs with a plastic modulus that is proportional to the distance of the yield surface from the bounding surface. The plastic modulus is interpolated from an interpolation rule which is specified.

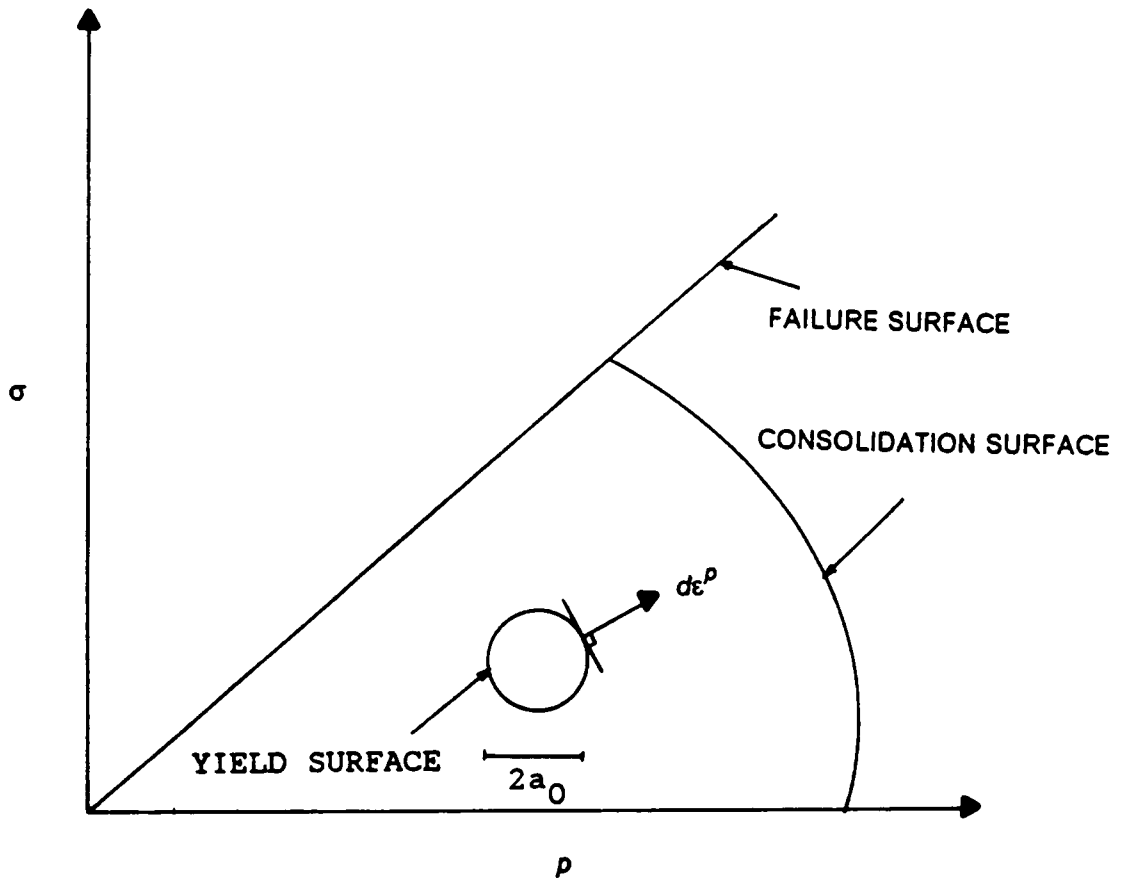

Figure 4.3 Two-Surface Model

Derivation of Elastic-Plastic Matrix

The bounding surface is defined as before;

$$F(\bar{\sigma},p,k) = (p - a)^2 + \frac{\bar{\sigma}^2}{n^2} - a^2(k) = 0 \tag{4.17}$$

The yield surface is assumed to be;

$$F(\sigma,p,\alpha,k) = (p - \bar{\alpha})^2 + \frac{(\sigma - \alpha)^T \mathbf{M} (\sigma - \alpha)}{n^2} - a_0^2(k) = 0 \tag{4.18}$$

where α is the translation vector which locates the yield surface in stress space, $\bar{\alpha}$ is the translation vector along the p axis, 'a' is the size of the bounding surface and a_0 is the size of the yield surface. For isotropic materials and under triaxial conditions, the yield function reduces to the form used by Mroz, Norris and Zienkiewicz (44) .

For the yield surface, translation and hardening rules have to be specified. The translation rule is (44);

$$d\alpha = d\mu \frac{(a_0\alpha - a\bar{\alpha} + \sigma(a - a_0))}{a_0} + \frac{(da - da_0)}{da_0}(\sigma - \alpha) \tag{4.19}$$

where $d\alpha$ is the incremental translation vector and $d\mu$ a constant to be calculated from the consistency condition. The first term in equatiion 4.19 represents the translation terms and the second term in the equation represents the expansion terms. The consistency condition states that;

$$dF = \frac{\partial F_0}{\partial \sigma}(d\sigma - d\alpha) + \frac{\partial F_0}{\partial a_0} da_0 = 0 \tag{4.20}$$

To determine $d\mu$, da_0 is to be evaluated from the hardening rule. The hardening rule is given below. As the ratio of the sizes of the yield and consolidation surfaces is assumed to be constant during deformation, da_0 can be written as;

$$da_0 = \frac{\partial a_0}{\partial e^p} de^p = (\frac{a}{a_0}) \frac{\partial a}{\partial e^p} de^p \tag{4.21}$$

An expression for $\frac{\partial a}{\partial e^p}$ is given in equation 4.14. Substituting equation (4.19)and equation (4.21)into equation (4.20) the constant $d\mu$ can be calculated.

The only thing left is to specify the interpolation rule, from which the plastic modulus can be calculated. This is done by assuming an interpolation for the plastic modulus such that the plastic modulus is proportional to the distance of the yield surface from the bounding surface. Define $\delta^{\times}$ as the distance between the stress point and the conjugate point on the bounding surface (44).

$$\delta^{\times} = (\frac{(\bar{\sigma}_0 - \bar{\sigma}_b)^2}{n^2} + (p_0 - p_b)^2)^{1/2} \tag{4.22}$$

where $\bar{\sigma}_0$ and p_0 are calculated on the yield surface and $\bar{\sigma}_b$ and p_0 are calculated on the bounding surface at the conjugate point. Then, the plastic modulus is defined as (44);

$$K_p = K_{p1} + (K_{p0} - K_{p1})(\frac{\delta^{\times}}{\delta_0^{\times}})^{(\gamma+1)} \tag{4.23}$$

$$\delta_0^{\times} = \mathrm{SUP}(\delta^{\times}) \tag{4.24}$$

K_p is the plastic modulus and K_{p1} is the plastic modulus on the bounding surface at the conjugate point and K_{p0} is the plastic modulus on the yield surface at $\delta^{\times} = \delta_0$. The constant γ is to be experimentally determined. SUP($\delta^{\times}$) is the largest value of δ previously reached. Therefore K_p will have a value of K_{p1} , when the yield surface is in contact with the bounding surface, and a value of k_{p0} when it is furtherest from the bounding surface.

the model developed in this section can be used for both normally- consolidated and over-consolidated soils. It can model both initial and induced anisotropy. It can be used for drained and undrained conditions.

Determination of Parameters

In this section the parameters required for the pressure-dependent models will be discussed. The parameters to be determined are;

(1) λ the slope of the loading path in isotropic consolidation test,

(2) κ the slope of the unloading path in isotropic consolidation test,

(3) n slope of failure surface,

(4) components of the **M** matrix,

(5) K_{p0} and γ , interpolation constants for two-surface model

λ and κ can be obtained from the isotropic consolidation test. For the isotropic-hardening model, unloading is assumed to be elastic (figure 4.2).

The constant n and the components of the M-matrix can be determined from the effective failure stresses. Here a method is given to determine the parameters for the isotropic hardening model from triaxial tests. Consider a cross-anisotropic material with the 1-2 plane as the plane of isotropy. From a triaxial test in the 1-direction,

$$\bar{\sigma} = \sigma_1 - \sigma_c \tag{4.25}$$

where σ_1 is the effective axial stress at failure in the 1-direction (horizontal direction) and σ_c is the confining pressure. Solving for n from equation 4.1;

$$n = \frac{3(\sigma_1 - \sigma_c)}{(\sigma_1 + 2\sigma_c)} \tag{4.26}$$

Equation 4.26 represents a straight line of slope n in a plot of the deviatoric stress at failure versus the mean pressure at failure. M_{33} can be determined from a triaxial test in the 3-direction, Solving for M_{33} from equation 4.1;

$$M_{33} = \frac{n^2(\sigma_3 + 2\sigma_c)^2}{9(\sigma_3 - \sigma_c)^2} \tag{4.27}$$

where σ_3 is the effective axial failure stress in the 3-direction (vertical direction) and σ_c is the confining pressure. Under triaxial conditions n can be related to the friction angle(Mohr-Columb failure condition);

$$n = \frac{3 \sin \varphi}{6 - \sin \varphi} \tag{4.28}$$

To obtain a physical interpretation of M_{33}, define b as a anisotropic strength factor. Where $M_{33} = \frac{1}{b^2}$. Here b is the ratio of the slope of the failure surface in the triaxial test in the 3-direction to the slope of the failure surface in the 1-direction (equation 4.26). The other parameters can be obtained from inclined tests.

For the two-surface model, the two interpolation constants K_{p0} and g, and the size of the yield surface a_0 are needed. These can be determined from the isotropic consolidation test (figure 4.2). Figure 4.2 shows the e-log(p) plot. The unloading path is usually not a straight line as assumed in the isotropic model. The value of a_0 is determined as the distance AB (figure 4.2). B is the point on the e-log(p) plot where the unloading curve deviates from a straight line. The interpolation constants are obtained by curve fitting this unloading path (44).

General Response and Comparison

The models described in the previous sections were implemented into a finite element program. In this section the general response of the models and some comparison with experimental data is studied. A single element is used in this analysis. The procedure is identical to the one used in Chapter 3. The purpose is to test the models developed in this chapter, with other models and to validate the program.

Isotropic Media

To test the model and the program, the finite element results will be compared with the results of similar models (exact solutions) for isotropic media. The finite element results are compared with the constitutive law of Mroz, Norris and Zienkiceiwz (44). This is a generalization of the modified Cam-Clay model. Figure 4.4 shows the comparison of IHM-PD results with the constitutive law of reference (44), for weald clay. The clay was modelled under drained triaxial conditions, at a confining pressure of 120. psi. The initial void ratio was .50. The hardening parameters were obtained from an isotropic consolidation test and n was obtained from the failure stresses in the triaxial test(44). As the clay is isotropic and normally consolidated, no anisotropic parameters are required. The parameters used are;

$e_0 = .5$

$n = .87$

$\nu = .3$

$G = 1000.$ psi

$\lambda = .092$

$\kappa = .027$

Where σ_a is the axial stress and σ_c is the confining pressure. The stress strain curve and the volume strain are plotted. Good comparison is observed. Note the strains are in percent.

Figure 4.5 shows the response of the same clay under undrained conditions. To model the undrained condition the procedure described in section 4.2 is used. The solid-fluid bulk modulus is taken as 50 times the elastic modulus. In the finite element analysis the imcompressibility condition can only be maintained approximately, whereas in the constitutive law this condition is exactly maintained. Inspite of this approximation, good results are obtained, for stress strain response, pore-pressure development and stress-path.

Figure 4.6 compares the response of the two-surface model (TSM), with the constitutive law of Mroz, Norris and Zienkiewicz(44) for weald clay. Figure 4.6 shows the unloading response of the clay in an isotropic consolidation test. The clay was unloaded from a initial isotropic pressure of 120 psi, at a void ratio of .50. The parameters are identical to those used to model the clay in figures 4.4 and 4.5. In addition to the parameters used to model the clay for figures 4.4 and 4.5 , the two-surface model parameters are required. These are obtained by curve fitting the unloading path in the test. The size of the yield surface is obtained by determining the point where the unloading path deviates from a straight line. The two-surface parameters are;

$K_{po} = 24000.$

$\gamma = 2.5$

$\frac{a}{a_0} = 6.$

Excellent agreement is obtained. The above examples validate the model and the finite element program.

Figure 4.7 compares the results of IHM-PD, with the results of the associated cam-clay model(ACCM) and the associated modified cam-clay model (AMCCM), for a labotory prepared isotropic soft clay (7). The clay has an initial void ratio of .95 at a confining pressure of 53.0 psi. It is sheared under undrained triaxial conditions. The parameters are taken from reference 7.

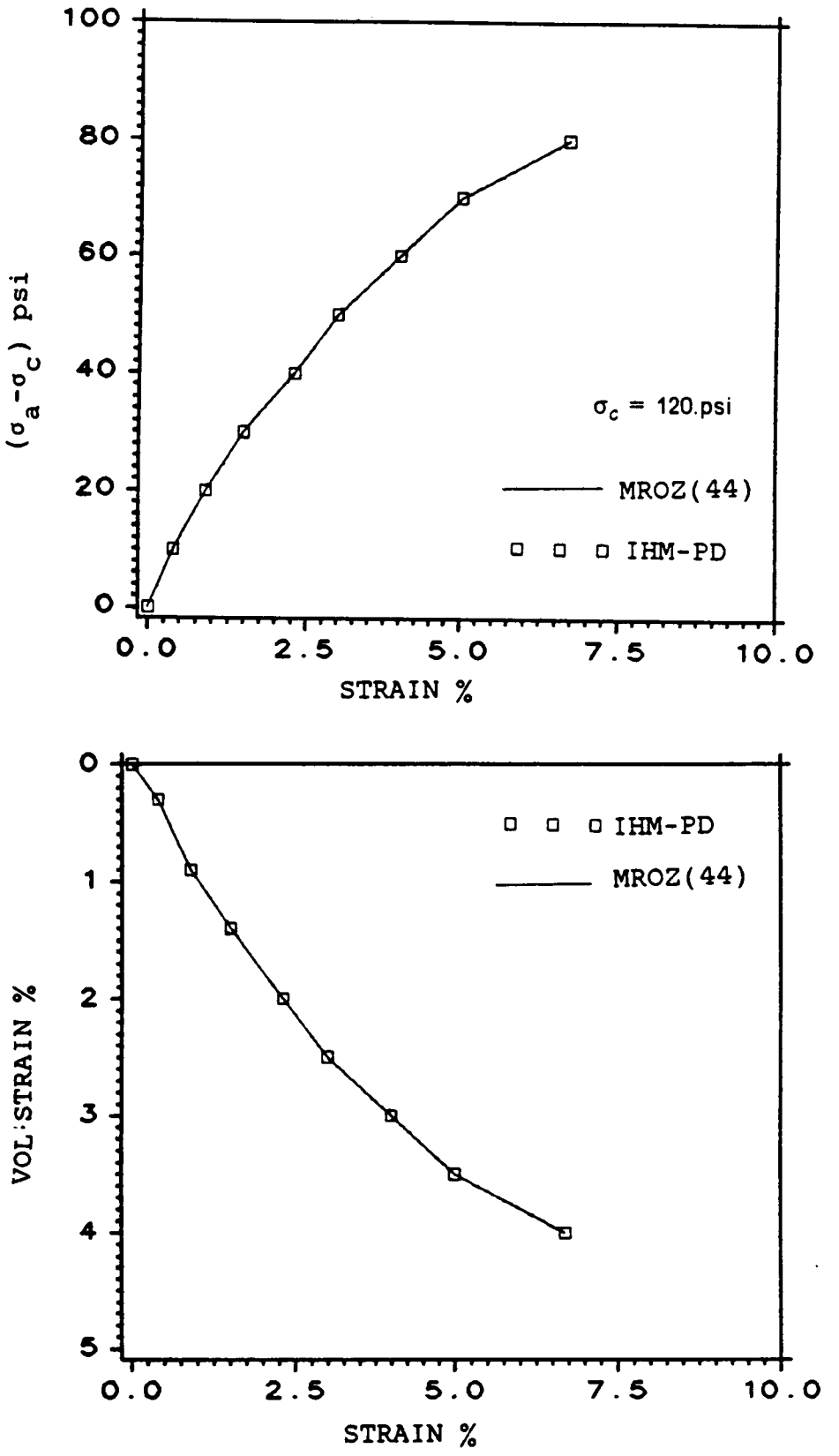

Figure 4.4: Comparison of model prediction with Mroz Constitutive law-Drained response

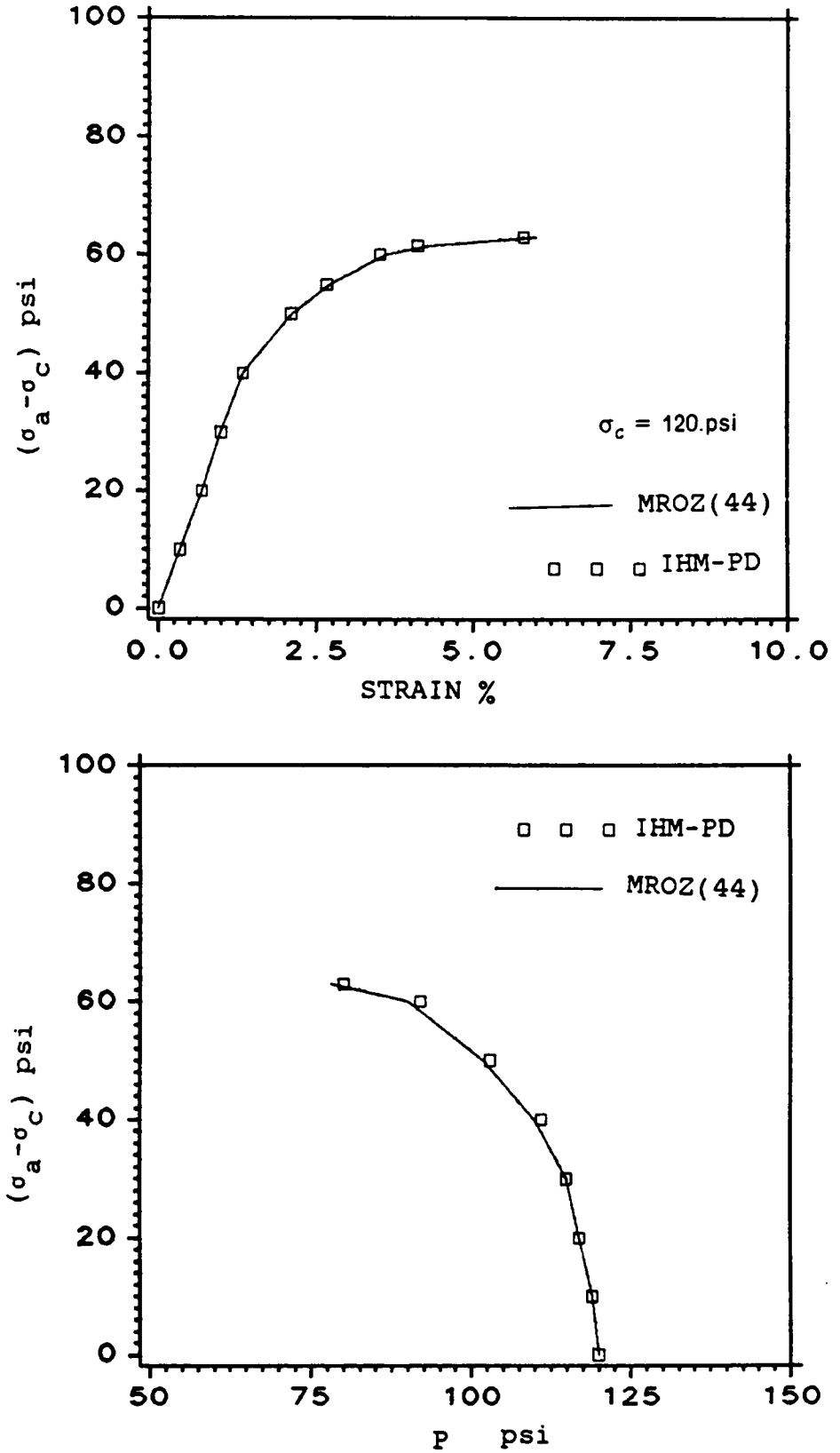

Figure 4.5: Comparison of model prediction with Mroz Constitutive law-Undrained response

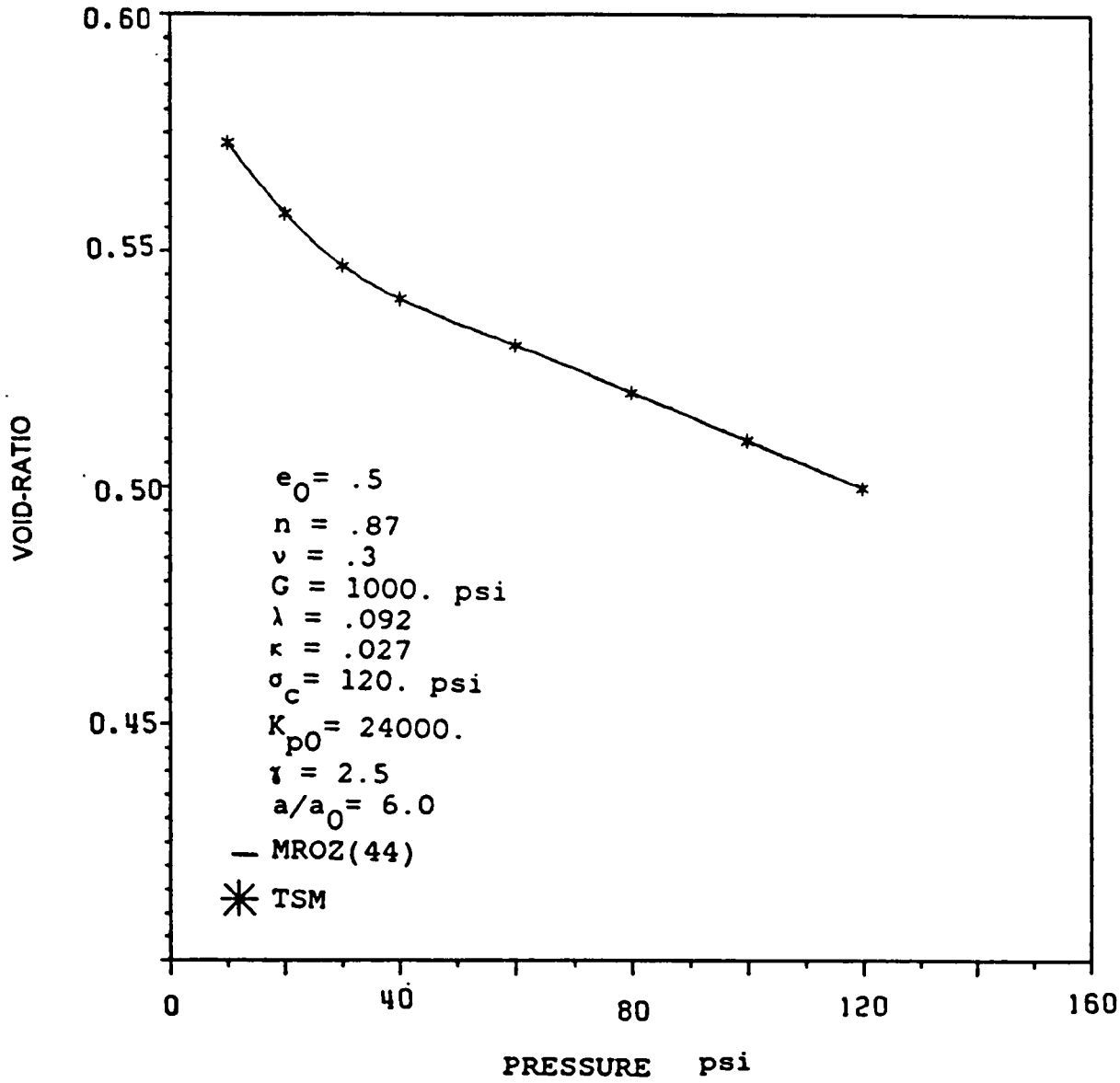

Figure 4.6: Comparison of model prediction with Mroz Constitutive law-Two surface model

e_0 = .95

n = 1.05

ν = .3

G = 1000. psi

λ = .140

κ = .05

Figure 4.7 compares the stress strain response and the pore-pressure development predicted by the models. It can be observed that the IHM-PD and the AMCCM give identical results, whereas the stress strain response predicted by the ACCM is significantly different. This is because IHM-PD reduces to the AMCCM for isotropic media. However, all the models predict essentially the same pore-pressure development.

Figure 4.8 shows the same clay now overconsolidated with an OCR = 1.2 (7). To model the overconsolidation, the soil is loaded isotropically to the consolidation pressure and then unloaded isotropically to obtain the appropriate overconsolidation ratio. Similar results are observed. The AMCCM gives similar results as the IHM-PD.

Anisotropic Media

The comparisons made above were for isotropic media. In this section the general response of the models for anisotropic media will be investigated. Some comparisons will be made with experimental data.

To study the influence of anisotropy, b is defined as the strength in the vertical direction to the strength in the horizontal direction (here b is the ratio of the slope of the failure surface in a triaxial test in the vertical direction to the slope of a similar text in the horizontal direction). The stress strain response is studied for various values of b. The material parameters used in this simulation are taken from the data of weald clay (44). For example b = 1.0 corresponds to isotropic clay, hence it is identical to the clay used in figure 4.4, with a friction

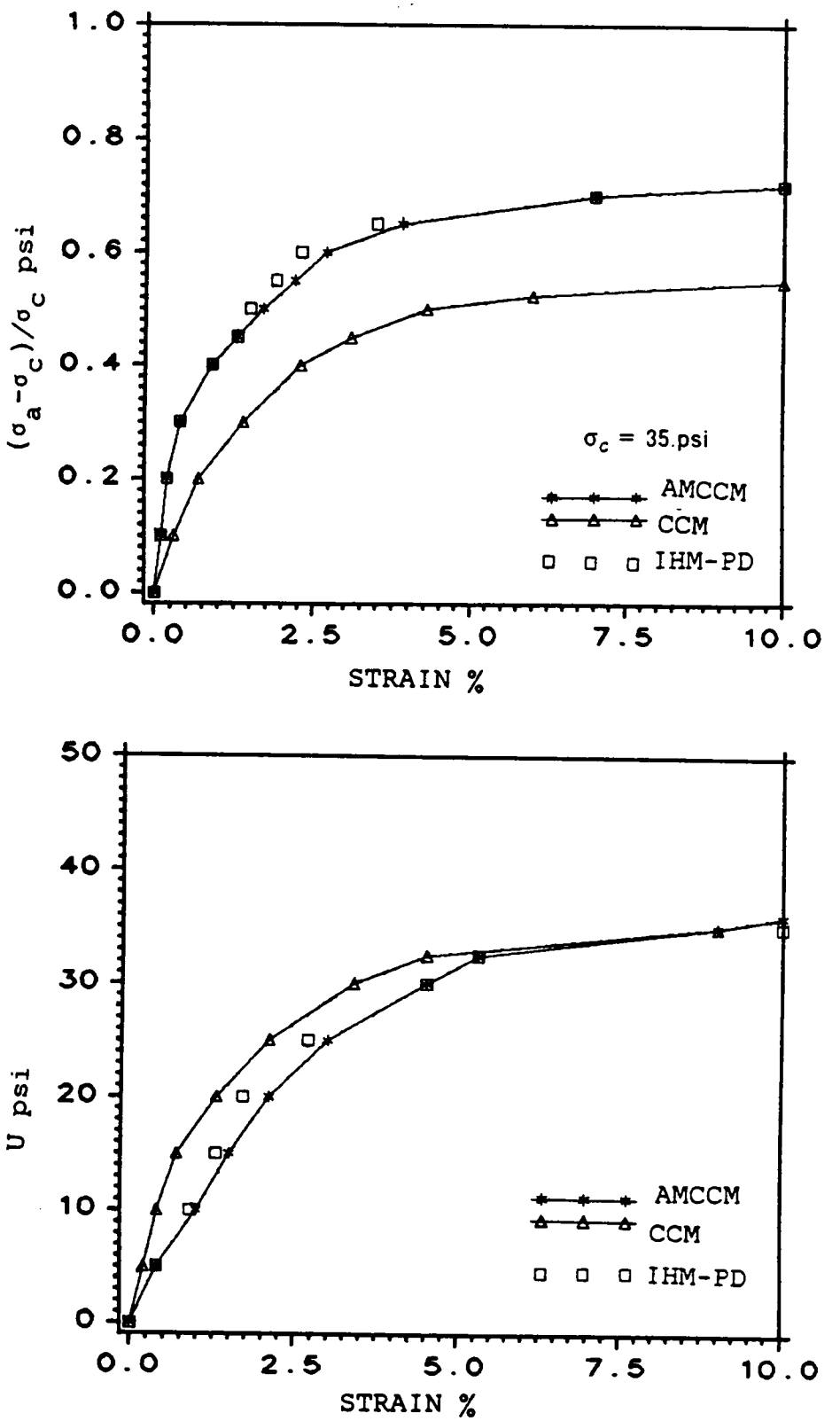

Figure 4.7: Comparison of model prediction with ACCM and AMCCM (OCR = 1.0)

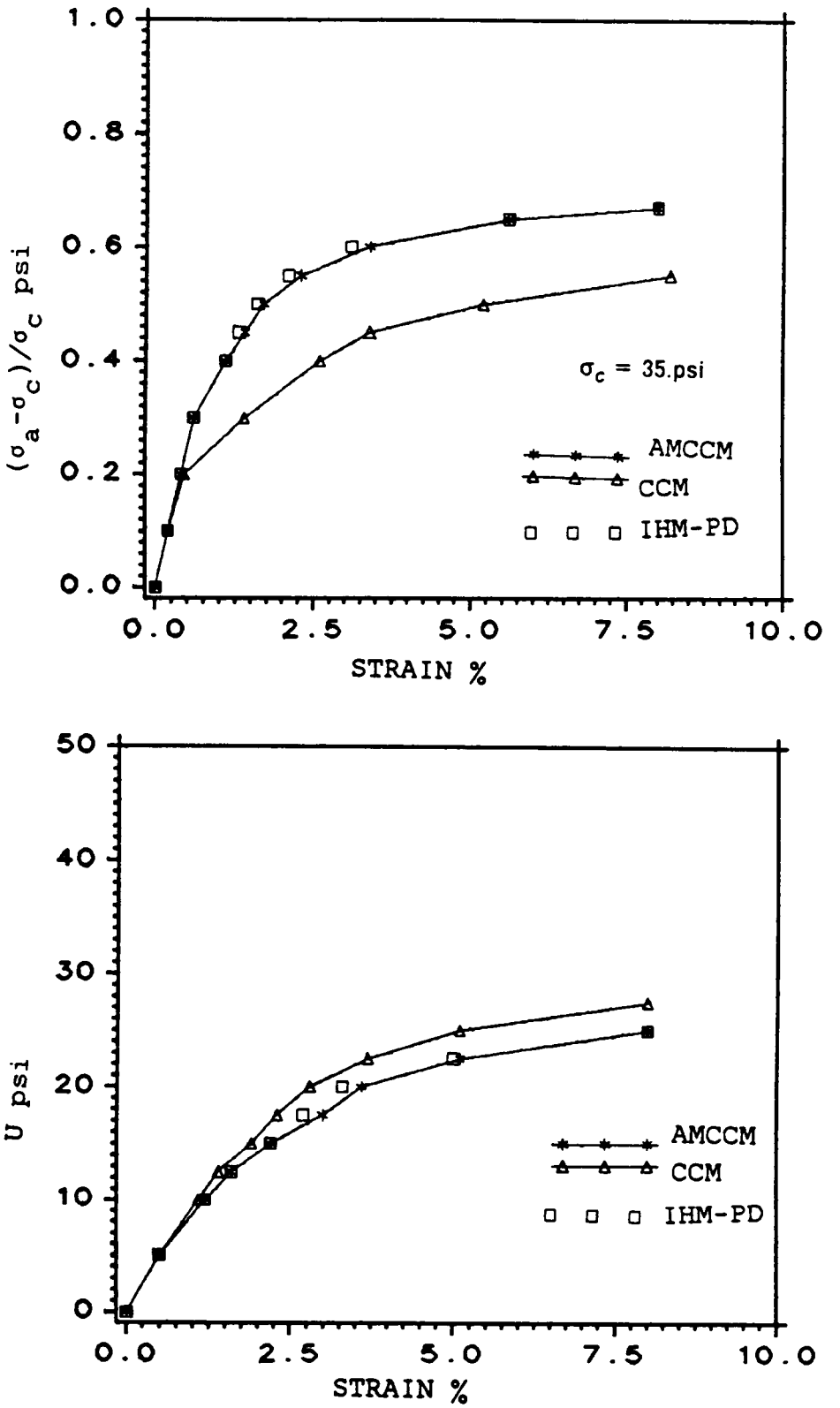

Figure 4.8: Comparison of model prediction with ACCM and AMCCM (OCR = 1.2)

angle of 22. degrees, and the clay with b=1.42 corresponds to a clay with a horizontal frictional angle of 22.0 degrees and a vertical frictional angle of 29.7 degrees under triaxial conditions. In addition to the data in figure 4.4, the anisotropic parameters are needed. As the response is investigated in the material principal planes, the shear terms are not needed. The only anisotropic parameter needed is M_{33} . The elastic response is assumed to be isotropic.

$e_0 = .5$

$n = .87$

$\nu = .3$

$G = 1000.$ psi

$\lambda = .092$

$\kappa = .027$

$M_{33} = \frac{1}{b^2}$

Figure 4.9 shows the stress strain response for various values of b. Some volume change curves are also plotted. It is observed that anisotropy influences both the stress strain and volumetric strain response, a higher value of b leading to a stiffer response.

In figure 4.10 the stress strain curves of a clay with b=1.42. (figure 4.9). are plotted for samples inclined to the principal directions of anisotropy under drained triaxial conditions. Where θ is the angle of inclination of the sample from the 1-direction (horizontal direction). The elastic response is assumed isotropic and M_{66} is assumed proportional to M_{33} . The anisotropic parameters used are;

$M_{33} = .5$

$M_{66} = 1.5$

This response is typical of senstive clays and sands (69).

So far, the drained response was analyzed. Now the response of the same soil will be studied under undrained conditions. The procedure described in section 4.3 for imposing the undrained condition is used. Figure 4.11 and Figure 4.12 shows the stress strain response,

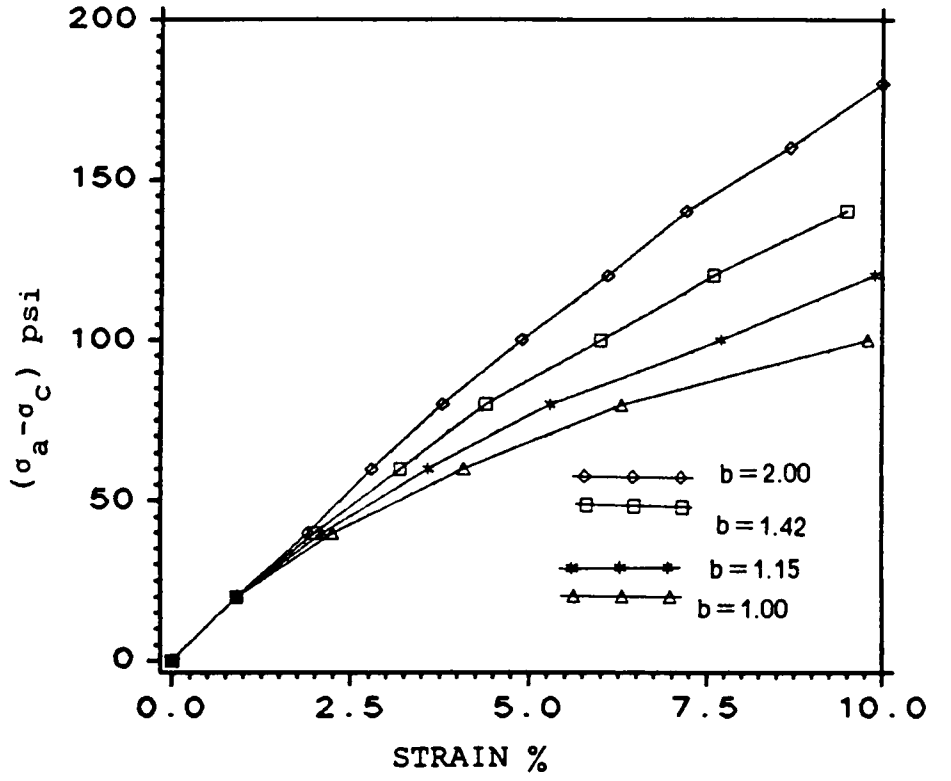

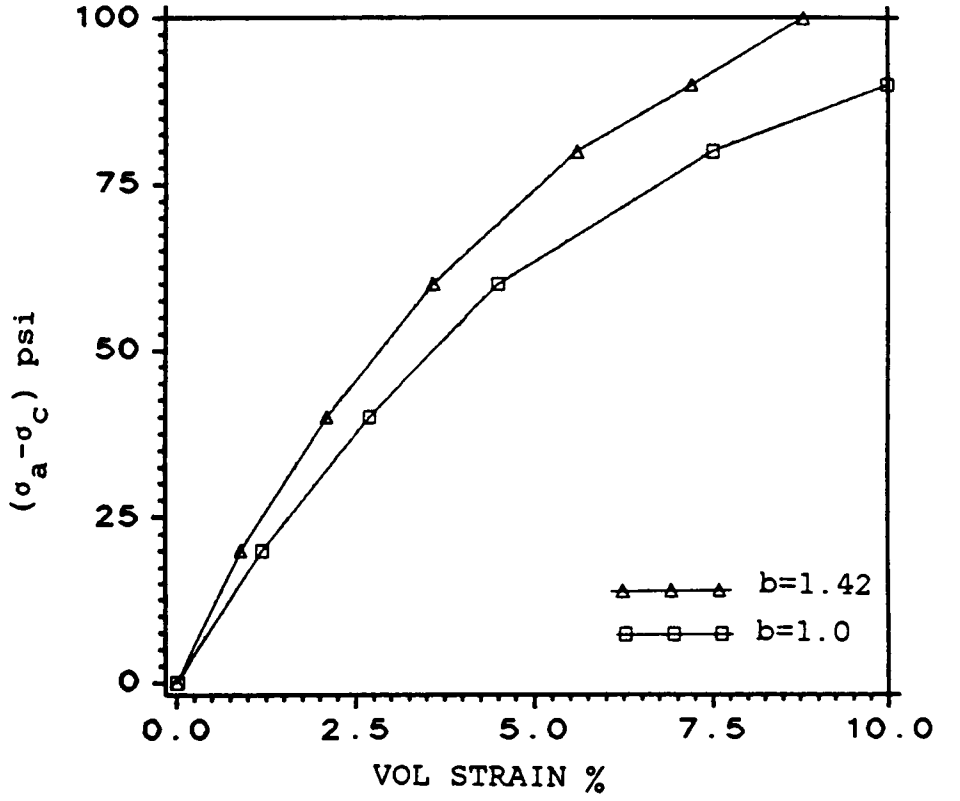

Figure 4.9: Constitutive Model Drained Response-Anisotropic Soil

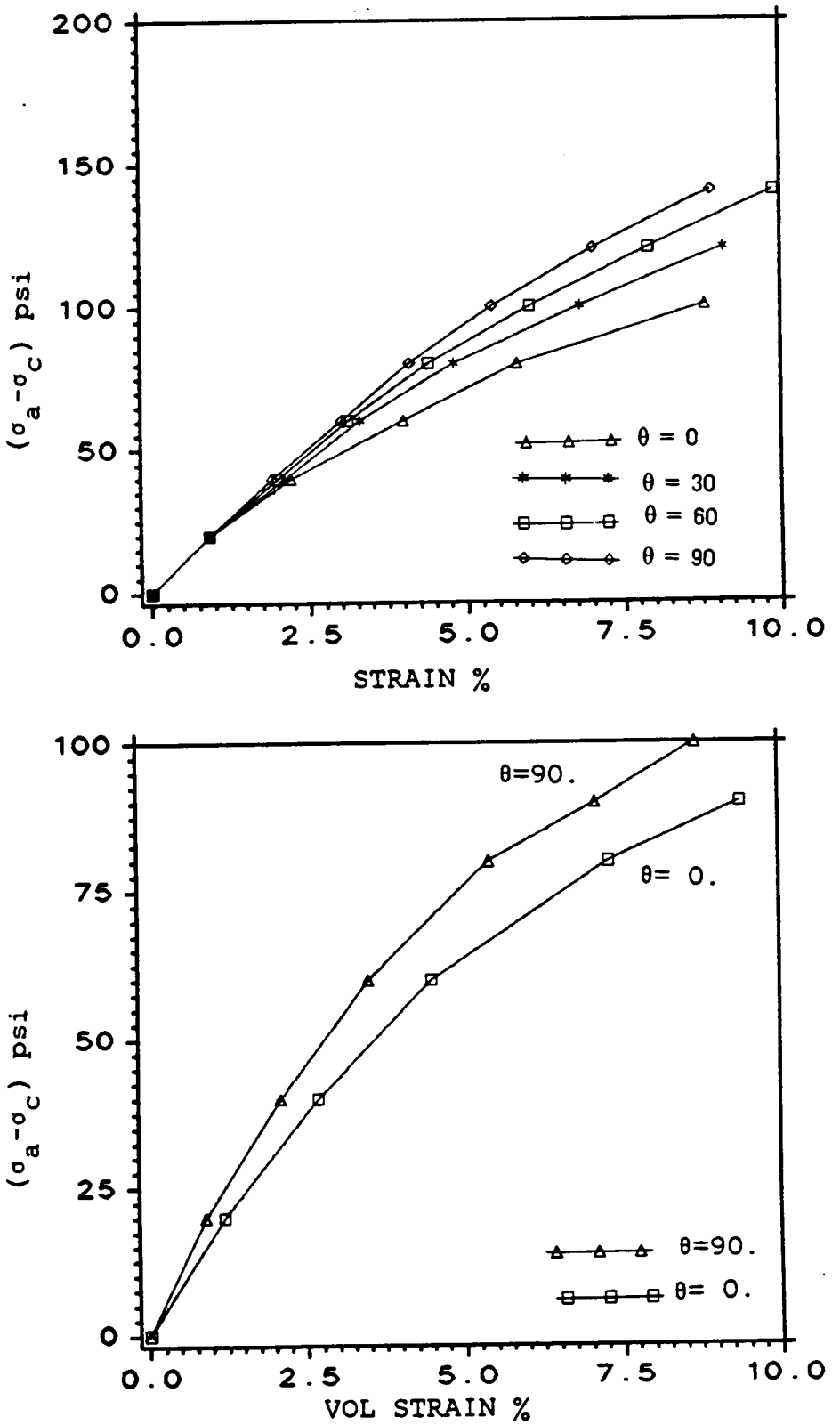

Figure 4.10: Constitutive Model Drained Response-Anisotropic Soil

stress path, and pore pressure curves for a isotropic (b = 1.0) and a cross anisotropic (b = 1.42) clay. The clay is identical to the one used in figures 4.9 and 4.10. It is found that a higher pore pressure is obtained for the isotropic material (b = 1.) than in the anisotropic material (b = 1.42). This is because under the same stress, greater plastic flow takes place in the isotropic material than in the anisotropic material. This leads to a higher pore pressure development. This undrained response is typical of some clays (1,37). The values of the parameters used in the analysis are taken from ref (44) and are given in the figures.

In the above analysis, it was assumed that the soil was normally-consolidated. Now the response of the same clay is investigated under overconsolidated conditions. Figure 4.13 shows the comparison between the isotropic hardening model and the TSM for an anisotropic overconsolidated soil (OCR = 2.,b = 1.42) under drained triaxial conditions. The procedure for overconsolidation is described in the previous section. The TSM parameters are taken from the data of weald clay (44) and are the same as those used in figure 4.6. Figure 4.13 illustrates the stress-strain response predicted by the two models for an anisotropic clay in both the vertical and horizontal directions. The isotropic-hardening model exhibits an initial elastic response followed by elastic-plastic deformation, whereas the two-surface model exhibits plastic flow at a very low stress level.

Figure 4.14 shows the failure stress state under triaxial conditions for an anisotropic sand(2). The sand used is rounded Leighton Buzzard sand, with a specific gravity of 2.64 and porosity of 34.1 percent. Figure 4.14 shows the failure stresses on the p-q plane. The sand was tested at various angles to the plane of deposition at a confining pressure of σ_c = 55.0 KN/ M^2 For an isotropic sand, all the data should have resulted in a single point on the p-q plane. As the sand exhibits anisotropy, several data points are obtained. This is because of different axial stresses at failure in each case. Figure 4.14 also shows the same data plotted on the $\bar{\sigma}$ -p plane(equation 4.1). It can be observed that the data plot as a straight line which passes through the origin. The experimental data approximately fit the straight line $\bar{\sigma}$ -p anisotropic failure criteria.

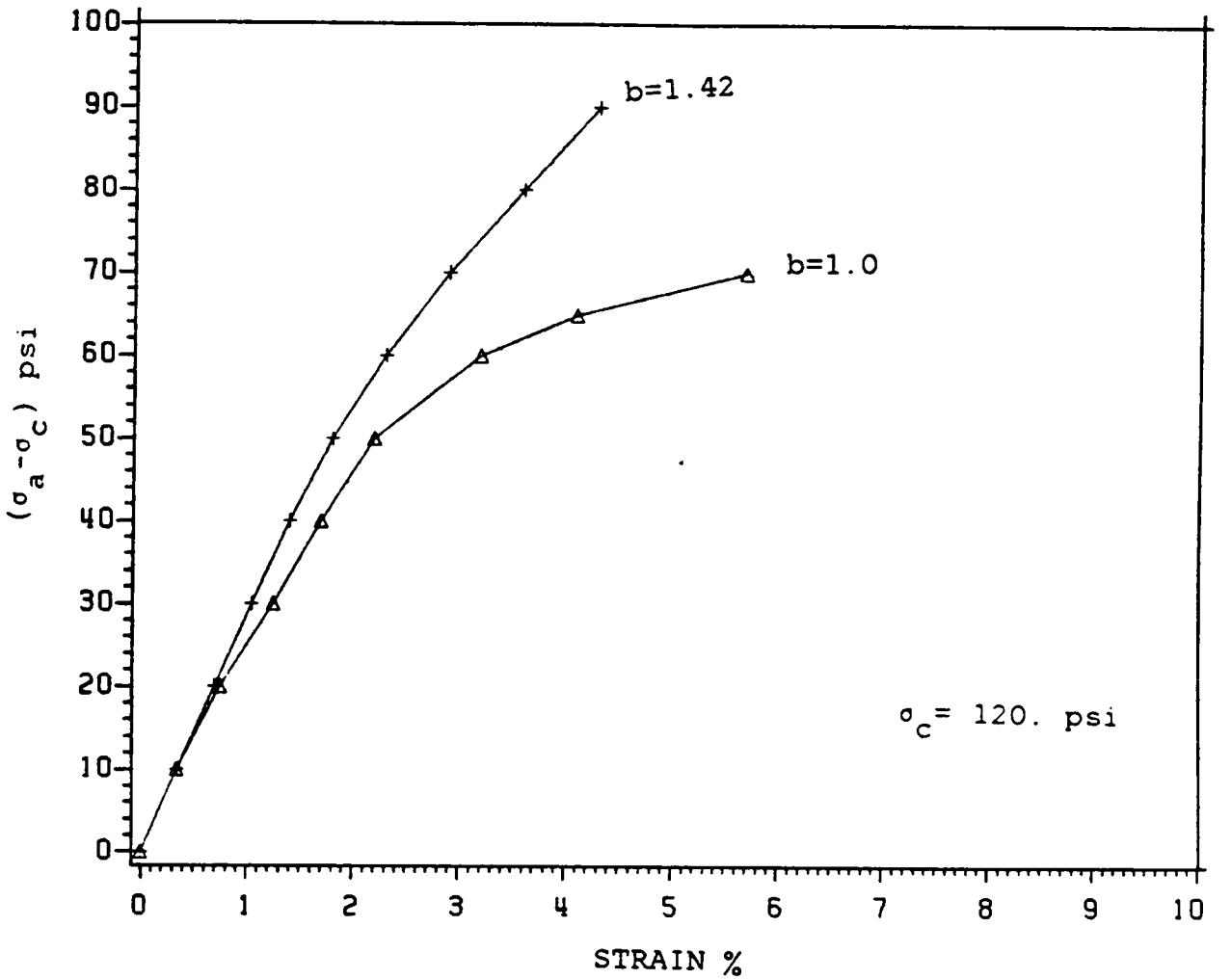

Figure 4.11 Constitutive model response-Undrained anisotropic soil

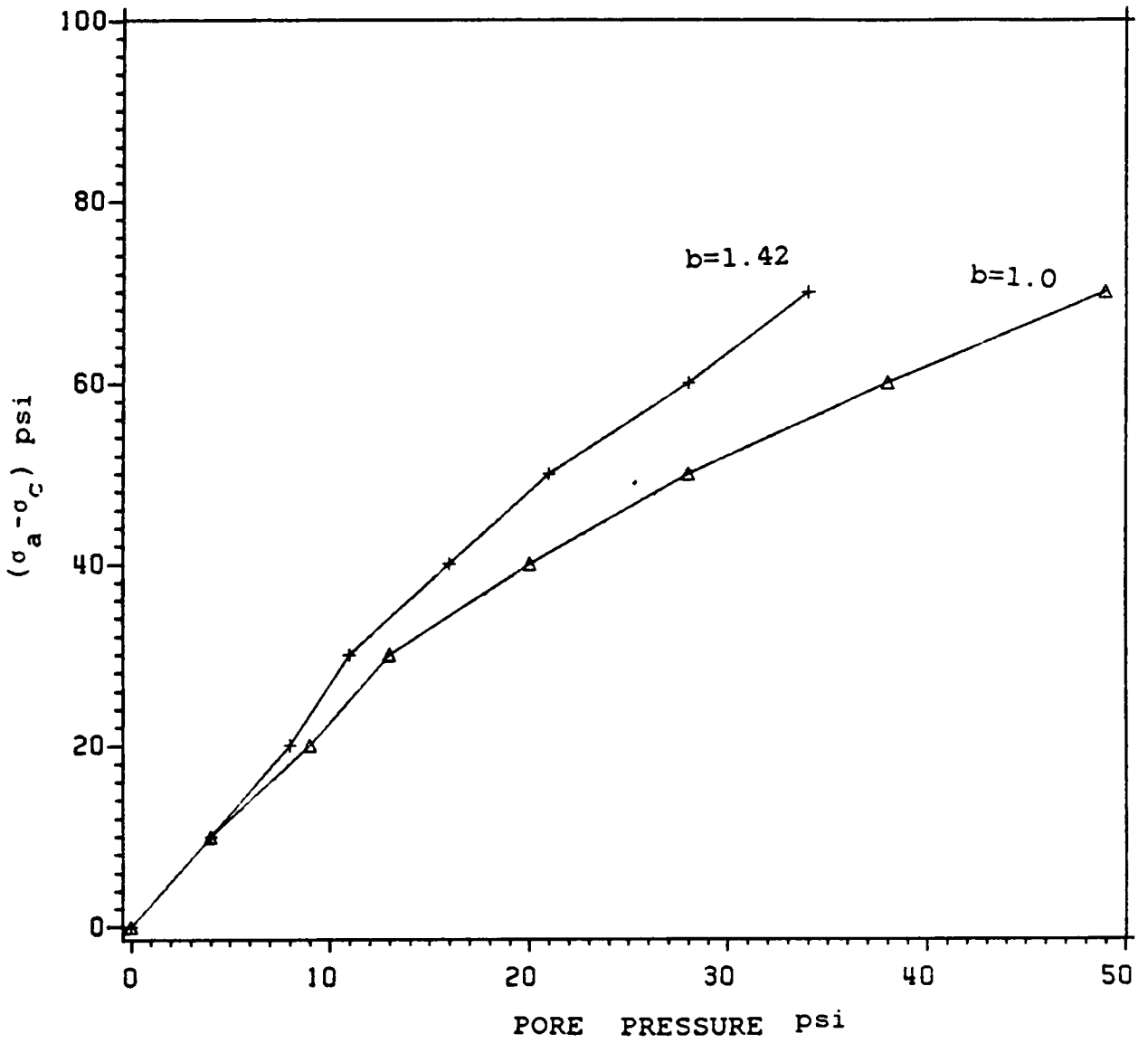

Figure 4.12 Constitutive model response-Undrained anisotropic soil

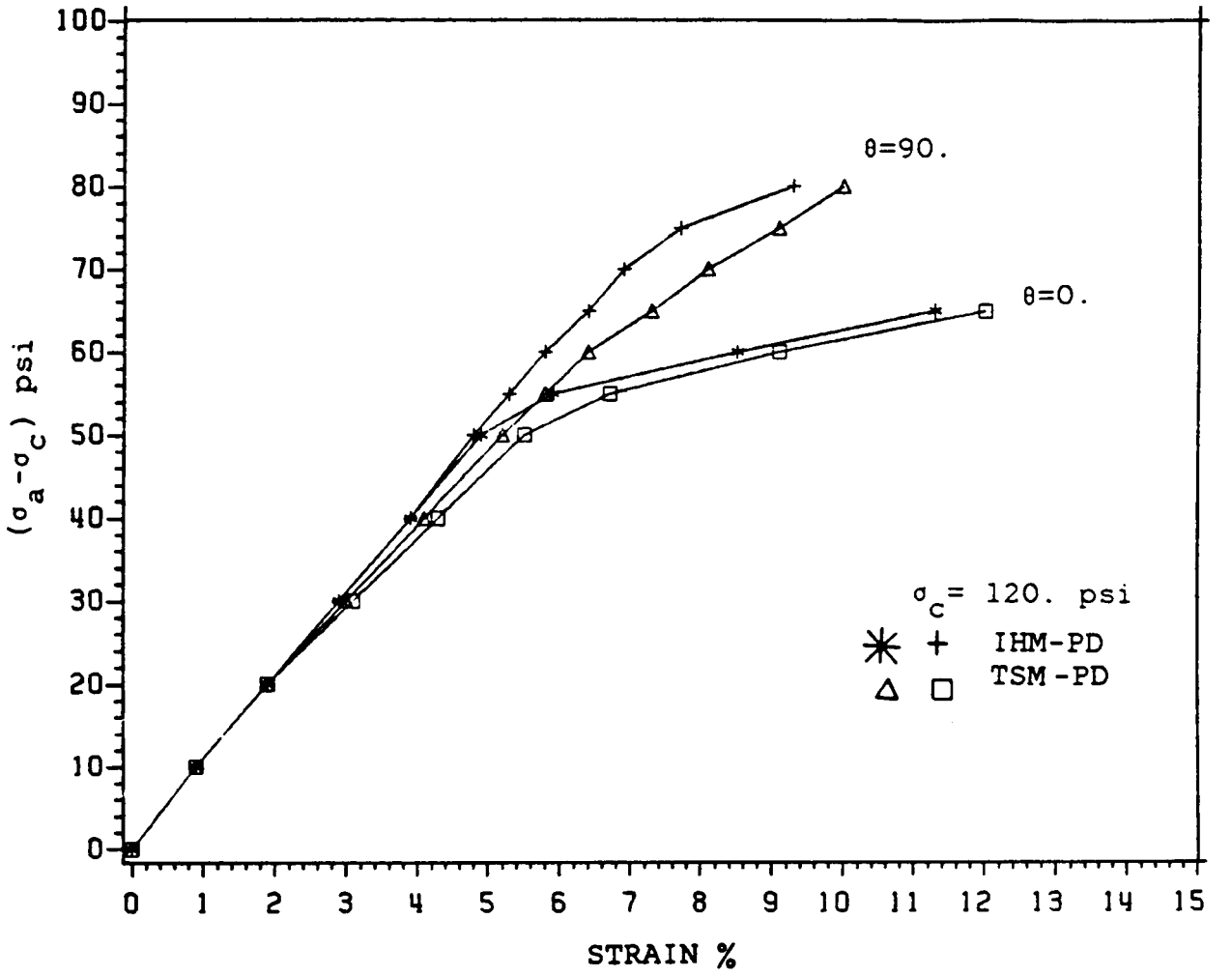

Figure 4.13: Constitutive Model Response-Overconsolidated Soil

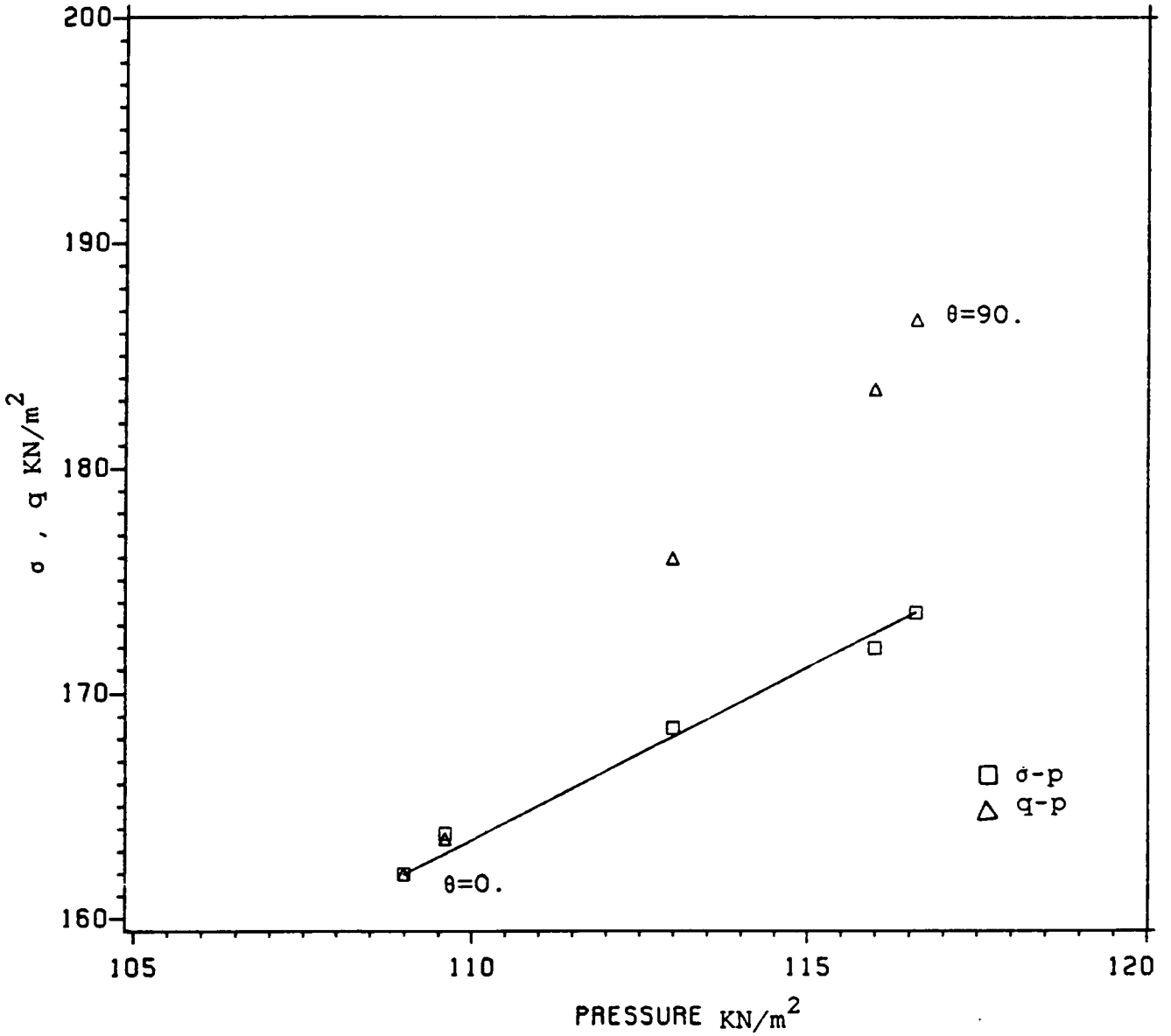

Figure 4.14: Comparison of model prediction with experimental data-Buzzard sand

Figure 4.15 shows the stress strain relations of anisotropic Toyoura sand tested under triaxial conditions (47). The sand has a mean grain size of .15 mm and a void ratio of .68 at a confining pressure of .5 kg/ cm^2 . The sand was tested in both the vertical and horizontal directions and at two different confining pressures. (.50 and 2.0 kg/ cm^2 The strength parameters n and M_{33} were calculated from the failure stresses from the test with a confining pressure of .5 kg/ cm^2 . The elastic moduli were calculated from the stress strain curves in the same test. The hardening parameters were taken from reference (47).

$e_0 = .68$

$n = 1.7$

$E_1 = 250.\ kg/cm^2$

$E_3 = 300.\ kg/cm^2$

$\nu = .15$

$\lambda = .025$

$\kappa = .007$

$M_{33} = .81$

The experimental results are compared with the results of the IHM-PD. It is observed that the model predictions compare well with the stress strain curve in the horizontal direction. Whereas for the vertical sample, the comparison is not good at low strains, but compares well near failure. Fair agreement is observed in both cases. The material parameters are given on the figure. Better agreement could be obtained if deviatroic-hardening is considered, because in sands deviatoric-hardening can be important (46).

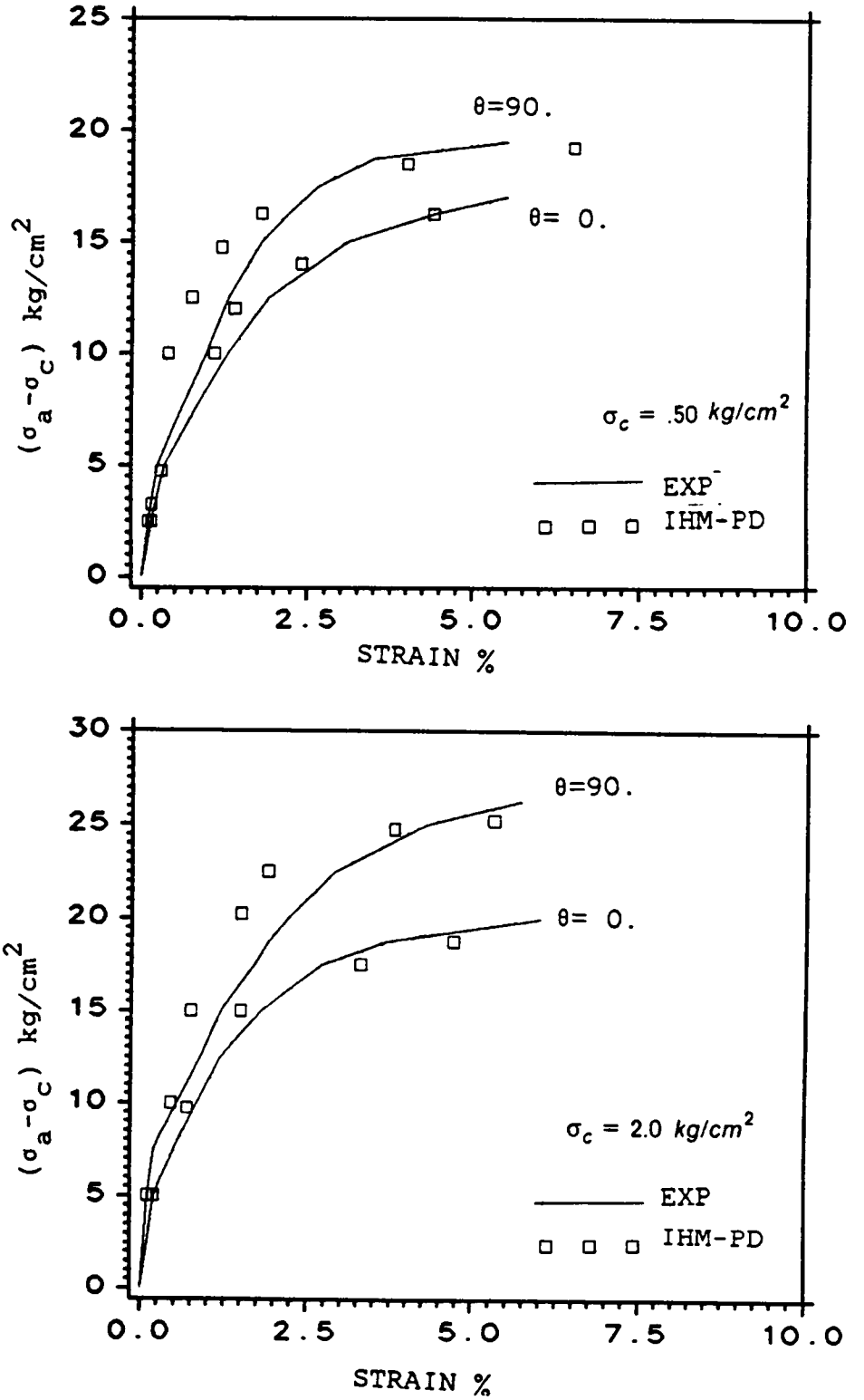

Figure 4.15: Comparison of model prediction with experimental data-Anisotropic Toyoura sand

CHAPTER 5

FINITE ELEMENT METHOD FOR PLASTICITY PROBLEMS

Introduction

In the previous Chapters constitutive models were developed to analyze nonlinear material behavior. These models are to be used in the solution of boundary value problems which are of interest in soil mechanics. Due to the nonlinear nature of the problems, a numerical method has to be used in the analysis. The finite element method has been successfully used in the solution of elastic-plastic boundary value problems.

In this Chapter the finite element method for elastic-plastic analysis will be described. As plastic deformations can result in large deformations, a method for large deformation analysis will also be described. Finally, the implementation of the models developed in the previous Chapters is discussed.

Finite Element Method

The basic concept of the finite element method is the idealization of an actual continuum as an assemblage of discrete elements interconnected at their nodal points (70). The unknowns, in this case the nodal displacements are interpolated over the element by shape functions. This reduces the boundary value problem to the solution of a set of algebraic equations of the form;

$$\mathbf{R} = \mathbf{K}^G\mathbf{U} \tag{5.1}$$

where $\mathbf{R}$ is the global load vector, $\mathbf{U}$ is the global nodal displacements and $\mathbf{K}^G$ is the global stiffness matrix.

For elasticity problems the global stiffness matrix is;

$$\mathbf{K}^G = \sum_{i=1}^{N} \mathbf{K}^e \tag{5.2}$$

where $\mathbf{K}^e$ is the element stiffness matrix and N is the number of elements. The element stiffness matrix is given by;

$$\mathbf{K}^e = \int_V \mathbf{B}^T\mathbf{D}\mathbf{B}dv \tag{5.3}$$

where $\mathbf{B}$ is the strain displacement matrix and $\mathbf{D}$ is the stress-strain matrix.

$$\boldsymbol{\varepsilon} = \mathbf{B}\mathbf{u} \tag{5.4}$$

$$\boldsymbol{\sigma} = \mathbf{D}\boldsymbol{\varepsilon} \tag{5.5}$$

The above method is complete for the solution of a linear elastic problem. For a material with a nonlinear stress-strain behavior, additional steps are needed. Several methods exist for the solution of nonlinear problems. Some of the commonly used methods are the tangent modulus method, Newton-Raphson and direct iteration (70).

In this thesis the tangent modulus method is used. In this method, the total load is applied in small load increments. At the beginning of each load increment, the appropiate stress strain matrix **D** is calculated for each element. The stiffness matrix is calculated for each element. Then the global stiffness matrix is assembled. This system of equations is solved to obtain the incremental nodal displacements and the incremental stress for each element. The total stresses and displacements are obtained by summing the results of each increment.

$$\mathbf{u}^i = \mathbf{u}^{i-1} + d\mathbf{u} \tag{5.6}$$

$$\sigma^i = \sigma^{i-1} + d\sigma$$

The accuracy of this method depends on the size of the load increment. Accuracy can be improved by iteration within each increment. Here the residual load vector correction approach is used. The residual load vector is defined as;

$$\psi = \int_V \mathbf{B}^T \sigma dv - \mathbf{R} \tag{5.7}$$

For equilibrium $\psi = 0$.

However, due to the nonlinearity of the material, ψ will not be zero. This residual load vector is added to the load vector as a correction. The system of equations is iterated till the residual load vector is below the allowable error. This procedure is good for monotonic loading. For cyclic loading small load steps are essential to maintain equilibrium.

The models described in the previous Chapters are implemented into finite element programs using the above method for nonlinear analysis. An 8-noded isoparametric three dimensional brick element is used in the analysis.

Large Deformation Analysis

Plastic deformations can result in large deformations and large changes in geometry. When large deformations occurs, the small strain theory is no longer valid. This can result in errors in the solution of some elastic-plastic boundary value problems.

For large deformation, analysis either the Lagrangian or the Eulerian formulations can be used. In the Lagrangian analysis, the coordinate system remains fixed during deformation (28,67). In the Eulerian formulation, the coordinate system moves during deformation (48).

In large deformation analysis of elastic-plastic materials it is important that the stress strain law be written using a stress measure that is frame indifferent. This is because the stress-strain tensor is a function of the stress tensor. It is shown by Prager (51) that the Jaumann rate of of the Cauchy and Kirchoff stress tensor is frame indifferent. Carter, Booker and Davis (14) used the Jaumann rate of the Cauchy tensor. This however leads to a non-symmetric matrix. In this work the formulation of Mcmeeking and Rice (38) is used. The Jaumann rate of the Kirchoff stress tensor is used. This gives a symmetric stiffness matrix. The stress-strain law is written as;

$$\tau_{ij}^{\times} = D_{ijkl}\varepsilon_{kl} \tag{5.8}$$

where $\varepsilon_{ij} = \frac{(u_{i,j} + u_{j,i})}{2}$ and $\tau_{ij}^{\times}$ is the Jaumann rate of the Kirchoff stress tensor. In this section both the tensor and vector notation are used for convenience.

It is shown by Mcmeeking and Rice (38) that for large displacement analysis, the stiffness matrix using the above definetion of stress can be written as;

$$\mathbf{K}^{e} = \int_{v}\mathbf{B}^{T}\mathbf{D}\mathbf{B}dv + \int_{v}((N_k)_{,i}^{T}\sigma_{ij}(N_k)_{,j} - 2(B_{kl})^{T}\sigma_{ij}(B_{kj}))dv \tag{5.9}$$

The second term is called the initial stiffness matrix and **B** is defined as;

$$B_{ij} = \frac{(N_{i,j} + N_{j,i})}{2} \tag{5.10}$$

Where N are the shape functions.

The true or Cauchy stress increment is;

$$d\sigma_{ij} = \tau_{ij}^{\times} - \sigma_{ij}\varepsilon_{ll} + \sigma_{ik}\omega_{kl} + \sigma_{jk}\omega_{kj} \tag{5.11}$$

where $\omega_{ij} = \frac{(u_{i,j} - u_{j,i})}{2}$ and $d\sigma_{ij}$ is the Caushy stress increment.

In the finite element calculation, the stiffness matrix is calculated at every load increment, using the current configuration and stress level. The finite element equations are solved to obtain the nodal displacements. Equation 5.8 is used to obtain the Kirchoff stress increment and equation 5.11 is then used to calculate the true stress increment. This stress increment is added to the previous stresses and stored. The mesh is updated using the calculated displacements. This configuration and the stresses obtained are used to calculate the stiffness matrix for the next load increment.

This large deformation formulation is implemented in the finite element program. To test this formulation, the finite element results were compared with analytical results for a simple problem. The problem chosen is a block compressed under plane strain conditions. Figure 5.2 shows the comparision of the two analysis for a body under homogenous plane strain conditions. One element was used in the analysis. The finite element results were compared with the results of Toh and Sloan (65). Excellent comparision is obtained. The parameters used in the analysis are taken from (65) and are given below.

Youngs modulus E = 100. kg/ cm^2

Possions ratio v = .3

Initial length L_0 = 1.0 cm

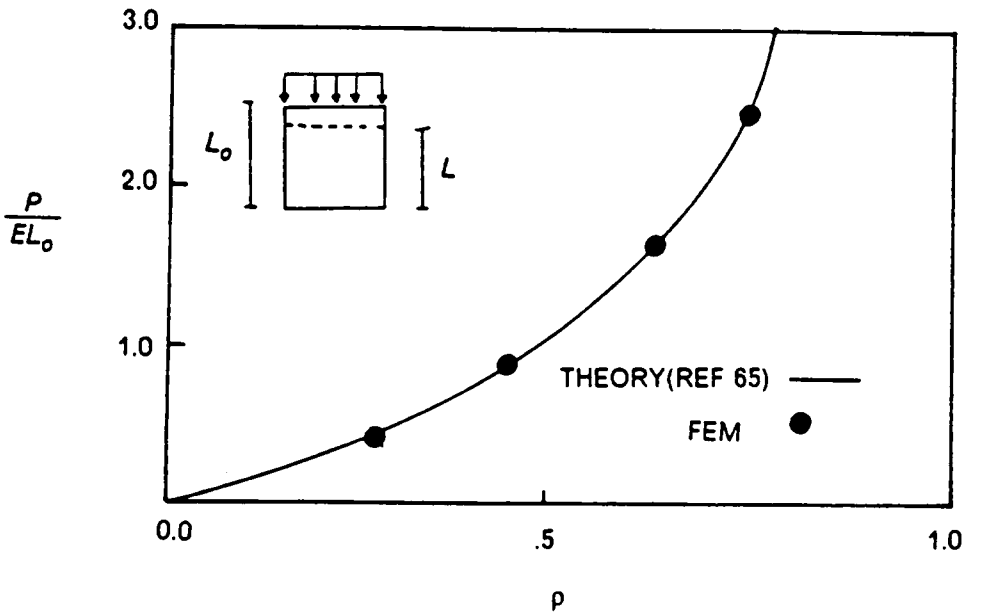

Figure 5.1 Large Deformation Analysis

Implementation of Models

In this section some of the details of the implementation of the models developed in Chapters three and four are discussed. As each model is very different from the others, it was decided to place each model in a separate program. However the basic program is the same in each case. This is a three dimensional finite element program with an eight noded brick element.

(a) Pressure-Independent Isotropic-Hardening Model (FEM3D-PIM)

The description of the model is given in Chapter 3. Here only a description of the computational aspects are described. Due to the presence of anisotropy, direction is important. Therefore, all stresses are transformed from the global coordinate system to the material coordinate system. The constitutive matrix is calculated in the material coordinate system and transformed back to the global coordinate system.

In an elasto-plastic problem two states of stress exist. For states of stress within the yield surface, the behavior is elastic and the elastic constitutive matrix is used in the calculation of the stiffness. For states of stress on the yield surface, the elasto-plastic matrix derived in Chapter 3 is used. As the hardening modulus usually varies nonlinearly the appropiate value of the modulus should be used.

As finite loading steps are used, an element which is elastic initially may turn plastic within the load increment. In this case, the stresses are scaled uniformly to the yield surface. This is done by reducing all the stresses uniformly such that the yield condition is satisfied. The left over stresses are added to the load vector as a correction. For elements which are plastic, the yield surface expands so that the stress point passes through it.

If during the analysis an element is found to have unloaded during a load step, the analysis is repeated using elastic properties for the element. The loading and unloading criteria are determined as (37);

$$\frac{\partial F}{\partial \sigma} d\sigma < 0 \quad \textit{unloading}$$

$$\frac{\partial F}{\partial \sigma} d\sigma = 0 \quad \textit{neutral loading} \tag{5.12}$$

$$\frac{\partial F}{\partial \sigma} d\sigma > 0 \quad \textit{loading}$$

During unloading the yield surface is unchanged and the response is elastic.

The program has a geometric nonlinear capability. As the updated Lagrangian description is used, the mesh is updated after each load increment. The program can also simulate incremental buildup. Before an element is buildup, it is treated as an air element with a very small stiffness. In the appropriate load step, the true material properties are assigned to the element, and gravity loads are calculated.

(b) Multisurface Model (FEM3D-MSM)

The implementation of this model is complex due to the presence of several yield surfaces. For each element the size and location of each surface has to be stored. In the calculation of the translation of the yield surface a large number of computations are needed. This results in larger memory space and increases computational costs. Also, very small loadsteps are needed to maintain stability. The isotropic-hardening model is generally stable compared to the multisurface model.

The elastic response is the same as the isotropic-hardening model. When the stress point reaches the first yield surface, the stresses are scaled as before. On futher loading the surface translates with the stress point and the appropriate hardening modulus is used. The incremental translation vector is calculated from the translation rule given in Chapter 3. The stiffness matrix is calculated using the current plastic modulus, stress state, and translation vector.

If during loading the stress point reaches the next surface, the first surface is discarded and the new surface is used for futher calculations. This includes both the plastic modulus and the translation vector. This procedure is repeated with other surfaces. The last or outermost yield surface is usually assigned a low value for the plastic modulus. Thus the material behaves as an elastic perfectly-plastic media.

If an element is found to have unloaded during a load increment, the results of this increment are discarded. Immediate unloading is assumed to be elastic. The analysis is repeated with the new properties.

(c) Pressure-Dependent Isotropic-Hardening Model (FEM3D-PDM)

The derivation of this model is given in Chapter 4. The implementation of the model is similar to the pressure-independent isotropic- hardening model. For states of stress within the yield surface the behavior is elastic. The elastic properties are dependent on the pressure.

For states of stress on the yield surface the elastic-plastic matrix derived in Chapter 4 is used along with the appropiate hardening modulus. During initial yield the stresses are scaled to the surface. During loading the yield surface expands with the stress point. If an element is found to have unloaded during the loadstep the analysis is repeated using the elastic matrix.

The program has a large displacement analysis option based on the updated Lagrangian scheme. The nonlinear analysis is similar to that of the pressure-independent isotropic-hardening model.

As the size of the yield surface depends on the consolidation pressure, the initial stress calculation is important. The initial size of the yield surface is calculated as,

$$a = \frac{OCR(\frac{\bar{\sigma}^2}{n^2} + P^2)}{2p} \tag{5.13}$$

where $\bar{\sigma}$, p and n are defined previously. The program can also be used for undrained analysis. The method for calculating the system bulk modulus and the pore pressures are given in Chapter 4.

(d) Two-Surface Model (FEM3D-TSM)

This model is described in Chapter 4. The implementation of the model can be separated into two parts. When the state of stress is on the bounding surface, the implementation of the model is the same as the isotropic-hardening model. If the stress point is within the bounding surface and the yield surface, the behavior is elastic. The behavior is elasto-plastic if the stress point is on the yield surface.

For elastic states of stress the elastic pressure-dependent matrix is used. If the stress point is on the yield surface, the appropiate hardening modulus is used with the elastic-plastic constitutive matrix derived in Chapter 4. The surface can translate and expand during deformation and the translation and expansion rules given in Chapter 4 are used.

The loading and unloading condition is the same as described for the multisurface model. Initial unloading is elastic.

The initial size of the bounding surface is as described in the isotropic-hardening model. It is futher assumed that the ratio of the sizes of the bounding surface and the yield surface is a constant. The initial position of the yield surface may be specified or calculated. If the soil is normally consolidated the bounding surface and the yield surface pass through the stress point (initial stress). The position of the yield surface can be calculated from the translation rule.

If the soil is overconsolidated the position of the yield surface can be calculated from the initial stress and the size of the surface.

CHAPTER 6

APPLICATION OF MODELS TO SOME SOIL MECHANICS PROBLEMS

Introduction

In this chapter the models developed in chapters 3 and 4 are used to obtain solutions to some soil mechanics problems by the finite element procedure described in chapter-5. Particular importance is given to the influence of anisotropy in these problems. The influence of anisotropy on the load-displacement response, stress, displacement, and pore-pressure distribution and stability is studied. Where analytical solutions exist, comparisons will be made. As plastic deformation leads to large strains, geometric nonlinearity is included in the analysis.

Both two and three-dimensional problems are studied. In most cases, only monotonic loading conditions will be investigated, in order to keep computational costs low. In a few cases general loading conditions will be investigated.

The problems analysed are;

(a) Strip Footing(plane strain analysis)

(b) Rectangular Footings(three-dimensional analysis)

(c) An Embankment on clay layer(plane strain analysis)

Strip Footing(Plane Strain analysis)

Pressure-Independent Model

In this section the models developed in chapter-3 are used in the analysis of a footing on a layer of clay under plane strain and undrained conditions. The pressure-independent models are used in the short-term undrained analysis of clays. These models give no information on the pore-pressure-development. However, the pressure-independent models are easy to use and can give good information on the displacement and stability of structures on undrained clays. For monotonic loading conditions, the isotropic-hardening model can be used to give reasonable answers (44). Therefore in most cases studied here, the isotropic-hardening model will be used as it is simple to use and computational costs are low.

In figure 6.1 the curve labeled b=1.0 shows the load displacement response of a strip footing of total width 2.0 ft on a layer of isotropic undrained clay. The clay is assumed to behave as a perfectly plastic material. The properties required for the analysis are the elastic modulus E and the yield strength or cohesion. The value of the possions ratio is taken as .485 which is calculated from the incompressibility condition (The exact value should be .5, but this

leads to a singular matrix and an alternate formulation has to be used). The values of the parameters used in the analysis are assumed as,

$$E = 30000.\ psi$$

$$\nu = .485$$

$$C = 17.5\ psi$$

The clay layer is analysed by using 36 elements and 15 load increments. Geometric nonlinearity is also included in the analysis. The load displacement curve shows an initial linear response. At a load of about 55.0 psi initial yielding takes place. From here, the load displacement curve shows a nonlinear response and reaches collapse at a load of 95. psi. Figure 6.1 also shows the limit load for isotropic clay. This is calculated as 5.14 C where C is the cohesion. The finite element results are close to the exact solution. The theoritical value of the limit load is 90. psi, where as the finite element analysis predicts a value 95. psi. It is extremely difficult to capture numerically the exact limit loads for perfectly-plastic media. A very fine mesh and small load increments are needed. However the limit loads obtained are cloase enough. Also in the analysis a clay layer of finite depth was assumed, where as in the theory a layer of infinite thickness is assumed.

To study the influence of anisotropy, a parameter b is defined as the ratio of the strength in the vertical direction to the strength in the horizontal direction. Two cases of anisotropy are studied, $b = 1.42$ and $b = .707$. The strength terms in shear and the elastic moduli are assumed to be proportional to b. The parameters used are given in the table 6.1. Figure 6.1 illustrates the influence of anisotropy on the load displacement response and limit loads.

The Poisson ratios are calculated from the incompressibility condition and $M_{33} = \frac{1}{b^2}$ It can be seen that anisotropy influences both the load displacement response and the limit loads. Table 6.2 compares the theoritical limit loads for the anisotropic clay with the finite element results. Theoritical results for the limit load on anisotropic clay have been obtained by Christian and Davis (19) and Chen (26). Christian and Davis (19) used the results of Hill(29) to obtain a lower bound solution for the limit loads of a strip footing on anisotropic undrained clays. Chen (26) used limit analysis to obtain limit loads. The finite element results are close

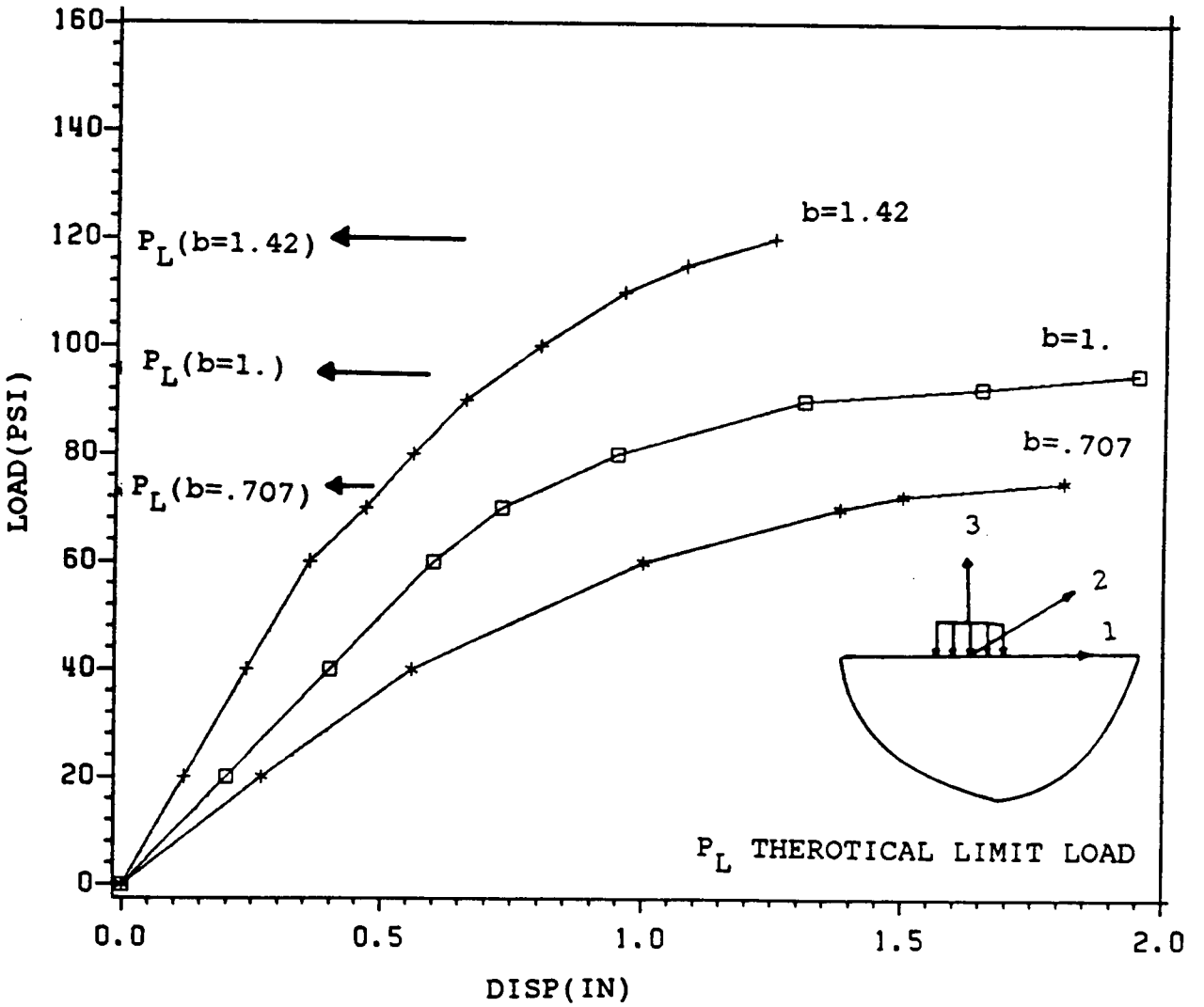

Figure 6.1: Influence of Anisotropy

Table 6.1 Properties for plane strain analysis-Undrained

b	E_1 psi	E_3 psi	G_{13} psi	G_{12} psi	M_{66}
.707	30000.	21210.	7189.	10170.	6.0
1.00	30000.	30000.	10170.	10170.	3.0
1.42	30000.	44260.	14400.	10170.	1.5

to the theoritical results, even though the failure criteria used in the theoritical analysis is different from the one developed in chapter 3.

The above analysis shows that the model along with the finite element analysis are satisfactory to obtain limit loads and load displacement relations for undrained anisotropic clays.

In figure 6.2 the ratio of the bearing capacity for anisotropic clays, to the bearing capacity for isotropic clays R_{pu}, is plotted for various values of b. As b tends to zero, the bearing capacity also tends to zero. For values of b less than 1.0, the bearing capacity is influenced essentially by the vertical strength. For values of b greater than 1.0, the bearing capacity increases with b, and the bearing capacity is influenced by both the vertical and horizontal strengths.

The results presented above are obtained assuming the clay behaves as an elastic-perfectly plastic media. This assumption is useful for obtaining limit loads. Most soils exhibit an initial elastic response, followed by a elastic-plastic hardening behavior. Finially at failure a perfectly plastic state is reached. To obtain the complete response of the footing, the hardening behavior of the clay has to be taken into account. In many cases linear hardening may be assumed. A linear hardening material is one which has a linear stress-strain response after initial yield.

Figure 6.3 shows the influence of hardening on the load displacement response. To study the influence of hardening, an anisotropic clay with b=.707 is analyzed. The properties of this clay are given in table 6.1. For simplicity, linear hardening is assumed. In this case there is no limit load and the load displacement curve always rises. The load displacement response is investigated for various values of H/E ratio, where H is the plastic modulus. H/E=0. implies perfectly plastic behavior and $H = \infty$ implies elastic behavior. Figure 6.3 shows the load displacement response for H/E ratios of 0, 1. and ∞ for an anisotropic clay. Hardening can greatly influence the load-displacement response.

Figure 6.4 compares the spread of yielding in anisotropic and isotropic clays at a load of 70. psi. The distribution of the yielded zone under the load is influenced greatly by the

Table 6.2 Comparison of limit loads

b	P_l(theory)	P_l(FEM)
.707	69.0	74.0
1.00	90.	95.0
1.42	116.0	120.0

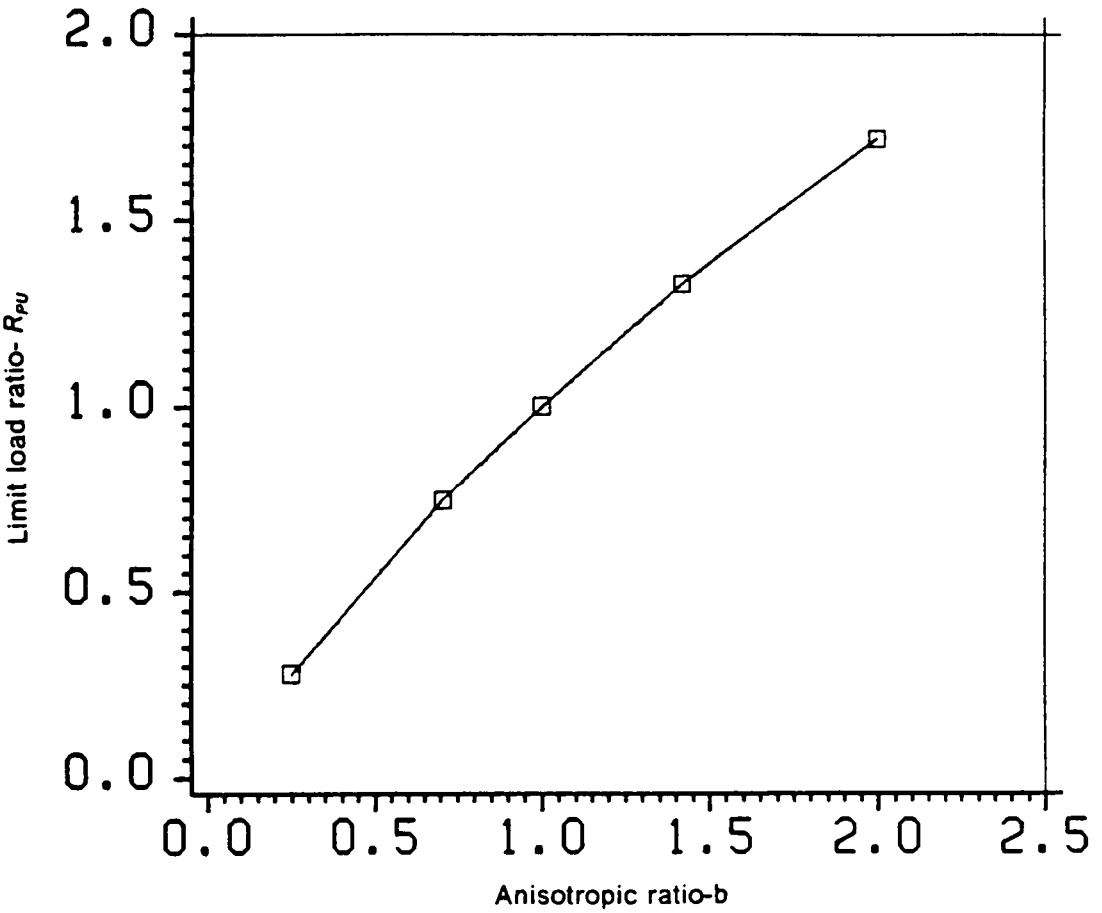

Figure 6.2:Influence of Anisotropy-Strip Footing

anisotropic strength of the soil. The anisotropic clay with b = .707 has reached collaspe at this load, where as the clay with b = 1.42 has just begun to yield.

Figure 6.5 compares the surface displacement profiles for both isotropic and anisotropic clays. It can be seen that anisotropy does not influence the surface profile, although the magnitude of the displacement is greatly influenced by the anisotropy of the clay.

The strip footing has also been analyzed using the multisurface model. An isotropic clay is used in the analysis. The properties of the clay are;

E = 30000. psi

v = .48

C = 17.5 psi

To simplify the analysis, a soil with linear hardening is assumed (E/H = 1.0). In this case only two surfaces are needed for the analysis. An inner yield surface and an outer failure surface. The parameters of the surfaces are given in table 6.3.

Figure 6.6 compares the response of the footing predicted by the multisurface model and the isotropic hardening model for monotonic loading conditions. The results of the two analysis sre similar. The results obtained are close because linear hardening has been assumed and the loading is monotonic and proportional. In general, the results would be different as the plastic modulus varies continuously in the isotropic-hardening model and varies in a piece-wise linear manner in the multisurface model. Note that in case of the multisurface model, the soil at the end of the loading is no longer isotropic.

The same problem is analysed for a single cycle of loading, using the multisurface model. Figure 6.7 shows the load-displacement response for a load-unload-reload condition. The initial response on loading is elastic. When the stress point reaches the yield surface, the surface translates with the stress point and both elastic and plastic strains are obtained. Upon unloading, the initial response is elastic. However, when the stress point reaches the yield surface, plastic flow occurs. On reloading, the initial response is again elastic, followed by plastic flow. The multisurface model can therefore predict the hysteric response of the soil.

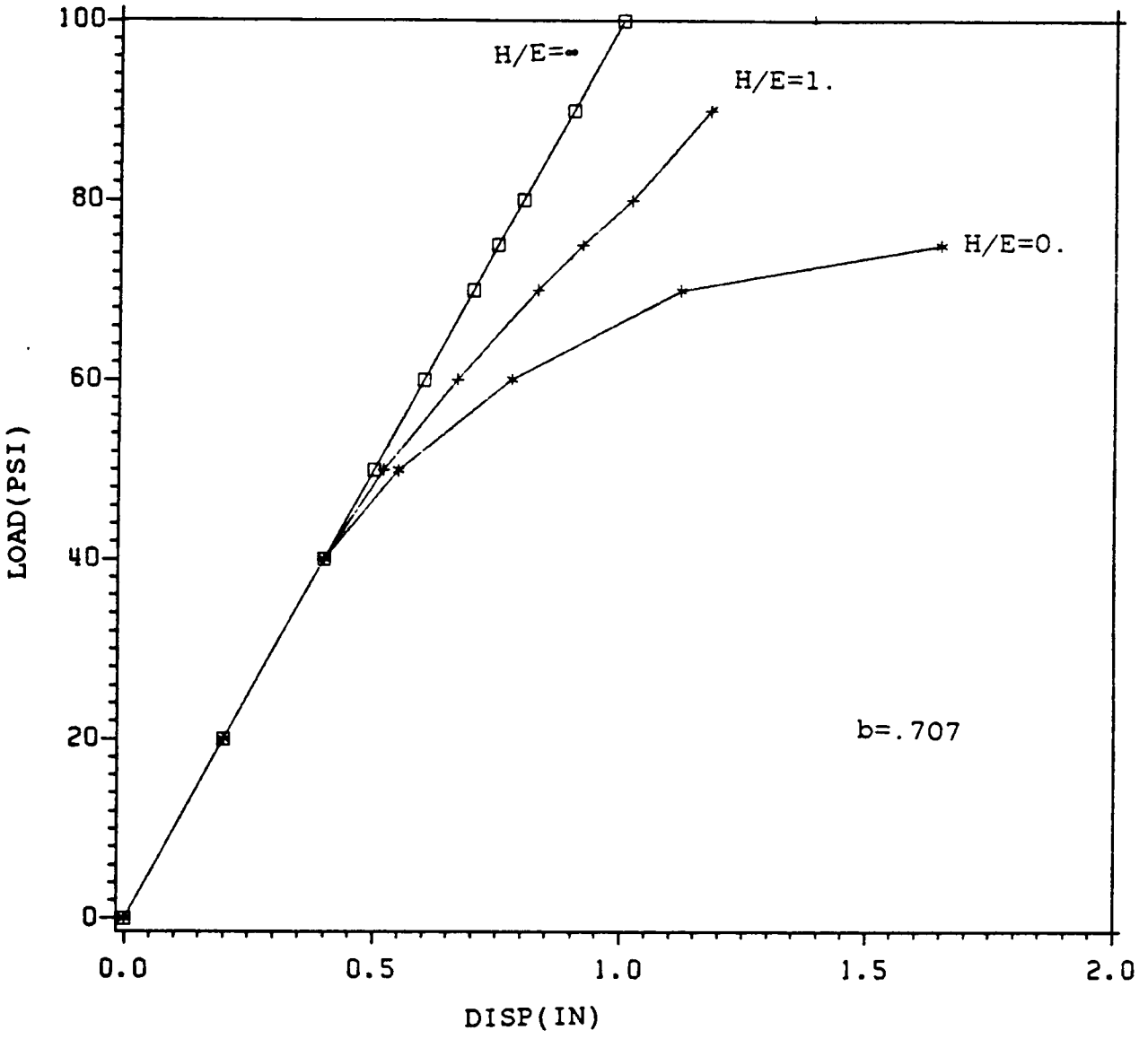

Figure 6.3: Influence of hardening on load displacement response of strip footing

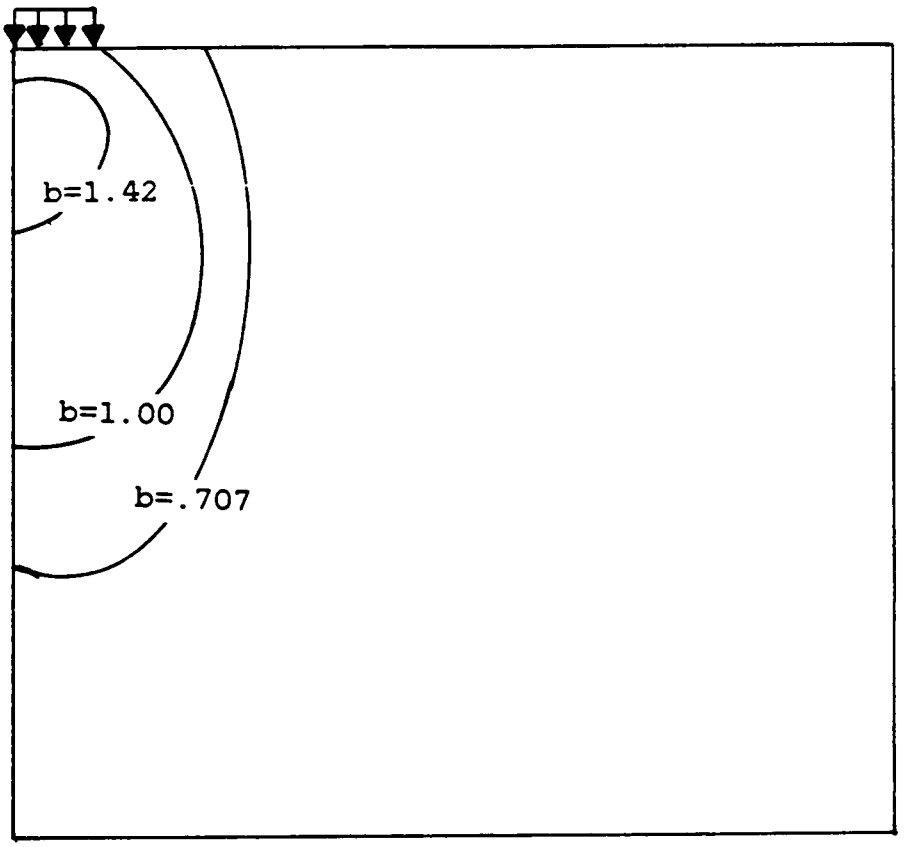

Figure 6.4: Yield zones under strip footing-Undrained condition

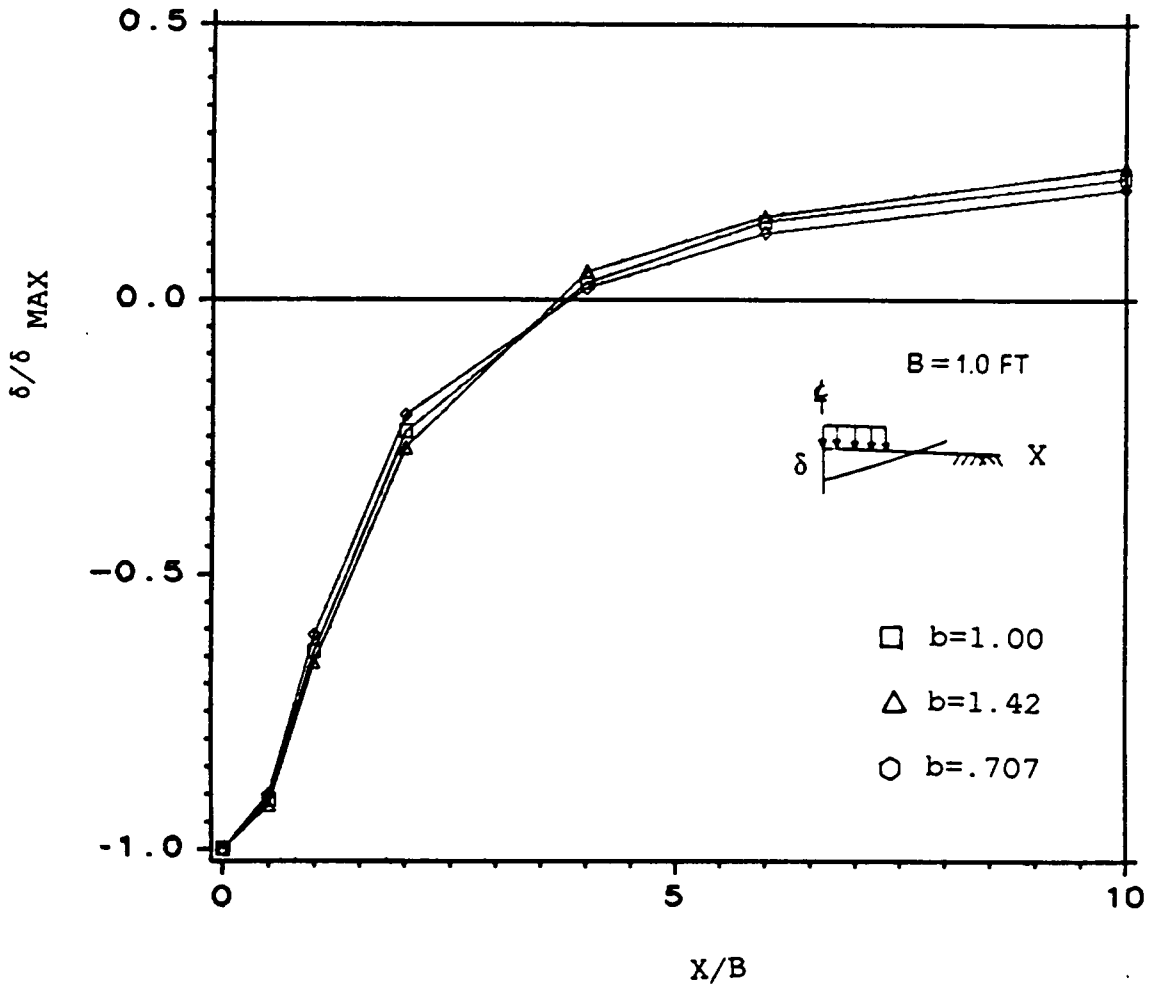

Figure 6.5: Surface profile-Undrained analysis

Table 6.3 Properties for multisurface model

N	size(P) psi	H psi	α psi
1	35.000	30000.	0.0
2	105.00	0.0	0.0

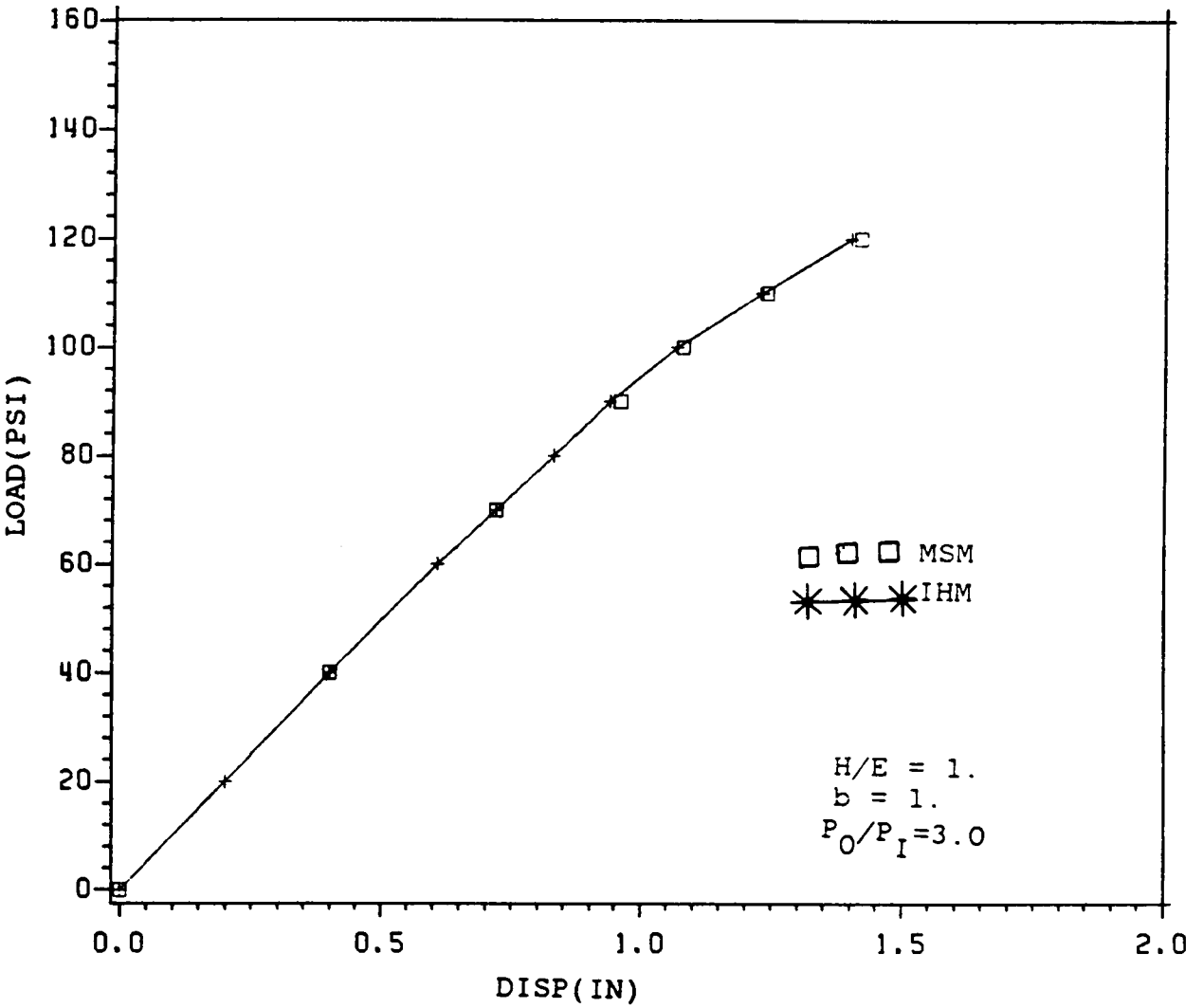

Figur Figure 6.6: Load displacement response of footing-Monotonic loading

In the isotropic-hardening model, the unloading is elastic; hence it cannot predict the hysteric behavior of the soil.

In the multisurface model developed here, the sizes of the yield surfaces do not change with plastic deformation. To predict realistic behavior of the clay under cyclic loads, the size of the yield surfaces should be made a function of the plastic strain. The size of the yield surfaces should decrease with increasing plastic strain. This gives better agreement with observed results. The model developed here assumes that the surfaces are of constant size. However, this model gives reasonable results for a small number of loading cycles.

In all the cases analysed the clay layer was assumed to be homogenous. Generally the clay strength increases linearly with depth and this case can be easily incorporated in the analysis.

Pressure-Dependent Model

(1) Drained Analysis

In this section the models developed in Chapter-4 are used in the analysis of a footing on a layer of clay under plane strain conditions. The problem analysed is a strip load on the surface of the soil. Also a surcharge of 250. psf is applied on the surface.

This problem is analysed under both drained and undrained conditions. The pressure-independent models which were used in the previous section gave no information about the pore-pressure-development. This information is needed for a complete understanding of the problem. The procedure for imposing the undrained condition and calculating the pore-pressures is given in Chapter-4. Because the behavior of the soil depends on the consolidation pressure, a method for calculating the initial conditions in the ground is given in Chapter 5. Here the influence of anisotropy is investigated on the load deformation response, pore-pressure-development, and stress and displacement distribution.

The clay used in the analysis is Weald clay. The properties of the clay are taken from reference (44). Figure 6.8 shows the load displacement response of a strip load on a

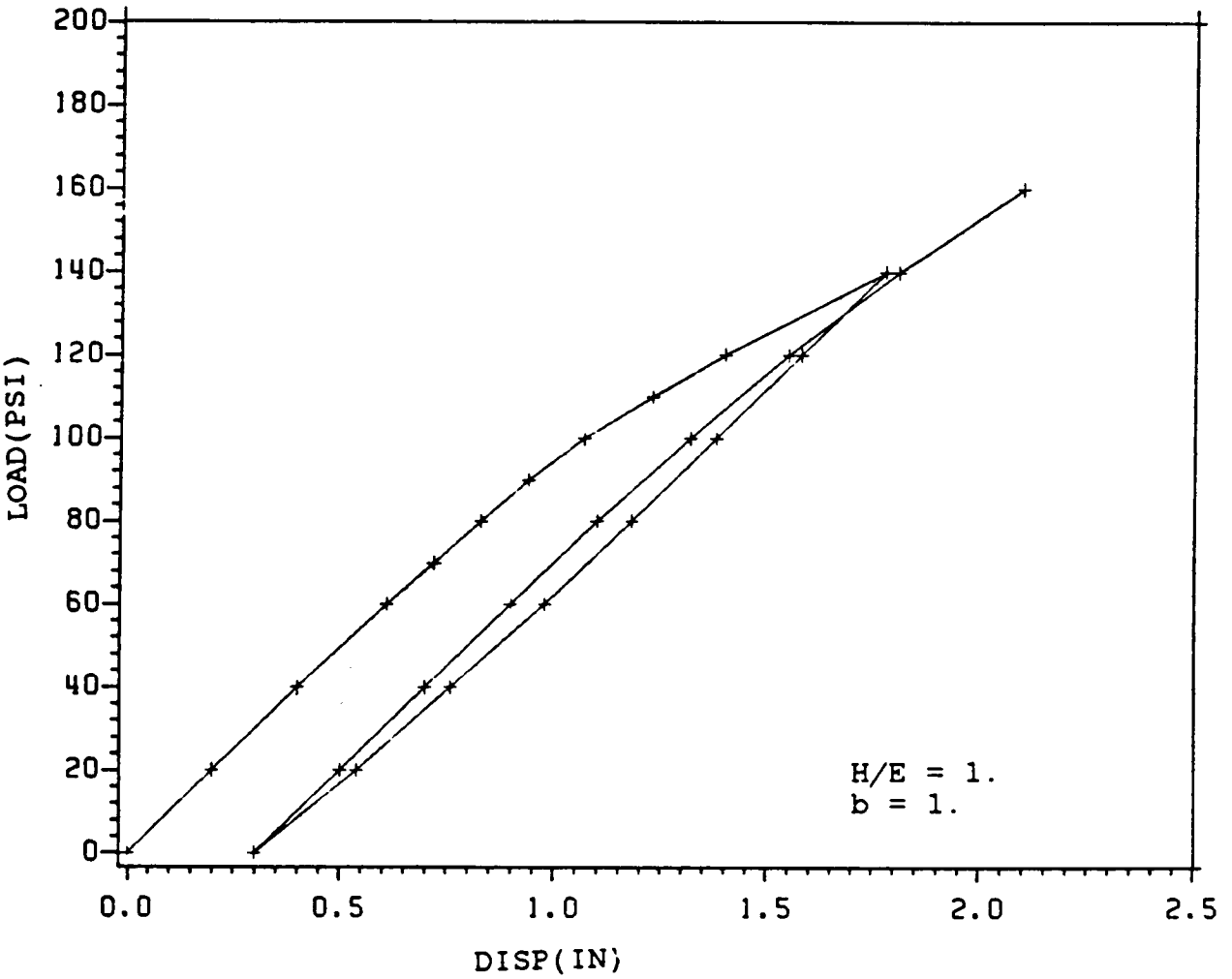

Figure 6.7: Load displacement response of footing-Cyclic loading

normally-consolidated isotropic clay (b=1.0). Figure 6.8 also illustrates the influence of anisotropy on the load displacement response for various values of b. Where b is the ratio of the effective failure strength in the vertical direction to the effective failure strength in the horizontal direction. (b is the ratio of the slope of the failure surface in the vertical direction to the slope of the failure surface in the horizontal direction). The shear strength and the elastic moduli are taken in proportion to b. These are given in table 6.4.

The properties of the isotropic clay are assumed as;

$K_0 = 1.0$

density = 100. psf

$\lambda = .092$

$\kappa = .027$

$\nu = .3$

G = 144000. psf

φ = 22. degrees (n=.87)

For the isotropic soil, φ = 22. degrees corresponds to a n value of .87 in the triaxial test. Under plane strain conditions, the failure condition for the isotropic soil can be made equivalent to the Mohr-Columb criteria by replacing n by n_{mc} . Where n_{mc} is given as;

$$n_{mc} = \frac{\sin\varphi}{(3 + \sin^2\varphi)^{.5}} \tag{6.1}$$

This equation can be obtained by equating the Mohr-Columb criteria and the failure criteria of the isotropic soil under plane strain conditions. For φ = 22. degrees the value of n_{mc} is .215. This value of n is used in the analysis. This is done because in most limit analysis of frictional media, the Mohr-Columb criteria is used to obtain limit loads. The elastic properties and the anisotropic strength parameters are given in the table below. Geometric nonlinearity is also included in this analysis.

Table 6.4 Properties for plane strain analysis-Drained

b	E_1 psi	E_3 psi	G_{13} psi	G_{12} psi	M_{66}
1.00	374400.	374400.	144000.	144000.	3.0
1.20	374400.	449280.	177400.	144000.	2.1
1.42	374400.	541648.	204480.	144000.	1.5

The value of the Poisson ratios is taken as .30 and $M_{33} = \frac{1}{b^2}$. It can be observed in figure 6.8 that no limit condition is reached. This is because the mode of failure in the finite element analysis is very different from that assumed in limit analysis. The footing undergoes progressive failure in the finite element analysis. This is because the soil developes plastic strains from the start of loading,(in a normally consolidated soil the stress point at the start of loading is on the yield surface). This type of response is typical of many soils, as most soils exhibit a nonlinear response well before the failure state is reached. Hence the ultimate load is to be estimated from some ultimate deformation criteria. The theoritical limit load for the isotropic soil is 2400. psf.

To define the ultimate load, the displacement due to the theoritical limit load on an isotropic soil, is taken as the allowable displacement. The load which causes the same displacement on an anisotropic soil, is defined as the ultimate load for the anisotropic soil. Figure 6.9 plots the ratio of the ultimate load for an anisotropic soil to the ultimate load for an isotropic soil R_{pd} versus b. It is observed that a small change in b, causes a large change in the ultimate load. this is in contrast with the undrained analysis of the previous section, where a small change in b causes a proportional change in the ultimate load. This is because for frictional media, the ultimate load is proportional to the tangent of the friction angle, whereas for a cohesive media the ultimate load is directly proportional to the cohesive strength. It should be noted that unlike the undrained case, the bearing capacity is also a function of the footing width. However the above analysis gives a indication of the influence of anisotropy on the displacements and failure of the footing. To obtain the response of a specific problem, the program developed will have to be used.

Figure 6.10 illustrates the surface profile under drained loading. As before anisotropy influences the maximum displacement, but not the shape of the profile. Note also that the shape of the profile is different from the shape of the profile under undrained loading. This is because in this case volume change under loading takes place, whereas under undrained loading there is no volume change.

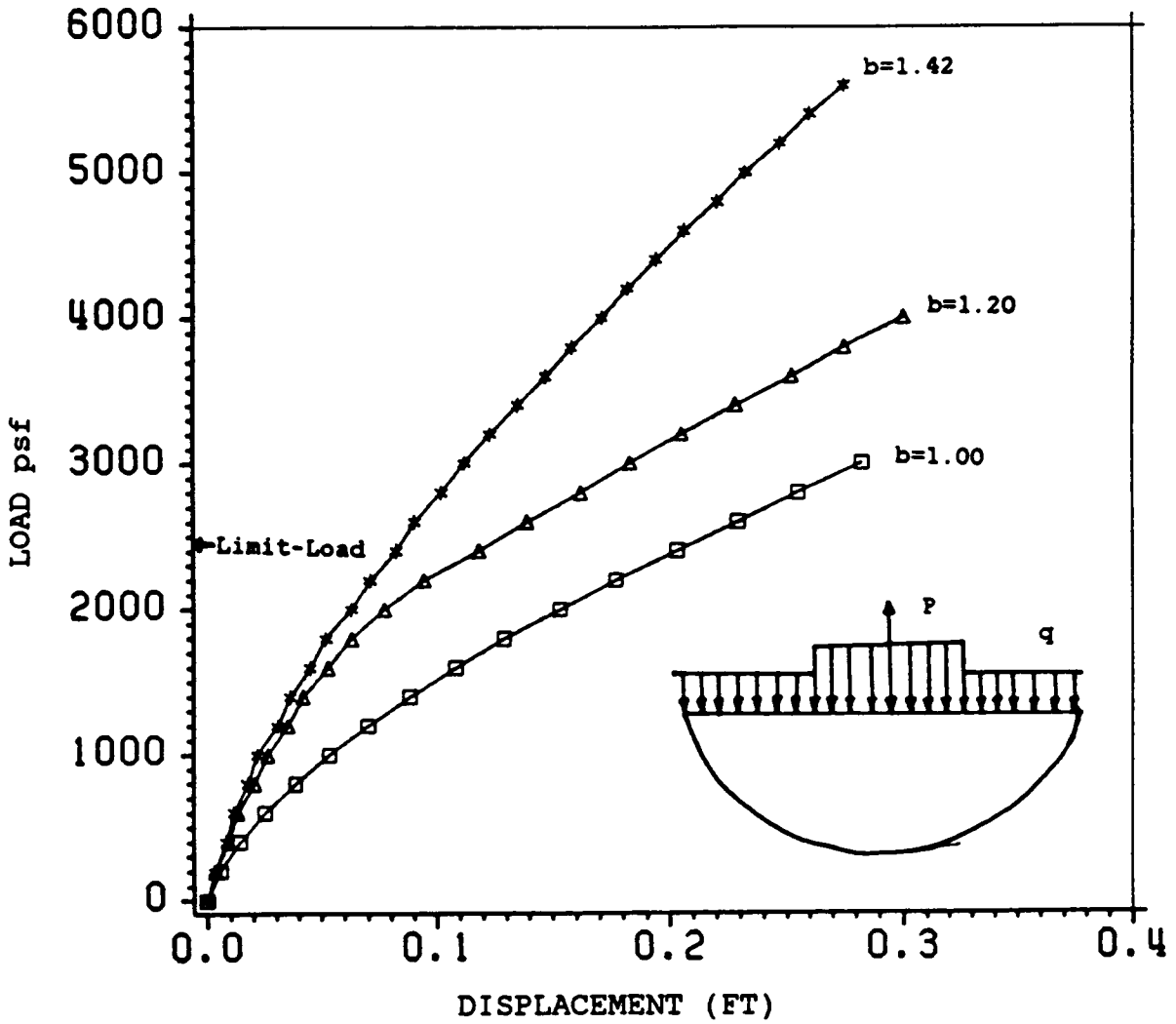

Figure 6.8 Drained Load-Displacement Response-Strip Footing

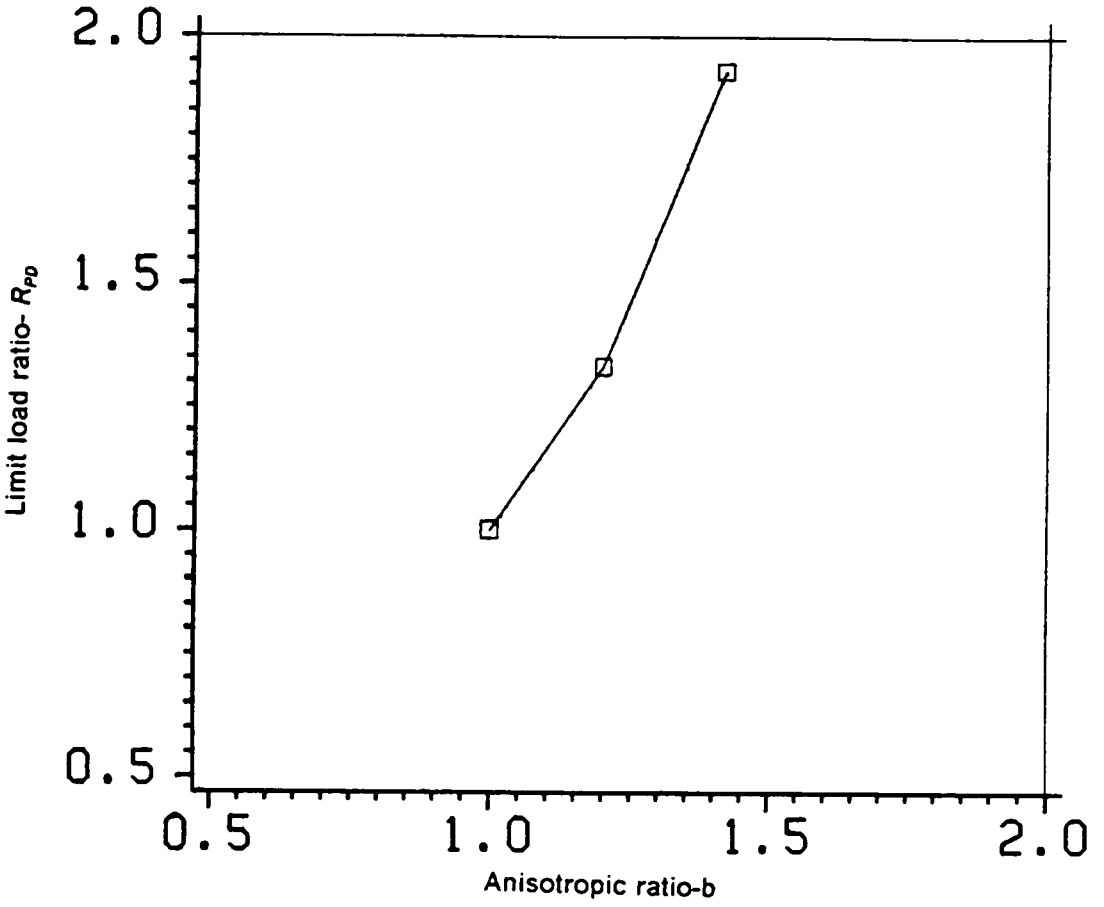

Figure 6.9:Influence of Anisotropy-Strip Footing

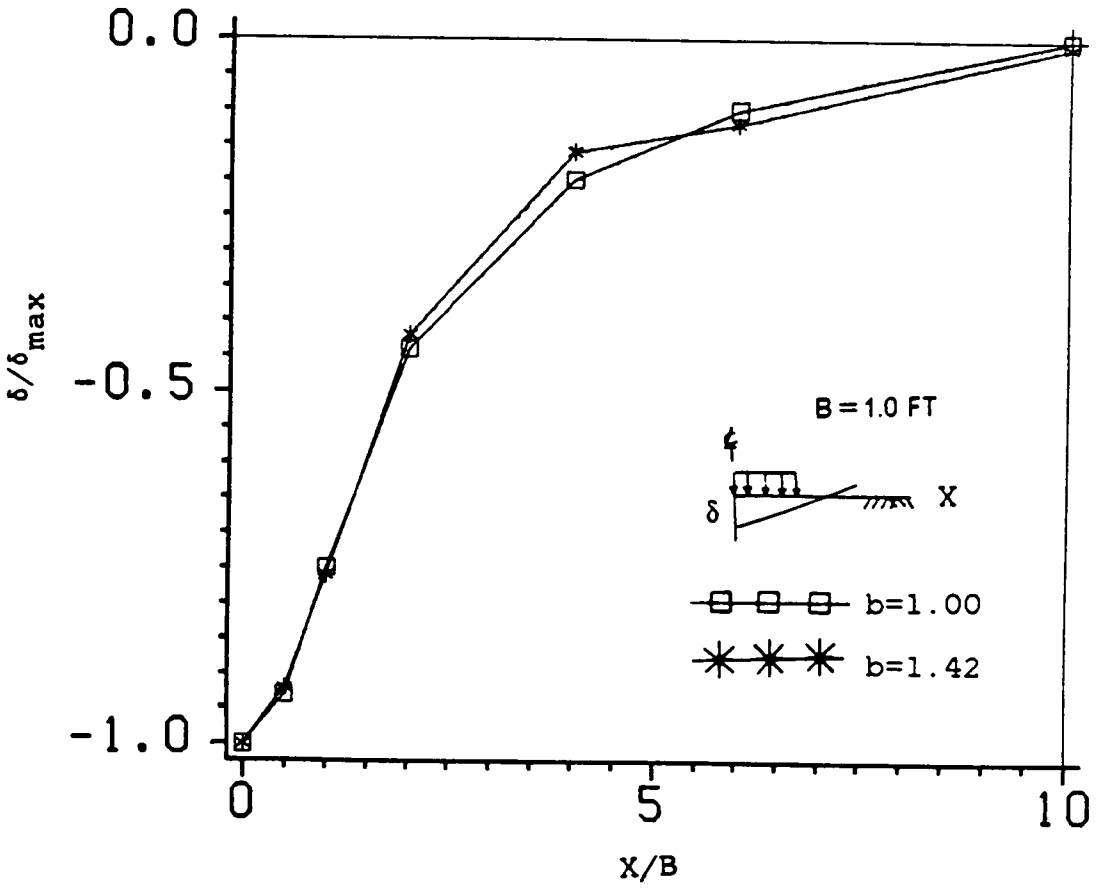

Figure 6.10:Surface Profiles-Drained Analysis

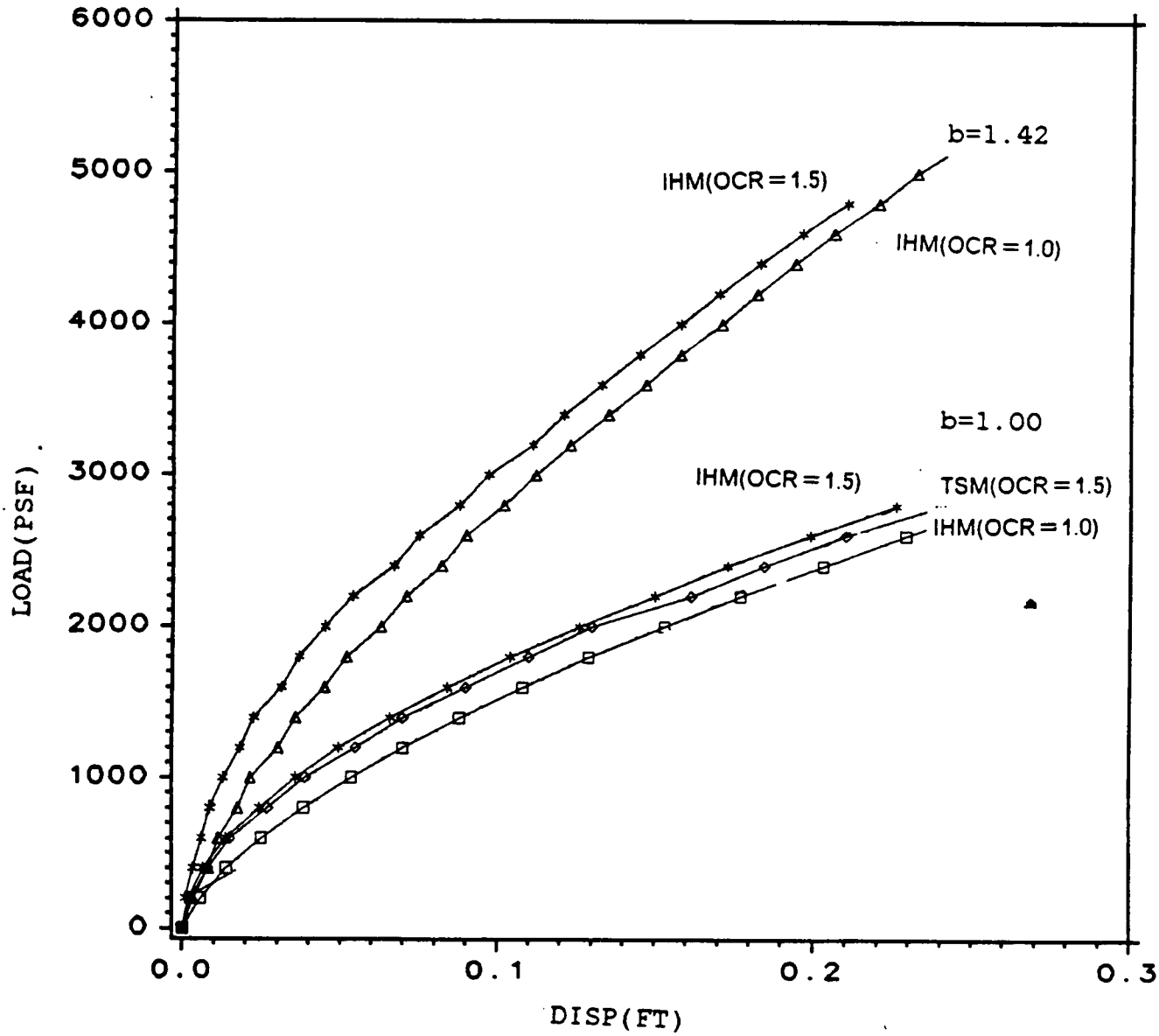

Figure 6.11: Influence of OCR on load displacement response of footing

Figure 6.11 compares the load-displacement responses of a normally consolidated clay with a clay of overconsolidation ratio of 1.5. Both isotropic and anisotropic clays are analysed. It it observed that the overconsolidated clay exhibits a stiffer resonse. This is because initially the load response of the overconsolidated clay is elastic, where as the normally consolidated exhibits an elasto-plasto response from the start. Figure 6.11 also compares the response of the overconsolidated soil predicted by the isotropic hardening model and the two-surface model. The two-surface model response is softer than the response of the isotropic hardening model. This is because of plastic flow below the consolidation surface. However at this low overconsolidation ratio, the responses predicted by the two models are not very different. At higher overconsolidation ratios the predictions can be significantly different. Clays with higher overconsolidation ratios are not analysed, as these clays exhibit softening.

(2) Undained Analysis

Here the same problem is analysed under undrained conditions, using the pressure dependent model. The procedure for imposing the undrained condition is given in chapter 4. Figure 6.12 illustrates the undrained load displacement response for an isotropic and an anisotropic soil. The influence of anisotropy on the load displacement response is significant, but not as large as in the drained analysis. Compared to the drained analysis, the undrained response is stiffer. This is to be expected, as the undrained modulus is always higher than the drained modulus.

Figure 6.13 illustrates the surface profiles for undrained loading. The surface profiles are similar to those obtained using the pressure-independent model, but are different from the profile in the drained analysis. This is because no volume change takes place in the undrained analysis.

Figure 6.14 illustrates the influence of anisotropy on the pore-pressure development below the footing. In figure 6.14 the ratio of the pore pressure to the pore-pressure developed

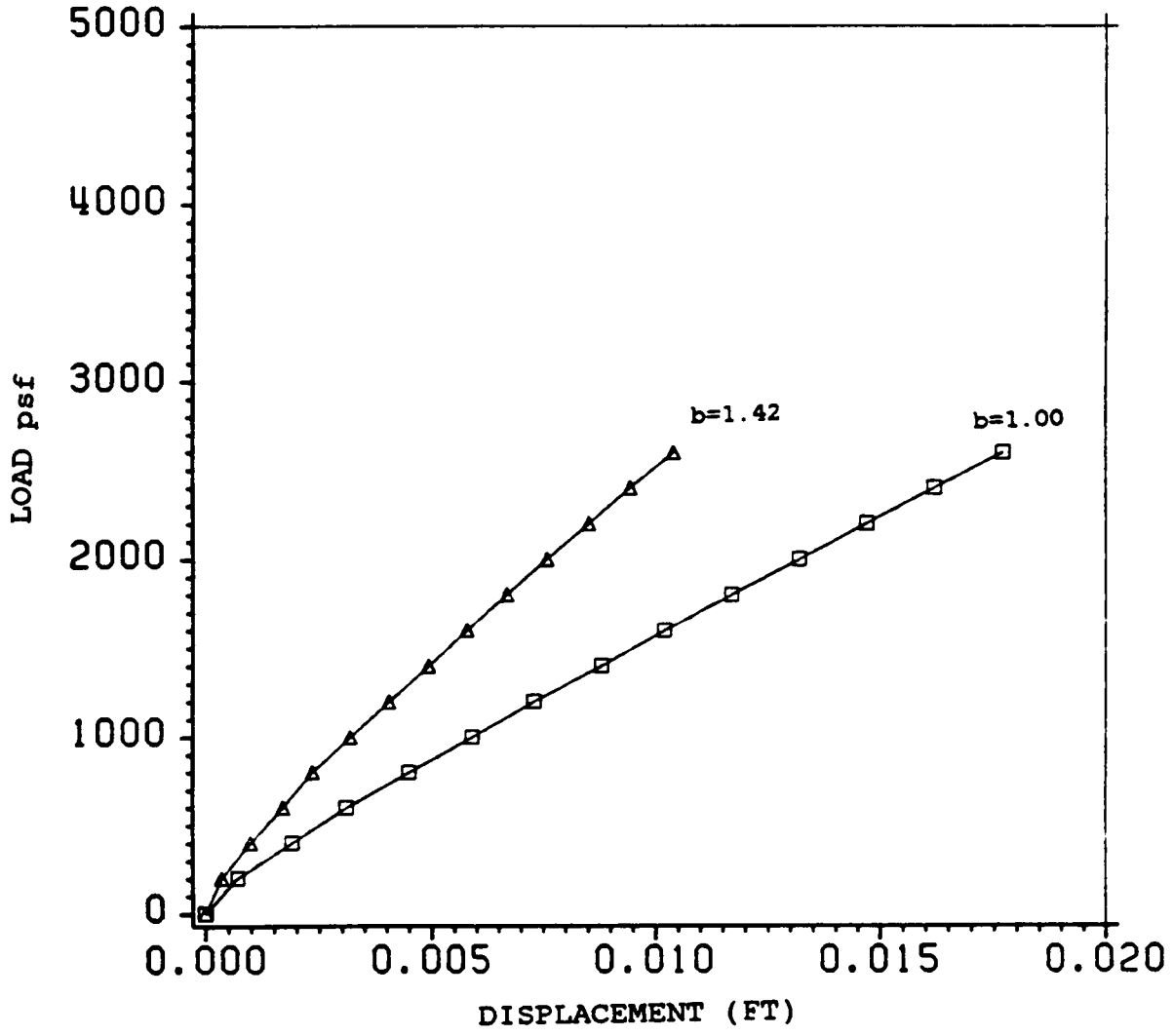

Figure 6.12 Load-Displacement Response-Undrained Analysis

at the surface of the isotropic soil is plotted with depth. The isotropic soil developes a higher pore-pressure, as it undergoes higher plastic straining compared to the stiffer anisotropic soil.

It should be noted that unlike the elastic case, the pore-pressure profiles change with the level of loading. This is because the pore-pressure developed at any depth dependes on its stress state. The pore-pressure profiles plotted in figure 6.14 are plotted at low stress levels. This is because at stress states close to failure, the method used to obtain the undrained condition leads to numerical problems.

Rectangular Footings(Three-Dimensional Analysis)

Pressure-Independent Model

In this section the response of rectangular footings on undrained clays is analysed and the isotropic-hardening model is used in the analysis.

Figure 6.15 shows the load displacement response of a square footing of size 2.0 ft by 2.0 ft on a layer of isotropic clay. The material is assumed to be perfectly-plastic. The parameters used in the analysis are assumed as,

$$E = 30000.\ psi$$

$$v = .485$$

$$C = 17.5\ psi$$

Figure 6.15 also compares the limit load (classical solution 6.0C) with the results of the finite element analysis. Good comparison is obtained. The theoretical limit load is 100. psi, where as the finite element analysis predicts a value of 104.0 psi.

Figure 6.15 also shows the influence of anisotropy on the load displacement response and limit loads. As before, both the shear strength and the elastic moduli are taken proportional to b. The parameters assumed in the analysis are given in table 6.5.

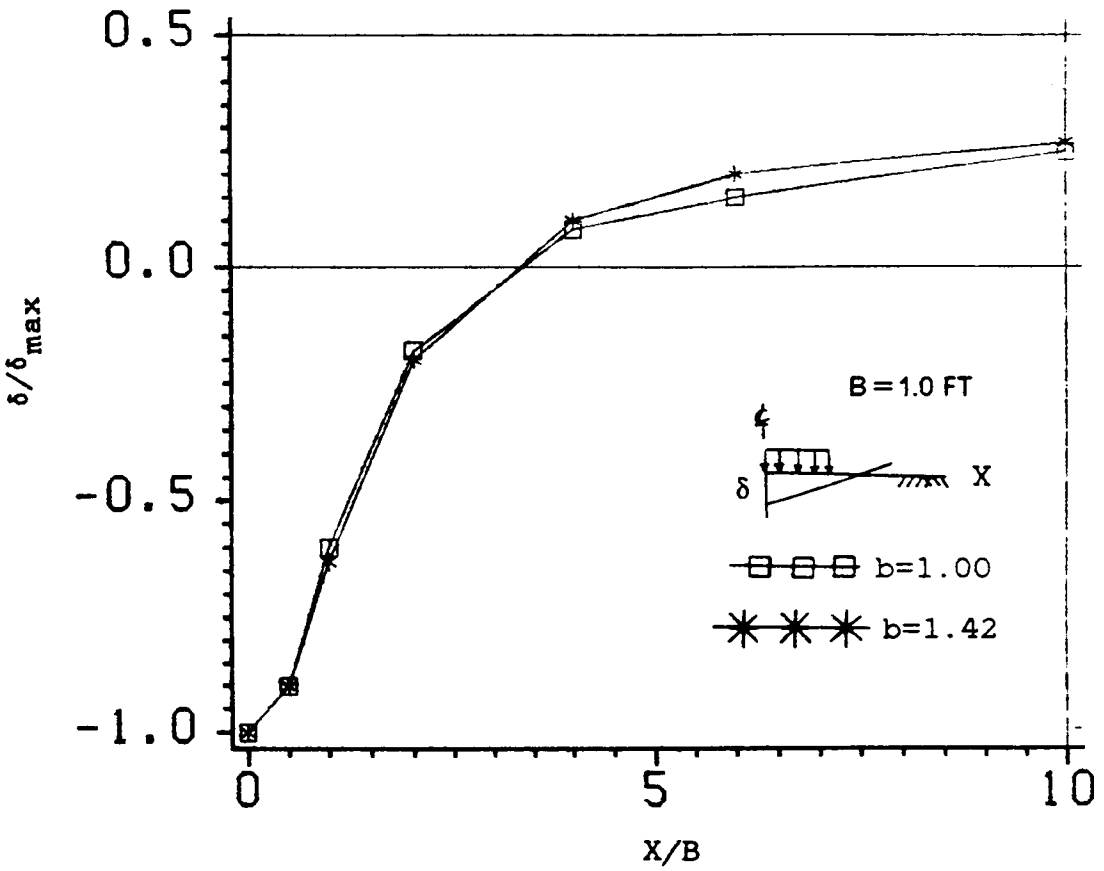

Figure 6.13:Surface profile-Undrained Analysis

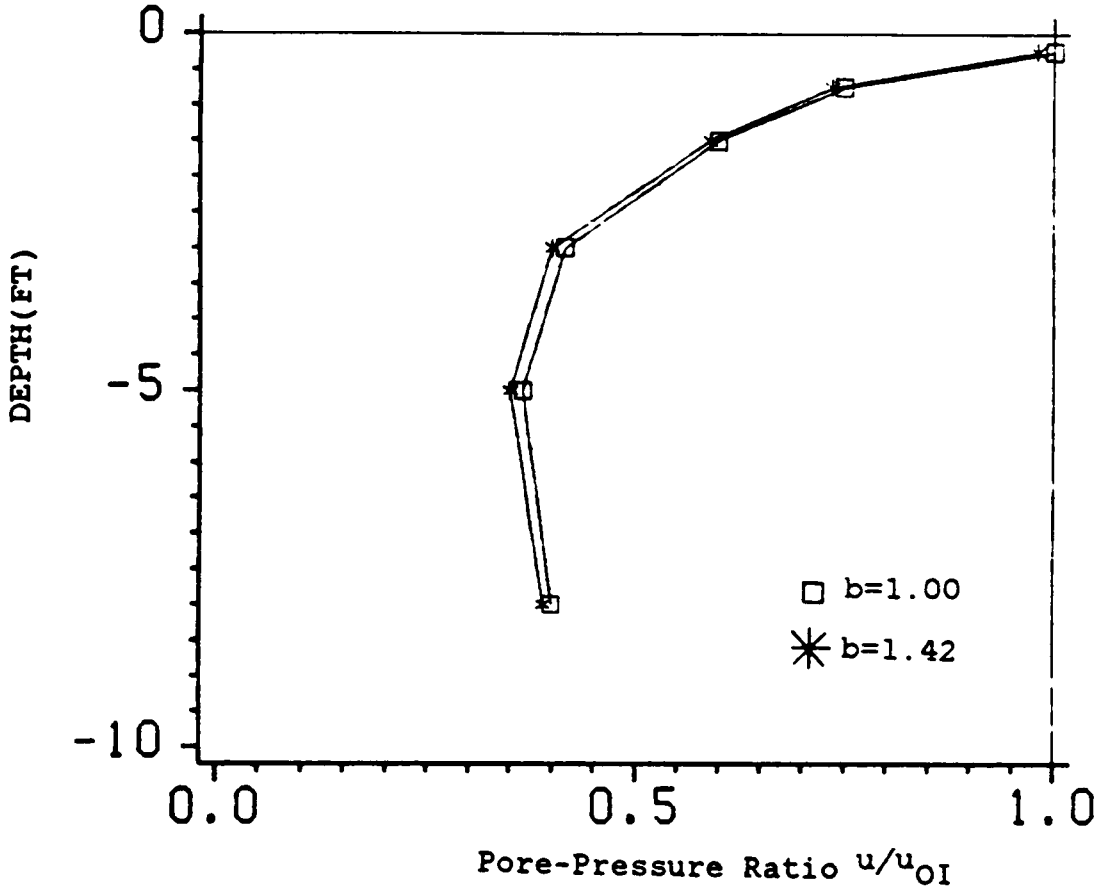

Figure 6.14 Pore-Pressure Distribution-Strip Footing

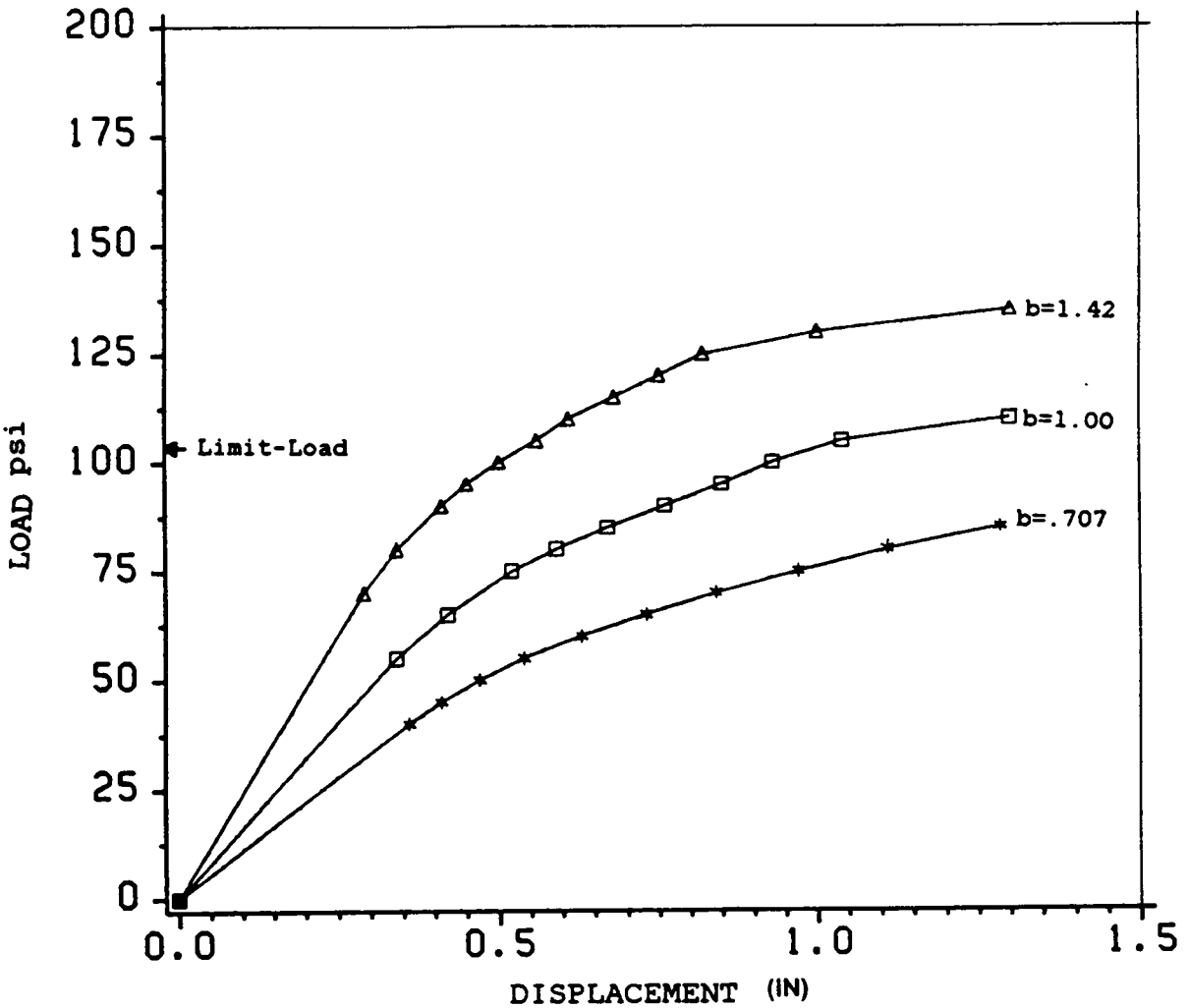

Figure 6.15 Undrained Load-Displacement Response-Square Footing

Table 6.5 Properties for three dimensional analysis-Square footing

b	E_1 psi	E_3 psi	G_{13} psi	G_{12} psi	M_{66}
.707	30000.	21210.	7189.	10170.	6.0
1.00	30000.	30000.	10170.	10170.	3.0
1.42	30000.	44260.	14400.	10170.	1.5

The anisotropy of the clay has a significant influence on the deformation and failure of the footing. In figure 6.16 the ratio of the anisotropic limit load to the isotropic limit load R_{su} is plotted versus b. As b increases the anisotropic limit load increases. Compared to the plane strain case, the influence of b is less siginificant for the square footing. This is because of the three dimensional stress distribution below the footing and the limited zone of influence of the square footing.

Figures 6.17 and 6.18 illustrate the surface profiles and yielding for isotropic and anisotropic clays. Anisotropy influences the maximum displacement, but not the shape of the profile. However both the surface profile and the spread of yield are different compared to the plane strain analysis. This is again due to the three dimensional nature of the problem.

Figures 6.19 and 6.20 illustrate the influence of orthotropy on the response of a square footing. To study the influence of orthotropy, o is defined as the ratio of the lateral strength to the horizontal strength. o=1.0 represents a cross anisotropic soil. In this case a soil with b=1.42 is used in the analysis, where b is the ratio of vertical strength to horizontal strength. The properties used in the analysis are given below and table 6.6.

The elastic and strength parameters in the 1-3 plane are, E_1 = 30000. psi, G_{13} = G_{23} = 14400. psi and M_{55} = M_{66} = 1.50. It can be observed that orthotropy can have a significant effect on the limit loads. In figure 6.20 the ratio of the limit load for the orthotropic soil to the limit load for the cross-anisotropic soil R_{sou} is plotted versus o. Orhotropy can have a large effect on the limit loads, but the effect of orthotropy on the limit loads is less significant than the effect of cross-anisotropy.

Figures 6.21 and 6.22 illustrate the response of a rectangular footing of size 2.0 ft by 4.0 ft on undrained anisotropic clays. The parameters used in the analysis are the same as used in the analysis of the square footing. As before anisotropy influences both the deformation and failure of the footing. In figure 6.22 the ratio of the limit load for anisotropic soil to the limit load for an isotropic soil for a rectangular footing R_{ru} is plotted versus b. Also plotted are similar curves for a strip and square footing. The rectangular footing exhibits a response in between the strip and square footing.

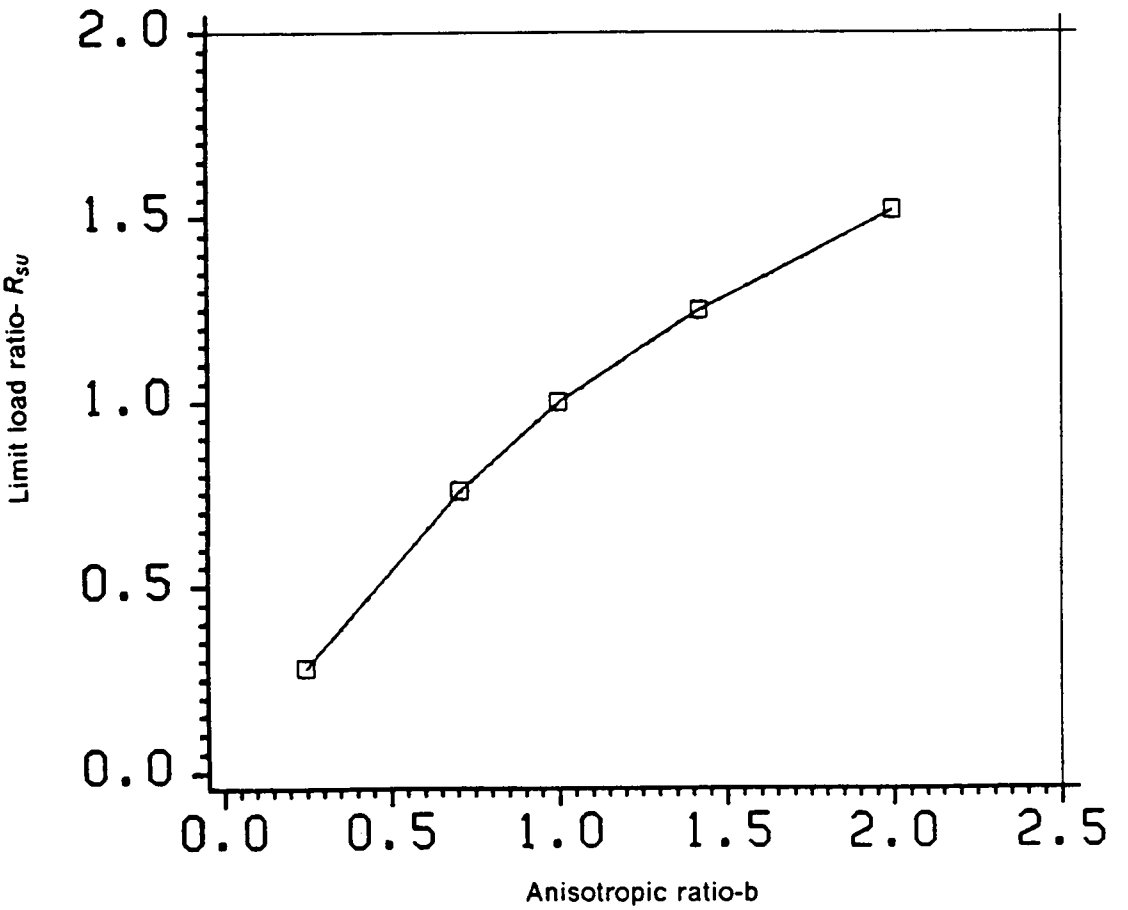

Figure 6.16: Influence of Anisotropy-Square Footing

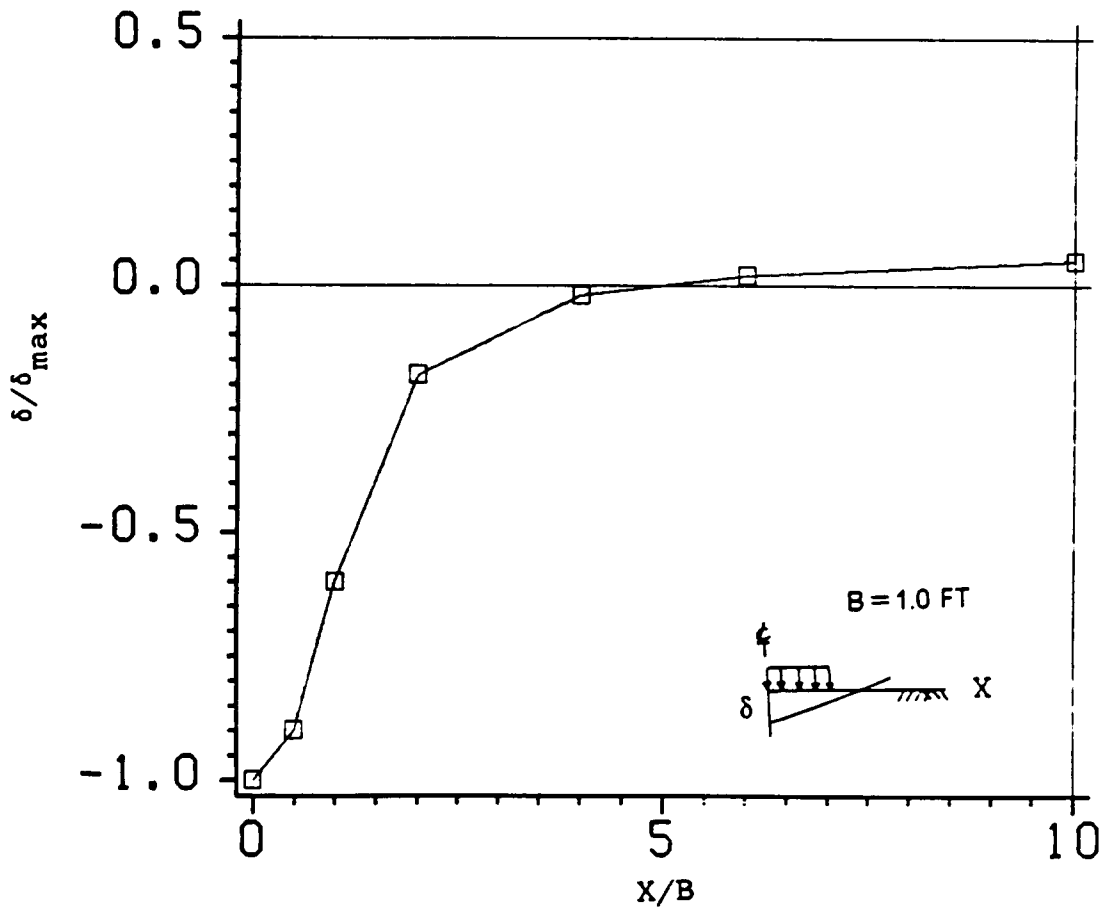

Figure 6.17:Surface Profile-Square Footing

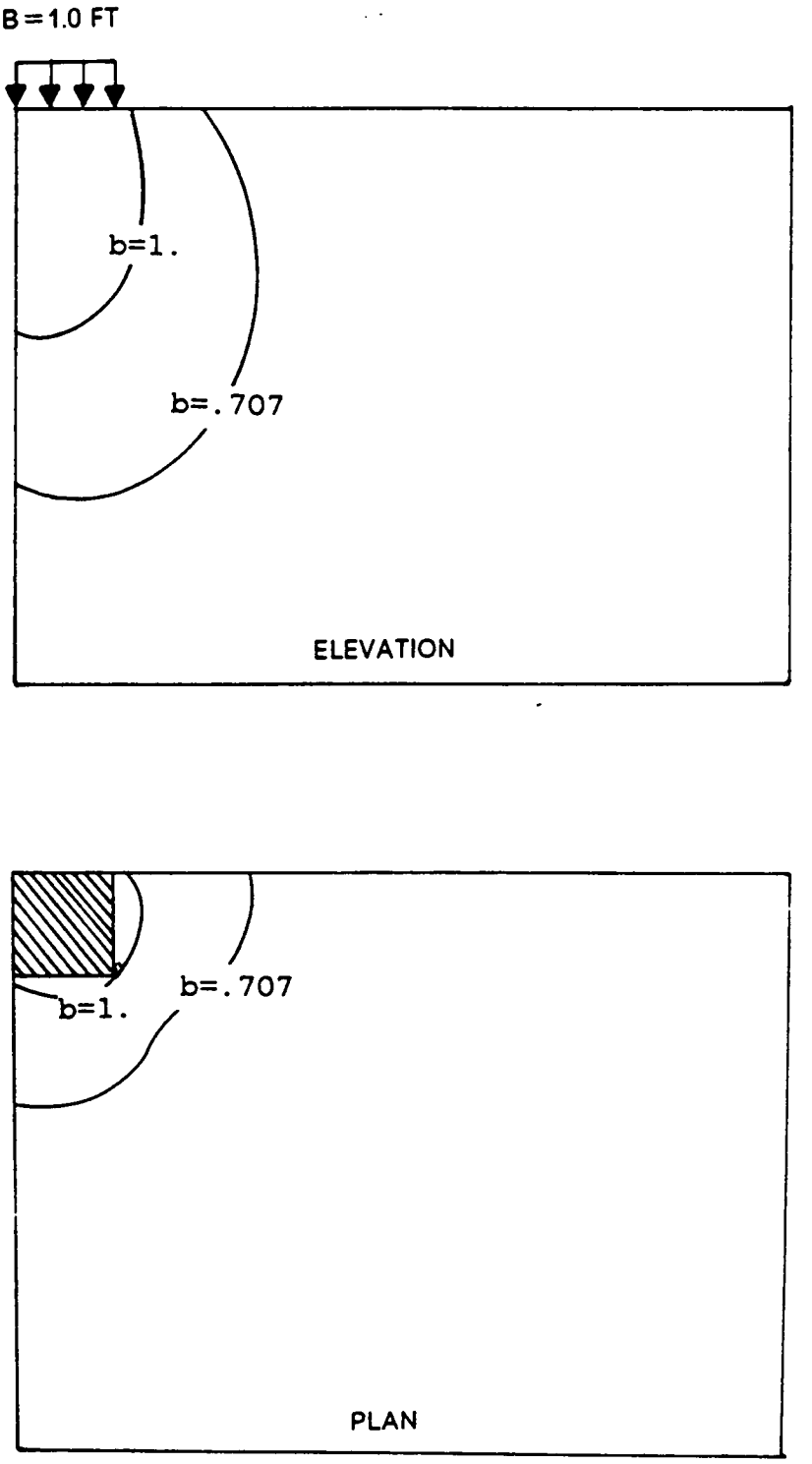

Figure 6.18: Yield zones under square footing-Undrained condition

Table 6.6 Propertied for three dimensional analysis-Orthotropy

o-ratio	E_2 psi	E_3 psi	G_{12} psi	M_{12} psi	M_{44}
.707	21210.	44260.	7189.	2.00	6.0
1.00	30000.	44260.	10170.	1.00	3.0
1.42	44260.	44260.	14400.	.500	1.5

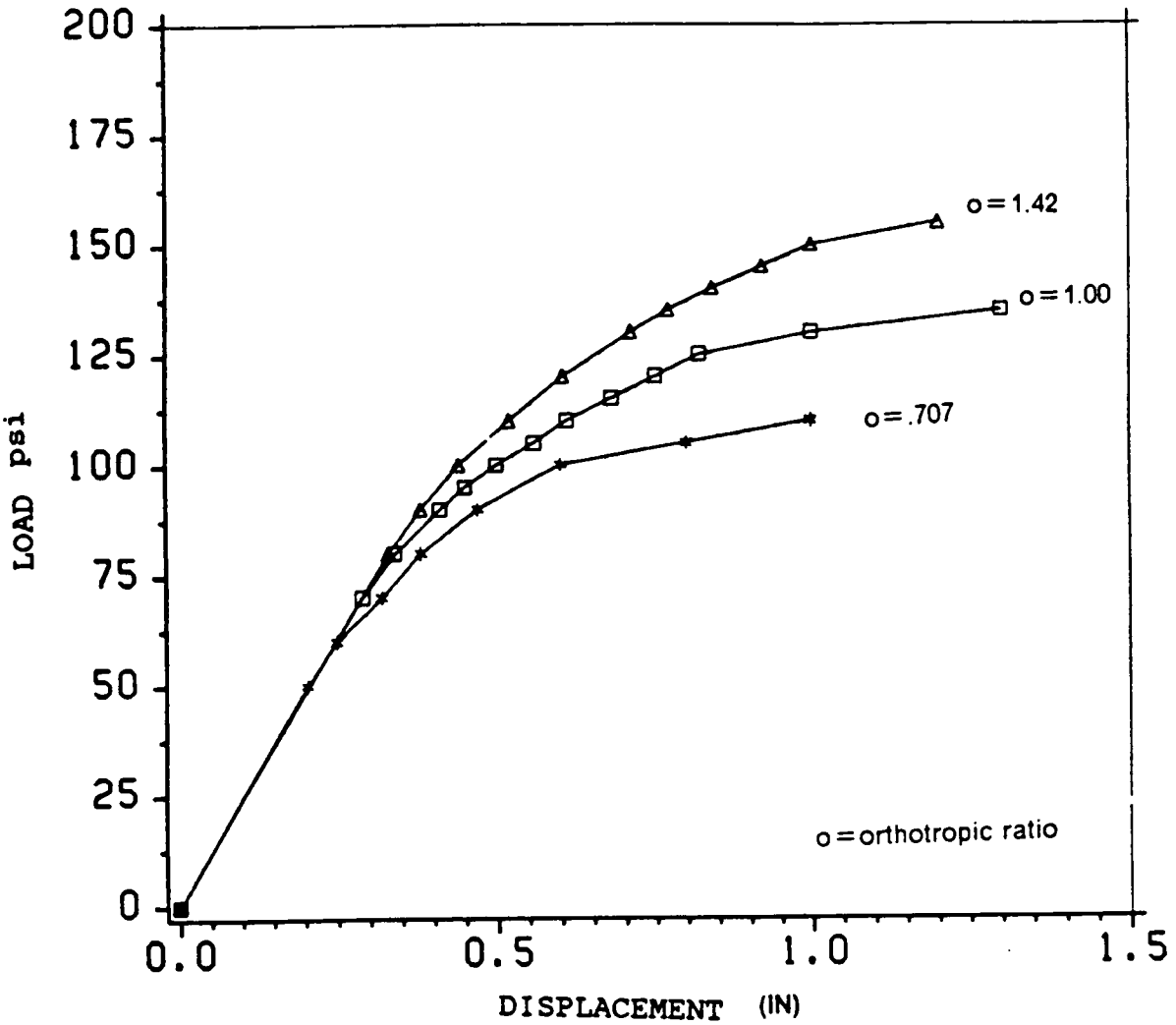

Figure 6.19 Influence of Orthotropy on Load-Displacement Response

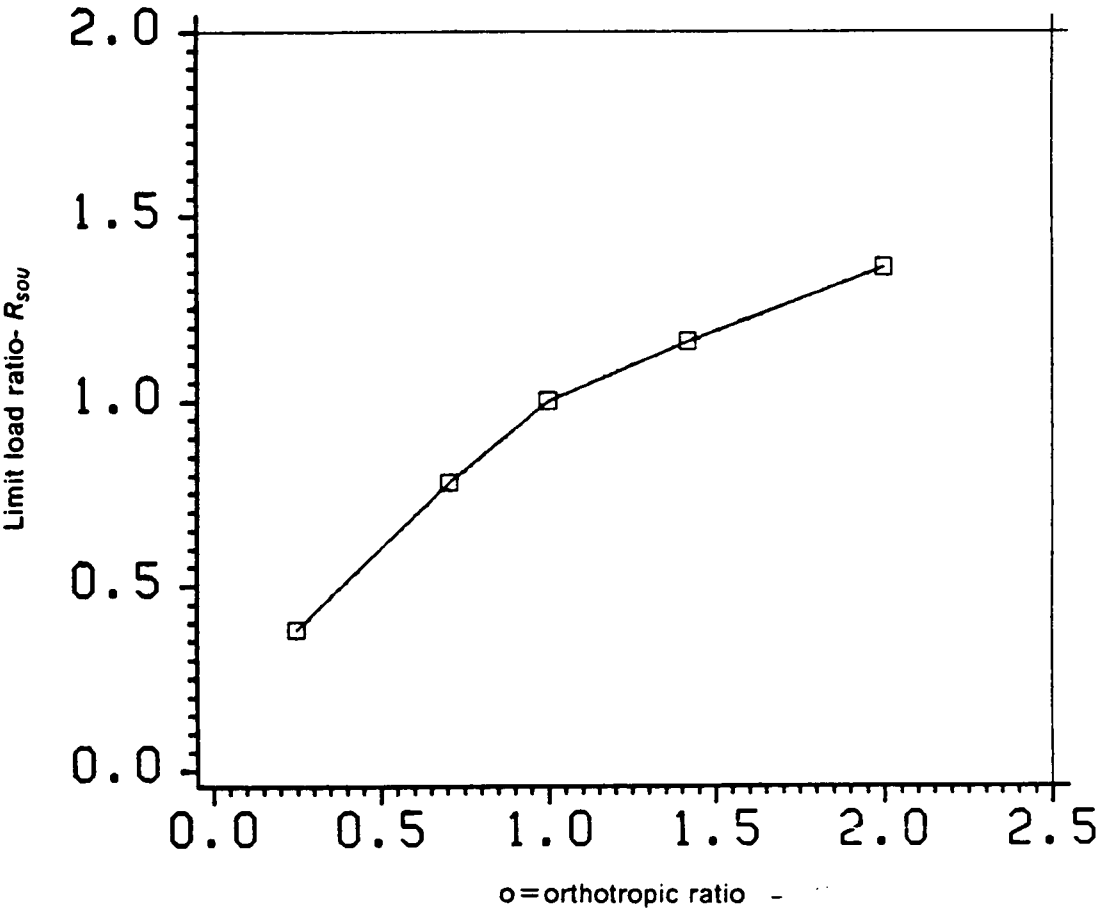

Figure 6.20: Influence of Orthotropy on Limit Loads

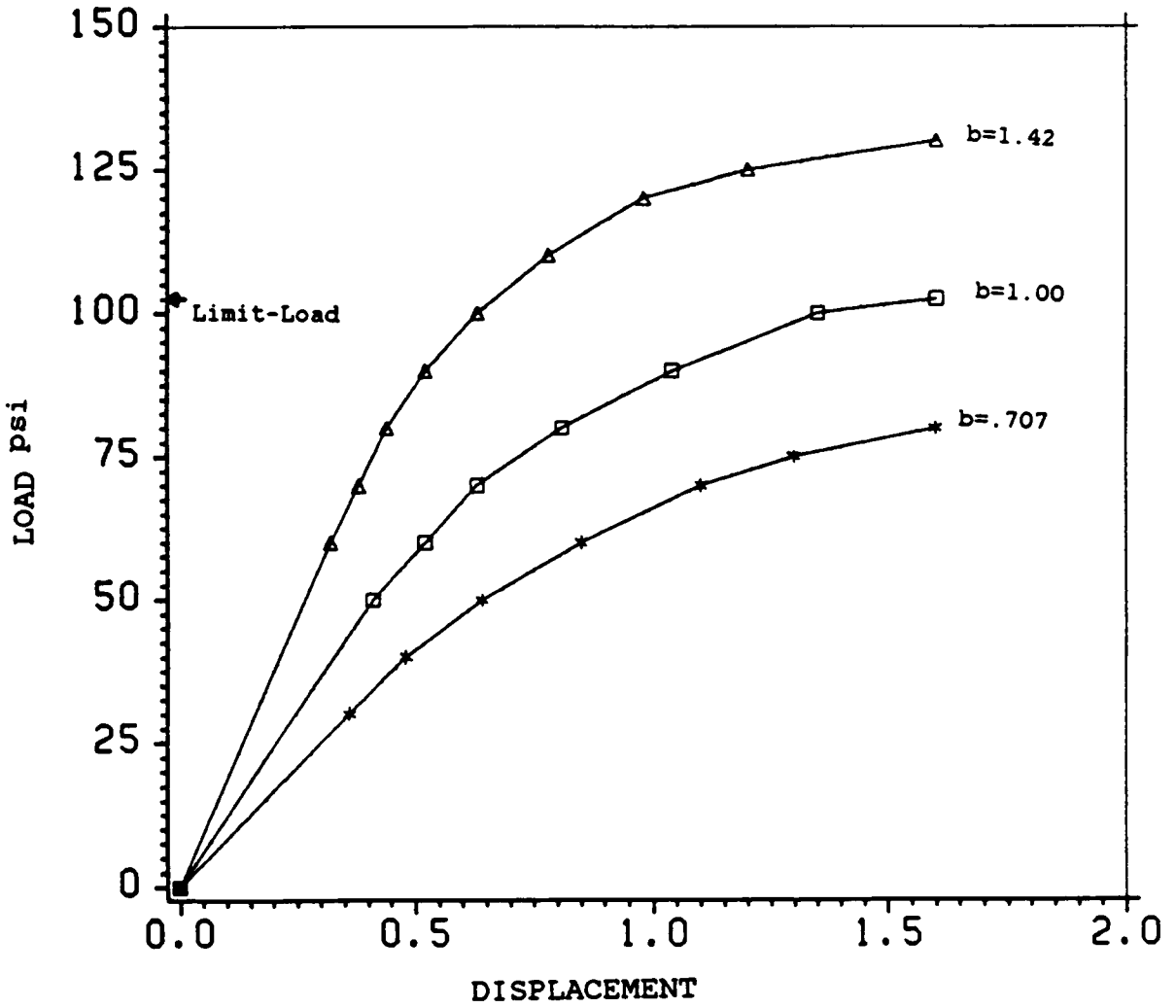

Figure 6.21 Undrained Load-Displacement Response-Rectangular Footings

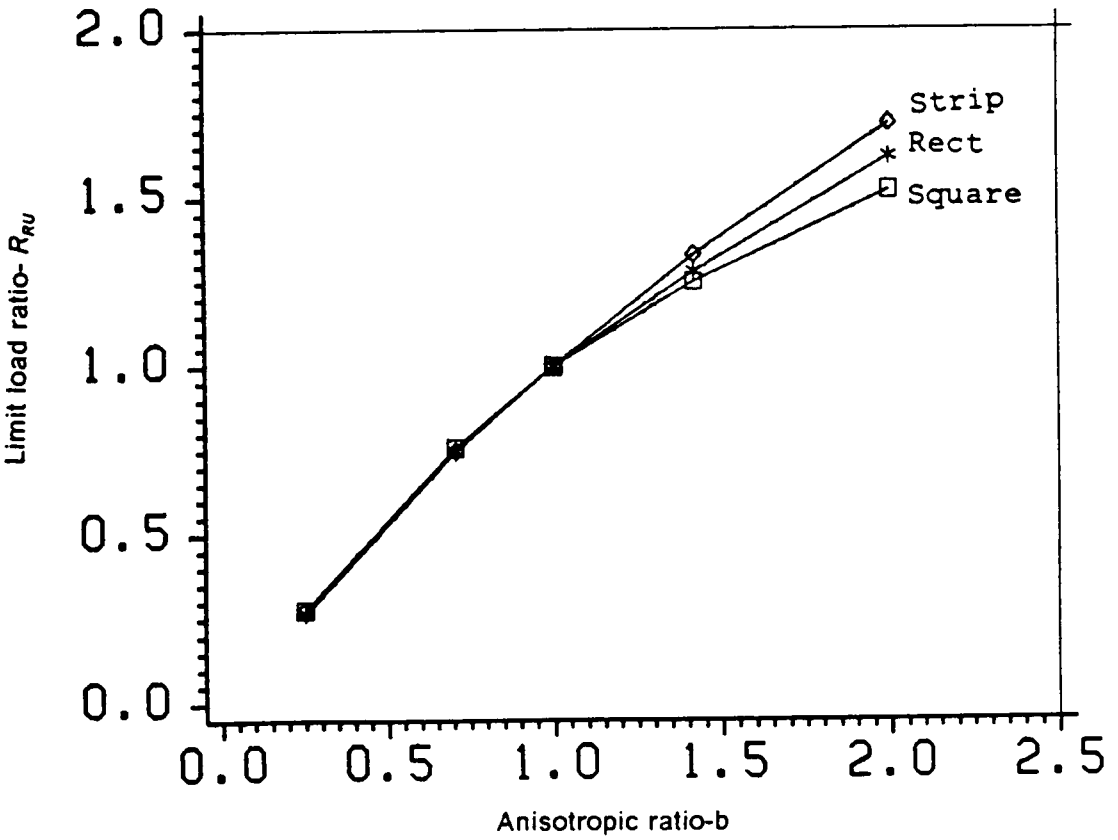

Figure 6.22:Influence of Anisotropy-Rectangular Footings

Figure 6.23 compares the influence of anisotropy on the elastic displacement, for square, rectangular and strip footings. Anisotropy has a large influence on the displacements in all cases. However the influence of anisotropy on the shape of the curves is the not significant.

Pressure Dependent Model

The same square footing has been analysed under drained conditions, using the pressure dependent model. The parameters used in the analysis are the same as those used in the drained analysis of the strip footing. Due to the three-dimensional nature of the problem, the failure criteria for the isotropic soil cannot be reduced to the Mohr-Columb criteria. However as the stress condition below the centre of the square footing is nearer to the triaxial condition, the n value obtained from triaxial tests will be used (n = .87). Figure 6.24 illustrates the load-deflection curves for isotropic and anisotropic clays. The theoritical limit load for the isotropic clay is 2320. psf. Again no limiting condition is reached and a ultimate load is defined as the load which causes the same deflection as a load of 2320. psf causes on an isotropic clay. No limiting condition is reached, because the mode of failure is different than that assumed in the limit analysis. Also in this case the failure condition is different than that assumed in the limit analysis.

Figure 6.25 illustrates the influence of anisotropy on the ultimate load. In figure 6.25 the ratio of the limit load for anisotropic soils to the limit load for isotropic soil R_{sd} is plotted versus b. Compared to the plane strain case the influence of anisotropy is less significant on the ultimate load. This is because of three-dimensional effects and the limited zone of influence of the square footing as compared to the strip footing. However the influence of anisotropy is large when compared to the undrained analysis.

Figure 6.26 illustrates the surface profile under drained conditions. The profile is not very different from the undrained case.

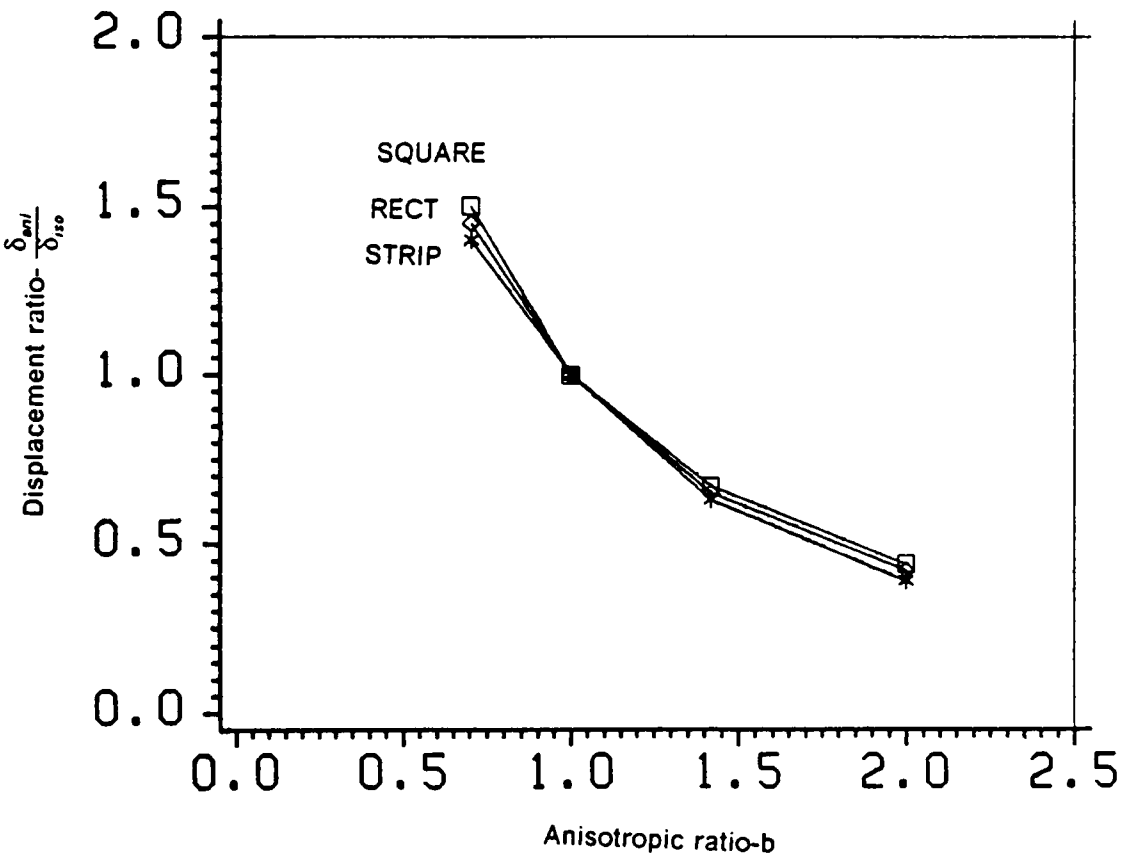

Figure 6.23: Influence of Anisotropy on Displacements

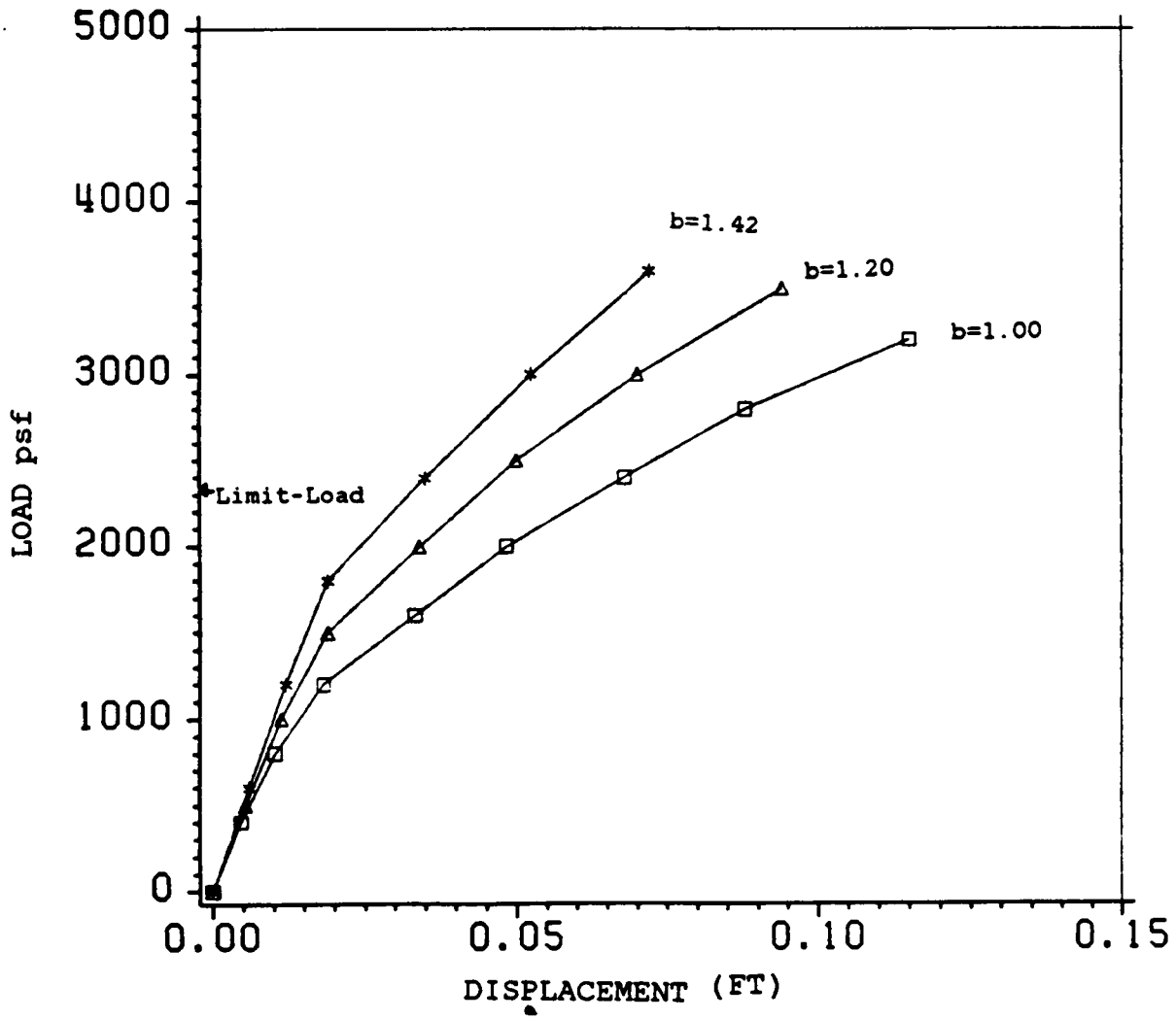

Figure 6.24 Drained Load-Displacement Response-Square Footing

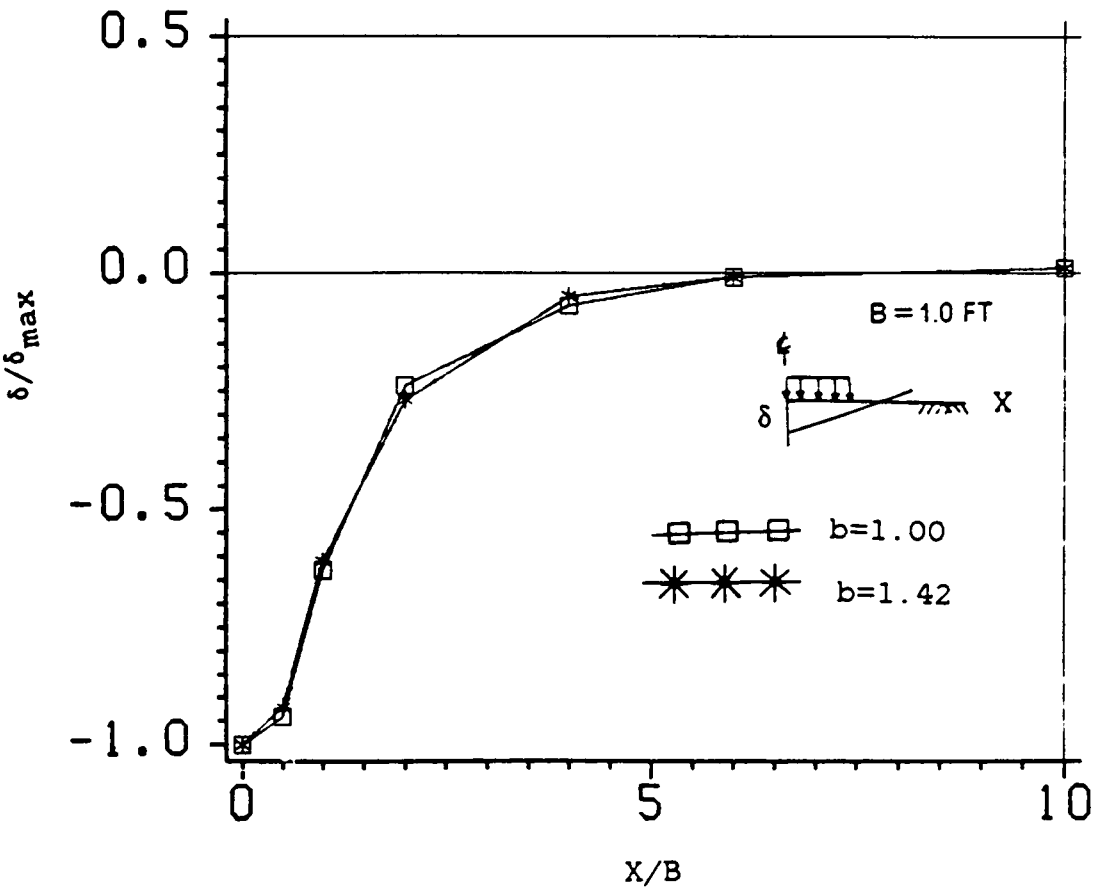

Figure 6.25:Surface Profile-Drained Analysis

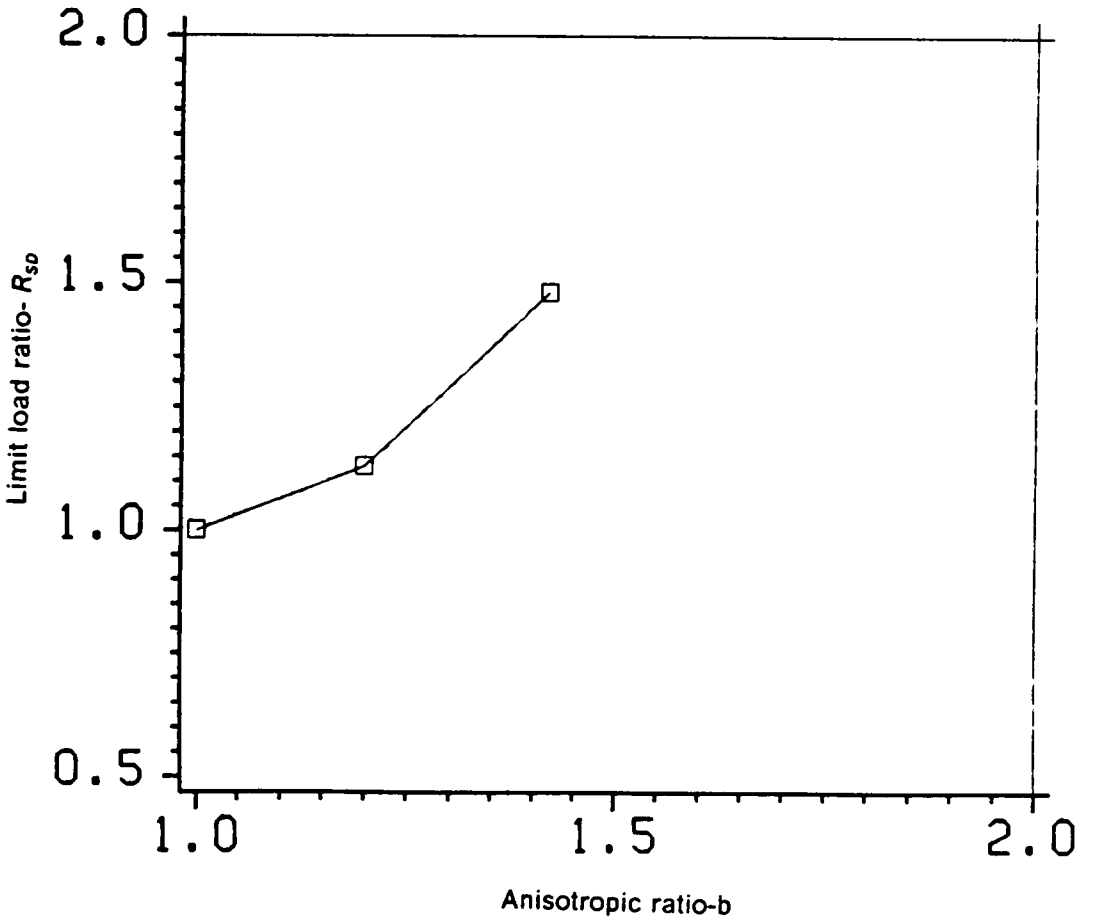

Figure 6.26: Influence of Anisotropy-Square Footing

Embankment on Shallow Clay Layer

The next problem analysed is an embankment on a shallow layer of clay. The embankment is analyzed under undrained conditions and under plane strain conditions. The pressure-independent model is used in the analysis. The loading is simulated by building up the embankment layer by layer. Five loading steps are used, and in each step, 20% of the layer is builtup. Details of this method are given in Chapter 5. The influence of initial anisotropy of the clay layer on the deformation and yielding are investigated. Three cases are analysed, b=.707, b=1.00 and b=1.42, where b is defined as before. The properties of the clay and the dimensions of the problem are given below;

E = 10000. psf

v = .48

C = 500. psf

$M_{33} = \frac{1}{b^2}$

$M_{66} = 3M_{33}$

$K_0 = 1.0$

density = 100. psf

L = 10. ft

D = 10. ft

H = 10. ft

Where L is the top width and H is the height of the embankment, and D is the depth of the layer. The slope of the embankment is 45. degrees. Figure 6.27 shows the deformation of the layer for a fixed height of the embankment for various degree's of anisotropy of the clay layer. It can be seen that the influence of anisotropy of the clay layer on the deformation can be significant. Table 6.7 compares the ratio of the maximum displacement at the centre of the embankment δ_{max} to the maximum displacement for the isotropic clay δ_{IMAX} with b.

Table 6.7 Influence of anisotropy on embankment displacements

b	$\delta_{max}/\delta_{IMAX}$
.707	1.22
1.00	1.00
1.42	.92

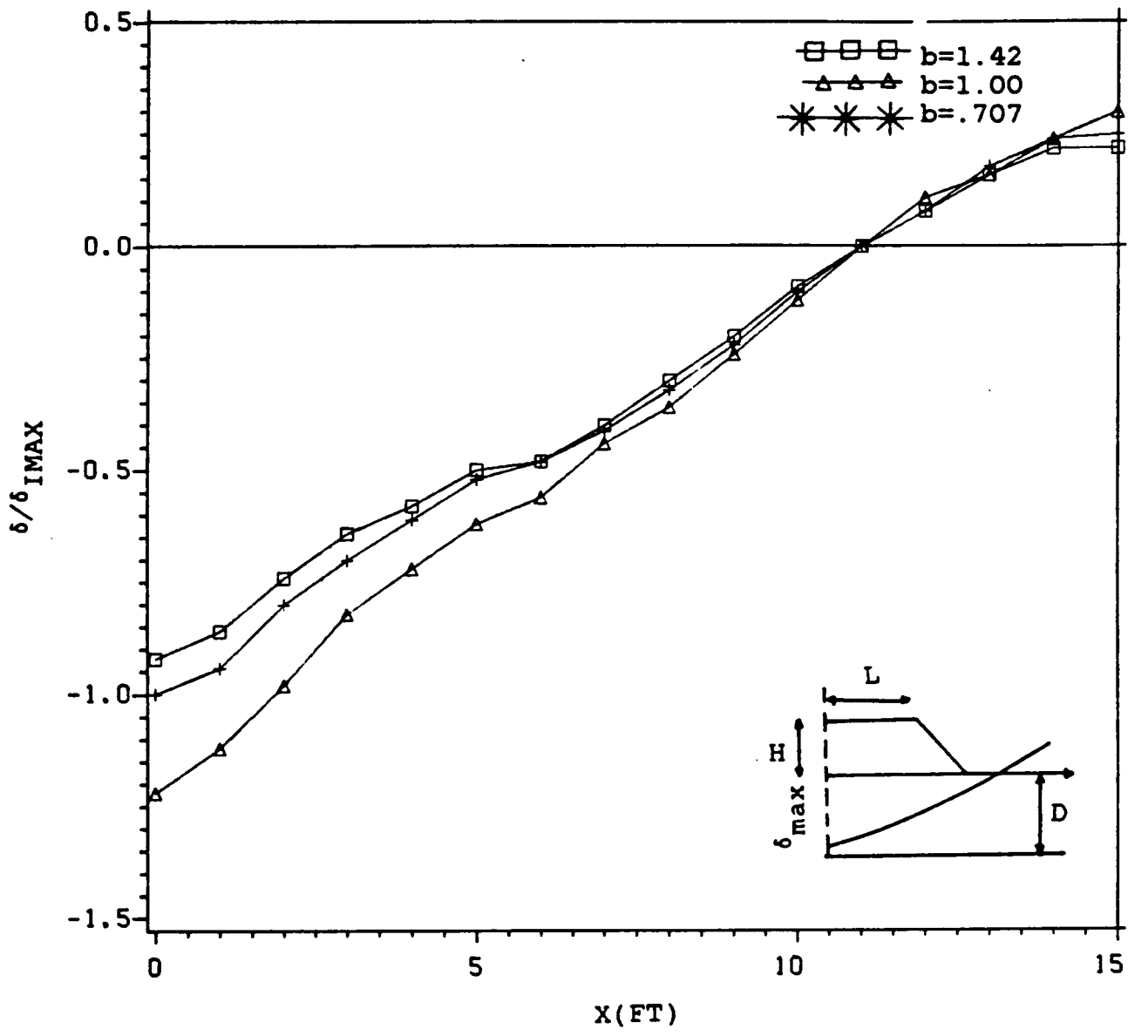

Figure 6.27:Embankment Displacement Profiles

Figure 6.28 shows the zones of yield at the end of construction of the embankment for various values of anisotropy of the clay layer. The anisotropic clay with b = 1.42, has just begun to yield at the end of construction, whereas for the anisotropic clay with b = .707 plastic collaspe has occoured. Hence anisotropy significantly influences the stability of the embankment.

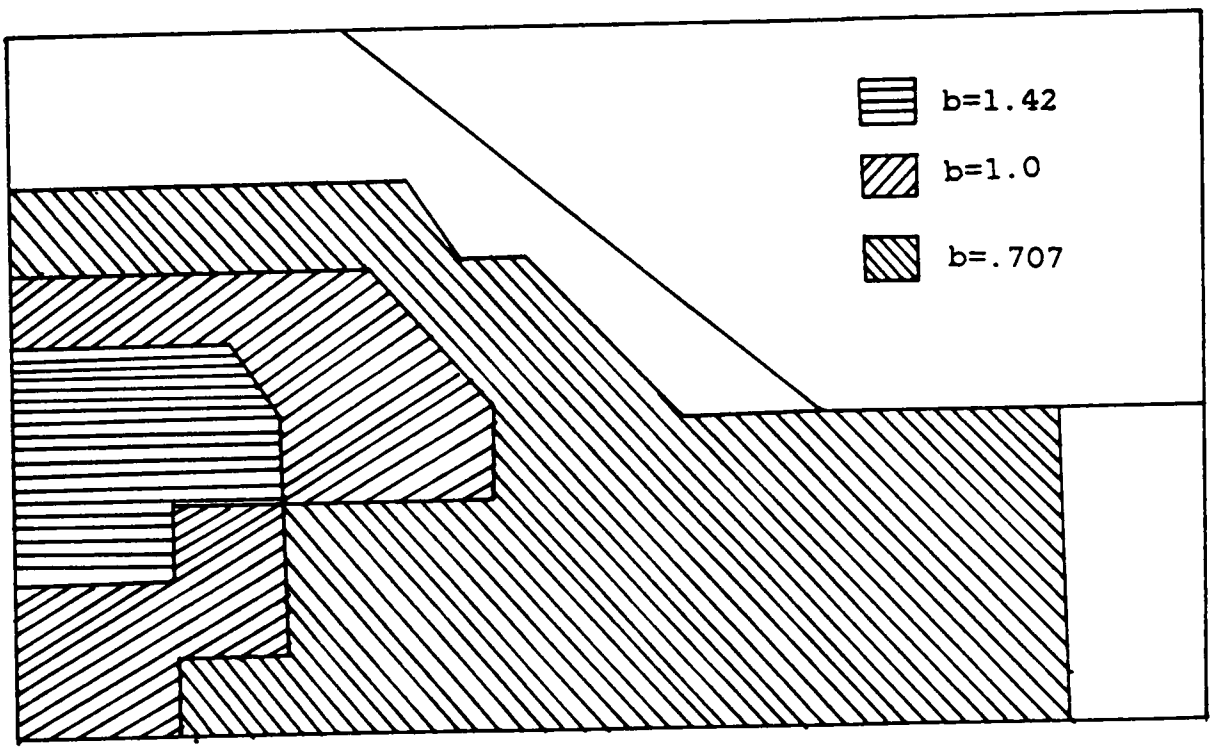

Figure 6.28 Embankment Yield Zones

CHAPTER 7

SUMMARY AND CONCLUSIONS

In recent years a large number of constitutive models have been developed to analyze the nonlinear behavior of soil, and these models have been used along with the finite element method to obtain solutions to a number of problems of practical interest. Most of these models have treated soil as an initially isotropic material. Yet most soils display some anisotropic behavior. The aim of this thesis has been to develop elasto-plastic models for initially anisotropic soils and to use these models along with the finite element method to obtain solutions to problems in which the soil displays initial anisotropy.

Models were developed for both pressure-independent media and pressure- dependent media. Pressure independent models can be used for the undrained/total stress analysis of clays. Pressure dependent models can be used for the effective stress analysis. Both isotropic and kinematic hardening theories were used in developing the models.

An isotropic-hardening model was developed for initially orthotropic pressure- independent media. This model is a generalization of the Von-Mises model. A method was developed to determine the hardening modulus and the anisotropic parameters. The model can

be used for monotonic loading conditions. However, the isotropic-hardening model cannot be used for general loading conditions, because it assumes elastic unloading and cannot account for induced anisotropy. To overcome these limitations, a multisurface model was developed for initially orthotropic pressure- independent media. In this model, several yield surfaces are introduced to model the anisotropic hardening behavior. This model can be used for complex loading conditions, as it can account for both initial and induced anisotropy. For both these models a simple method was developed to obtain the strength parameters and the plastic modulus. The response of these models was investigated under simple loading conditions. Some comparisons were made between undrained triaxial test data and theoritical model predictions for isotropic as well as anisotropic soils. Good comparisons were obtained.

The pressure-dependent models were based on Critical state concepts. To model the anisotropic behavior, an ellipicital cone was used as the failure surface and a distorted ellipsoid was used as the consolidation surface. To model complex loading conditions, a yield surface was introduced within the consolidation surface. This model can exhibit anisotropic-hardening and is called the two-surface model. A method was given to obtain the model parameters from simple tests. The response of the models was investigated under simple loading conditions. Comparisions were made with other constitutive laws and a limited amount of experimental data.

The general behavior of the models was investigated under various loading conditions and some comparisons were made with experimental data for both isotropic and anisotropic soils.

A nonlinear finite element program for elasto-plastic analysis was developed and the above models were incorporated into the program. A large deformation analysis based on the updated Lagrangian approach was included in the program. Also included were sequential buildup, automatic mesh generation, and graphics for three-dimensional analysis.

The finite element program was used to study the behavior of strip, rectangular and square footings. The models developed were used in the analysis. The aim was to investigate the influence of initial anisotropy, on the bearing capacity, deformation, and pore-pressure

development under footings under both plane strain and three-dimensional conditions. Both undrained and drained situations were analyzed. It was found that anisotropy can have a significant influence of the deformation and failure of the footings. For the range of anisotropy encountered in the field, the deformation can vary by over 100% of the isotropic deformation, and the bearing capacity by over 75% of the isotropic undrained bearing capacity. Under drained conditions, the anisotropy can result in similar results. However anisotropy has little influence on the surface displacement profile for both drained and undrained situations. The influence of anisotropy on the stability and deformation of embankments was also investigated.

From the above study, the following conclusions can be drawn.

The pressure-independent models can be used for undrained analysis of anisotropic clays. The models are simple to use and easy to implement. The determination of the parameters is simple and can be determined from undrained tests. The model predictions compare well with undrained triaxial data for both isotropic and anisotropic soils.

For monotonic loading conditions, both the isotropic-hardening model and the multisurface model gave similar results. The isotropic hardening model is simpler to use. However, it cannot account for induced anisotropy and assumes elastic unloading. The multisurface model can account for induced anisotropy and be used for nonmomotonic loading conditions.

The pressure-dependent models can be used for both drained and undrained conditions. The models are general and can be used for both clays and sands. These models are more complex compared to the pressure-independent models. However, with the pressure-dependent models information about the pore pressure-development can also be obtained. Futher comparisons are needed with experimental data to verify these models.

For overconsolidated soils the two surface model gives more reasonable results than the isotropic-hardening model. However, at low overconsolidation ratios the difference is not significant.

In the finite element analysis with monotonic loading conditions, both the isotropic-hardening models and the anisotropic-hardening models gave similar results. However, the

isotropic-hardening models are simpler to use, computationally economical, and numerically stable compared to the anisotropic-hardening models.

Finite element analysis of footings on undrained anisotropic clays show that anisotropy has a significant influence on both the deformation and bearing capacity of the footing. Anisotropy has the largest influence on the bearing capacity of the strip footing, and the least on the bearing capacity of the square footing. The rectangular footings exhibit a response inbetween the strip and square footing. The bearing capacity can differ by over 100% of the isotropic bearing capacity. Anisotropy has a significant influence on the undrained displacements. The anisotropic displacement can differ by over 100% of the isotropic displacement. The anisotropic displacement is not significantly influenced by the shape of the footing. Also the surface profile is not significantly influenced by anisotropy.

Some studies of square footings on orthotropic clays indicate that orhotropy of the clay can have some influence on the bearing capacity and deformation of the footing. However this is less important than the cross-anisotrpic influence.

Under drained conditions anisotropy has an even larger influence on the bearing capacity. As before the influence of anisotropy is larger in the strip footing. Anisotropy influences the magnitude of displacement, but not significantly the surface profile. However the drained surface profile is different from the undrained surface profile, specially for the strip footing. The difference is less significant for rectangular and square footings.

Some studies of strip footings under undrained conditions show that anisotropy influences the development of pore-pressure below the footing. A higher pore-pressure is developed in the isotropic soil compared to an anisotropic soil($b > 1.$). However the pore pressure profiles below the footing are not significantly different.

Anisotropy influences both the settlement and stability of embankments on clays. Both the displacement profile and the spread of yielding are influenced by the anisotropy of the clay.

The following recomendations are suggested for further study,

The constitutive models developed in this thesis can be extended to include softening and time dependent phenomenon. The models developed here are limited in application to a small number of loading cycles. These models can be extended for cyclic loading.

Futher comparisons with experimental data should be made to validate the models and investigate the applicability of the models to various soils.

Finally, the models along with the finite element method can be used to investigate the influence of anisotropy on various geotechnical structures.

REFERENCES

(1) Atkinson.J.H (1975), "Anisotropic elastic deformations in laboratory tests on undisturbed London clay", Geotechnique, 23, No 2, 357-374.

(2) Author.J.R.F (1972), "Inherent anisotropy in a sand", Geotechnique, 22, No.1, 115-128.

(3) Author.J.R.F, Chau.K.S and Dunstan.T (1973), "Induced anisotropy in a sand", Geotechnique, 27, No.1, 13-30.

(4) Baker.W.H and Krizek.R.J (1970), "Mohr-Coulomb strength theory for anisotropic soils", J. Geotech. Eng. Div, ASCE, Vol 96, 269-292.

(5) Baladi.G.Y and Sandler.I.S (1980), "Examples of the use of the cap model for simulating the stress strain behavior of soils", Pros. workshop on Limit equilibrium, plasticity and generalized stress strain in geotechnical engineering, 649-710.

(6) Baltov.A and Sawczuk.A (1964), "A rule for anisotropic hardening", Acta Mech 6, 81-92.

(7) Banerjee.P.K and Stipho.A.S (1978), "Associated and non-associated constitutive relations for the undrained behavior of isotropic soft clays", Int. J. Num. Anl. Meth. Geom., Vol 2, 35-56.

(8) Bhaskaran.R (1976), "Anisotropy for finite element analysis", Numerical methods in geomechanics, Vol 1, 345-356.

(9) Bishop.A.W and Hight.D.W (1977), "The value of possions ratio in saturated soils and rocks stressed under undrained conditions", Geotechnique, 27, No.3, 369-384.

(10) Boehler.J.P and Sawczuk.A (1977), "On yielding of oriented solids" Acta Mech, 27, 185-206.

(11) Bonaparte.R and Mitchel.J.K (1973), " The properties of San Francisco bay mud at Hamilton air force base", Report Dept. of Civil Eng., Univ. of Berkeley, CA.

(12) Clough.G.W and Hansen.L.A (1981), "Clay anisotropy and braced wall behavior", J. Geotech. Div, ASCE, Vol 107, 893-913.

(13) Cairncross.A.M and James.R.G (1977), "Anisotropy in overconsolidated clays", Geotechnique, 27, No. 1, 31-36.

(14) Carter.J.P, Booker.J.R and Davis.E.H (1977), "Finite deformation of an elasto-plastic soil", Int. J. Num. Meth. Geom., Vol 1, 25-43.

(15) Chen.W.H (1975), "Limit analysis in soil plasticity", Elsevier Scientific Publishing Company, New York.

(16) Dafalias.Y.F and Popov.E.P (1977), "A model of nonlinearly hardening materials for complex loadings", Acta Mech, Vol 21, 173-192.

(17) Dafalias.Y.F (1979), "Anisotropic hardening of initially orthotropic materials", ZAMM, 59, 437-446.

(18) Dafalias.Y.F and Herrmann.L.R (1980), "Bounding surface soil plasticity model", Int. Sym. on soils under cyclic and transient loading, 335-345.

(19) Davis.E.H and Christian.J.T (1971), "Bearing capacity of anisotropic cohesive soils", J. Geotech Eng. Div., ASCE, Vol 97,753-769.

(20) Desai.C.S and Abel.J.F (1972), "Introduction to the finite element method", Van Nostrand Reinhold Company, New York.

(21) Drucker.D.C, Gibson.R.E and Henkel.D.J (1957), "Soil mechanics and work hardening theories of plasticity", Trans. Am. Soc. Civ. Eng., 122, 338-346.

(22) Duncan.J.M and Seed.H.B (1968), Anisotropy and stress reorientation in clay", J. Geotech. Eng. Div., ASCE, Vol 92, 22-50.

(23) Edelman.F and Drucker.D.C (1951), "Some extensions of elementary plasticity theory", J. Fran. Ins., 581-605.

(24) Feda.J (1978), "Stress in in subsoil and methods of final settlement calculation", Elsevier Scientific Publishing company, New York.

(25) Ghaboussi.J and Momen.H (1984), "Plasticity model for inherently anisotropic behavior of sands", Int. J. Num. Anl. Meth. Geom., Vol 8, 1-17.

(26) Gibson.R.E (1974), "The analytical method in soil mechanics", Geotechnique, 24, No. 2, 115-140.

(27) Griffin.O.H, Kamat.M.P and Herakovich.C.T (1981), "Three dimensional inelastic finite element analysis of laminated composites", J. Comp. Mat., 5, 543-559.

(28) Hibbit.H.D, Marcal.P.V and Rice.J.R (1970), "A finite element formulation for problems of large strains and large deformations", Int. J. Sol. Stru., 6, 1069-1086.

(29) Hill.R (1950), "The mathematical theory of plasticity", Oxford University Press, London.

(30) Jones.R.M (1981), "Mathematical theory of plasticity", Class notes, V.P.I.

(31) Ko.H.Y and Sture.S (1974), "Three dimensional mechanical characterization of anisotropic composites", J. Comp. Mat.,Vol 8, 174-190.

(32) Krieg.R.D (1975), "A practical two surface theory", J. App. Mech., 641-646.

(33) Lekhitsky.S.G (1963), "Theory of elasticity of an anisotropic elastic body", Holden-day Inc, New York.

(34) Livhen.M and Shklarsky.E (1965), "Equations of failure stresses in materials with anisotropic strength parameters", Highway research Record, No. 74, 44-55.

(35) Lo.K.Y (1965), "Stability of slopes in anisotropic soils", J. Geotech. Eng. Div., ASCE, Vol 91,255-272.

(36) Lo.K.Y and Morin.J.P (1972), "Strength anisotropy and time effects of two senstitive clays", Can. Geotech. J., 9, 261-277.

(37) Lo.K.Y , Leonards.G.A and Yuen.C (1981), "Interpretation and significance of anisotropic behavior of soft clays", NGI, 1-16.

(38) McMeeking.R.M and Rice.J.R (1975), "Finite element formulation for problems of large elastic-plastic deformation", Int. J. Sol. Struc., Vol 11, 601-616.

(39) Mendelson.A (1968), "Plasticity, Theory and application", Macmillan Co., New York.

(40) Mitchell.R.J (1970), "The generalized failure of an Ottawa valley champlain clay", Can. Geot. J., Vol 10, 607-616.

(41) Mitchell.R.J (1972), "Some deviations from isotropy in lightly overconsolidated clay", Geotechnique, 22, No. 2, 459-467.

(42) Mroz.Z (1963), "Non-associated flow laws in plasticity", J. de Mecanique, Vol 11, NO. 1,27-40.

(43) Mroz.Z (1967), "On the description of anisotropic work hardening", J. Mech. Phys. Sol., Vol 15, 163-175.

(44) Mroz.Z, Norris.V.A and Zienkiewicz.O.C (1979), "Application of an anisotropic hardening model in the analysis of elasto-plastic deformation of soils", Geotechnique, 29, No. 1, 1-34,

(45) Mroz.Z, Norris.V.A and Zienkiewicz.O.C (1981), "An anisotropic critical state model for soils subject to cyclic loading", Geotechnique, 31, No.1, 451-469.

(46) Mroz.Z and Pietruszczak.ST (1983), "A constitutive model for sand with anisotropic hardening rule", Int. J. Num. Anl. Meth. Geot., Vol 7, 305-320.

(47) Oda.M, Koishikawa.I and Higuchi.T (1978), "Experimental study of anisotropic shear strength of sand by plane strain test", Soils and Foundations, Vol 18, No. 1, 25-38.

(48) Osias.J.R and Swedlow.J.L (1974), "Finite elasto-plastic deformation-1, Theory and numerical examples", Int. j. Sol. Struc., Vol 10, 321-339.

(49) Pickering.D.J (1970), "Anisotropic elastic parameters for soil", Geotechnique, 20, No. 3, 271-276.

(50) Pietruszczak.St and Mroz.Z (1983), "On hardening anisotropy of Ko consolidated clays", Int. J. Num. Anl. Meth. Geot., Vol 7, 19-38.

(51) Prager.W (1961), "An elementary discussion of defination of stress rate", J. App. Math., XVII, 403-407.

(52) Prevost.J.H (1977), "Mathematical modelling of monotonic and cyclic undrained clay behavior", Int. J. Num. Anl. Meth. Geot., Vol 1, 195-216.

(53) Prevost.J.H (1978), "Anisotropic undrained stress strain behavior of clays", J. geotech. Eng. Div., ASCE, Vol 105, 1076-1090.

(54) Prevost.J.h (1979), "Mathematical modelling of soil stress strain behavior", Int. Conf. Num. Meth. Geom., Aachen, 513-526.

(55) Prevost.J.h (1982), "Two surface versus multisurface plasticity theories, A critical assesment", Int. J. Num. Anl. Meth. Geom., Vol 6, 323-338.

(56) Ramberg.W and Osgood.W.P (1943), "Description of stress strain curves by three parameters", NACA Technical Note, No. 902.

(57) Roscoe.K.H, Schofield.A.N and Wroth.C.P (1958), "On the yielding of soils", Geotechnique, 8, No. 1, 22-53.

(58) Roscoe.K.H and Burland.J.B (1968), "ON the generalized stress strain behavior of 'wet clay'", Engineering Plasticity, Cambridge, 593-609.

(59) Saada.A.S and Zamani.K.K (1969), "The mechanical behavior of cross anisotropic clays", Pros. 7 Int. Con. Soil Mech. Foun. Engg., New Mexico, 351-359.

(60) Saada.A.S and Ou.C.D (1973), "Strain stress relations and the failure of anisotropic clay", J. Geotech. Eng. Div., ASCE, Vol 99, 1091-1111.

(61) Schofield.A and Wroth.P (1968), "Critical state soil mechanics", McGraw-Hill, New York.

(62) Shih.C.F and Lee.D (1978), "Futher developments in anisotropic plasticity", J. Engg. Mat. Tech., Vol 100, 294-302.

(63) Sokolovskii.V.V (1965), "Statics of granular media", Pergamon Press New york.

(64) Tsai.S.W and Wu.E.M (1971), "A general theory of strength for anisotropic materials", Composite Materials, Vol 5, 58-80.

(65) Toh.C.T and Sloan.S.W (1980), "Finite element analysis of isotropic and anisotropic cohesive soils with a view to correctlty predicting impending collaspe", Int. J. Num. Anl. Meth. Geom., Vol 4, 1-23.

(66) Valliappan.S, Boonlaulohr.P and Lee.I.K (1976), "Nonlinear analysis for anisotropic materials", IJNME, Vol 10, 597-606.

(67) Yamada.Y and Wifi.A.S (1977), "Large strain analysis of some geomechanics problems by the finite element method", Int. J. Num. Anl. Meth. Geom., Vol 1, 299-318.

(68) Yamada.Y and Ishihara.K (1979), "Anisotropic deformation characteristics of sand under three dimensional conditions", Soils and Foundations, Vol 19, No. 2, 79-94.

(69) Yong.R.N and Silvestri.V (1979), "Anisotropic behavior of a senstitive clay", Can Geotech. J., Vol 16, 335-350.

(70) Zienkiewicz.O.C (1971), "The finite element method in engineering science", McGraw-Hill, London.

(71) Zienkiewicz.O.C and Naylor.D.J (1971), "The adoption of the critical state model for use in the finite element method", Proc. Roscoe Memorial Sym., Cambridge, 537-547.

(72) Zyczkowski.M (1981), "Combined loadings in the theory of plasticity", PWN-Polish Scientific Publishers.

Appendix A. Elastic Relations For Orthotropic Media

For an orthotropic elastic material the stress strain relations in the material principal planes can be written as;

$$\varepsilon_1 = \frac{1}{E_1}\sigma_1 - \frac{\nu_{21}}{E_2}\sigma_2 - \frac{\nu_{31}}{E_3}\sigma_3$$

$$\varepsilon_2 = \frac{-\nu_{12}}{E_1}\sigma_1 + \frac{1}{E_2}\sigma_2 - \frac{\nu_{32}}{E_3}\sigma_3$$

$$\varepsilon_3 = \frac{-\nu_{13}}{E_1}\sigma_1 - \frac{\nu_{23}}{E_2}\sigma_2 + \frac{1}{E_3}\sigma_3 \qquad (A.1)$$

$$\gamma_{23} = \frac{\tau_{23}}{G_{23}} \quad \gamma_{13} = \frac{\tau_{23}}{G_{23}} \quad \gamma_{12} = \frac{\tau_{12}}{G_{12}}$$

Not all the constants are independent. For symmetry requirments;

$$E_1\nu_{21} = E_2\nu_{12}$$

$$E_2\nu_{32} = E_3\nu_{23} \tag{A.2}$$

$$E_3\nu_{13} = E_1\nu_{31}$$

For an incompressible orthotropic elastic material, three more conditions have to be satisfied.

$$\nu_{12} = \frac{n_3 + n_2 - 1}{n_1 n_3 + n_2}$$

$$\nu_{13} = 1 - \nu_{12} \tag{A.3}$$

$$\nu_{23} = \frac{1 - \nu_{13}}{n_3}$$

where $n_1 = \frac{E_2}{E_1}$, $n_2 = \frac{E_3}{E_1}$ and $n_3 = \frac{E_3}{E_2}$

For an cross anisotropic material with the 1-2 plane as the plane of isotropy, the stress strain relations in the material principal planes can be written as;

$$\varepsilon_1 = \frac{(\sigma_1 - \nu\sigma_2)}{E} - \frac{\nu^{\times}\sigma_3}{E^{\times}}$$

$$\varepsilon_2 = \frac{(\sigma_2 - \nu\sigma_1)}{E} - \frac{\nu^{\times}\sigma_3}{E^{\times}}$$

$$\varepsilon_3 = \frac{-\nu(\sigma_1 + \sigma_2)}{E} + \frac{\sigma_3}{E^{\times}} \tag{A.4}$$

$$\gamma_{23} = \frac{\tau_{23}}{G^{\times}} \quad \gamma_{12} = \frac{\tau_{12}}{G} \quad \gamma_{13} = \frac{\tau_{13}}{G^{\times}}$$

For an incompressible media, the following relations are valid;

$$\nu_{12} = 1 - .5n_2 \tag{A.5}$$

$$\nu_{13} = \nu_{23} = .5$$

Finally for an isotropic elastic material, the stress strain relations can be written as;

$$\varepsilon_1 = \frac{1}{E}(\sigma_1 - \nu(\sigma_2 + \sigma_3))$$

$$\varepsilon_2 = \frac{1}{E}(\sigma_2 - \nu(\sigma_1 + \sigma_3))$$

$$\varepsilon_3 = \frac{1}{E}(\sigma_3 - \nu(\sigma_1 + \sigma_2)) \tag{A.6}$$

$$\gamma_{23} = \frac{\tau_{23}}{G} \quad \gamma_{13} = \frac{\tau_{13}}{G} \quad \gamma_{12} = \frac{\tau_{12}}{G}$$

The elastic constitutive matrix for an orthotropic material in the material principal planes is given as;

$$\mathbf{D} = \begin{vmatrix} D_{11} & D_{12} & D_{13} & 0 & 0 & 0 \\ D_{12} & D_{22} & D_{23} & 0 & 0 & 0 \\ D_{13} & D_{23} & D_{33} & 0 & 0 & 0 \\ 0 & 0 & 0 & D_{44} & 0 & 0 \\ 0 & 0 & 0 & 0 & D_{55} & 0 \\ 0 & 0 & 0 & 0 & 0 & D_{66} \end{vmatrix} \tag{A.7}$$

Where

$$D_{11} = \frac{E_1(1 - \nu_{23}\nu_{32})}{F}$$

$$D_{12} = \frac{E_2(\nu_{12} + \nu_{13}\nu_{31})}{F}$$

$$D_{13} = \frac{E_3(\nu_{13} + \nu_{12}\nu_{21})}{F}$$

$$D_{22} = \frac{E_2(1 - \nu_{13}\nu_{31})}{F}$$

$$D_{23} = \frac{E_3(\nu_{23} + \nu_{21}\nu_{13})}{F}$$

$$D_{33} = \frac{E_3(1 - \nu_{12}\nu_{21})}{F}$$

$$D_{44} = G_{12} \quad D_{55} = G_{23} \quad D_{66} = G_{13}$$

$$F = 1 - \nu_{12}\nu_{21} - \nu_{13}\nu_{31} - \nu_{23}\nu_{32} - \nu_{12}\nu_{23}\nu_{31} - \nu_{21}\nu_{13}\nu_{32}$$

If the global coordinate system does not coincide with the material principal directions, the **D** matrix has to be transformed.

$$\mathbf{D}^{\times} = \mathbf{T}_{\varepsilon}^{T}\mathbf{D}\mathbf{T}_{\varepsilon} \qquad (A.8)$$

where $\mathbf{T}_{\varepsilon}$ is the transformation matrix. The components of $\mathbf{T}_{\varepsilon}$ consist of the direction cosines of the angles between the two coordinate system.

$$\boldsymbol{\varepsilon}^{\times} = \mathbf{T}_{\varepsilon}\boldsymbol{\varepsilon} \qquad (A.9)$$

$$\boldsymbol{\sigma}^{\times} = \mathbf{T}_{\sigma}\boldsymbol{\sigma} \qquad (A.10)$$

where $\mathbf{T}_{\varepsilon}$ is given as;

$$
\mathbf{T}_\varepsilon = \begin{vmatrix}
l_1^2 & m_1^2 & n_1^2 & l_1 m_1 & m_1 n_1 & n_1 l_1 \\
l_2^2 & m_2^2 & n_2^2 & l_2 m_2 & m_2 n_2 & n_2 l_2 \\
l_3^2 & m_3^2 & n_3^2 & l_3 m_3 & m_3 n_3 & n_3 l_3 \\
2l_1 l_2 & 2m_1 m_2 & 2n_1 n_2 & (l_1 m_2 + l_2 m_1) & (m_1 n_2 + m_2 n_1) & (n_1 l_2 + n_2 l_1) \\
2l_2 l_3 & 2m_2 m_3 & 2n_2 n_3 & (l_2 m_3 + l_3 m_2) & (m_2 n_3 + m_3 n_2) & (n_2 l_3 + n_2 l_3) \\
2l_3 l_1 & 2m_3 m_1 & 2n_3 n_1 & (l_3 m_1 + l_1 m_3) & (m_3 n_1 + m_1 n_3) & (n_3 l_1 + n_1 l_3)
\end{vmatrix}
$$

$\mathbf{T}_\varepsilon$ can be written as;

$$
\mathbf{T}_\varepsilon = \begin{bmatrix} \mathbf{T}_Q & \mathbf{T}_R \\ \mathbf{T}_S & \mathbf{T}_T \end{bmatrix} \tag{A.11}
$$

$\mathbf{T}_\sigma$ can be written as,

$$
\mathbf{T}_\sigma = \begin{bmatrix} \mathbf{T}_Q & 2\mathbf{T}_R \\ \dfrac{\mathbf{T}_S}{2} & \mathbf{T}_T \end{bmatrix} \tag{A.12}
$$

The vita has been removed from the scanned document